Effect of Different Nano-oxide Addition on Densification, Microstructure, Electrical and Mechanical Properties of $Ba(Zr_{0.2}Ti_{0.8})O_3$–$0.5(Ba_{0.7}Ca_{0.3})TiO_3$ (BZT–BCT) Ferroelectric Ceramics

A Thesis Submitted in Partial Fulfillment of the Requirements for the Degree of

MASTER OF TECHNOLOGY (RESEARCH)

By

PRATIVA ADHIKARI
(Roll No: 612CR6006)

Under the Guidance of

Prof. Ranabrata Mazumder

DEPARTMENT OF CERAMIC ENGINEERING

NATIONAL INSTITUTE OF TECHNOLOGY, ROURKELA

2015

NATIONAL INSTITUTE OF TECHNOLOGY

Rourkela, INDIA

CERTIFICATE

This is to certify that the thesis entitled **"Effect of Different Nano-oxide Addition on Densification, Microstructure, Electrical and Mechanical Properties of $Ba(Zr_{0.2}Ti_{0.8})O_3–0.5(Ba_{0.7}Ca_{0.3})TiO_3$ (BZT–BCT) Ferroelectric Ceramics"** being submitted by Mrs. Prativa Adhikari, for the degree of **Master of Technology (Research) in Ceramic Engineering** to the National Institute of Technology, Rourkela, is a record of bonafide research work carried out by her under my supervision and guidance.Her thesis, in my opinion, is worthy of consideration for the award of degree of Master of Technology (Research) in accordance with the regulations of the Institute.

The results embodied in this thesis have not been submitted to any other university or institute for the award of a Degree.

Dr. R. Mazumder
Associate Professor
Department of Ceramic Engineering
National Institute of Technology, Rourkela

Declaration

I hereby declare that my M.Tech (Research) thesis is entitled as "**Effect of Different Nano-oxide Addition on Densification, Microstructure, Electrical and Mechanical Properties of $Ba(Zr_{0.2}Ti_{0.8})O_3–0.5(Ba_{0.7}Ca_{0.3})TiO_3$ (BZT–BCT) Ferroelectric Ceramics".** This thesis is my own work and has not been submitted in any form for another degree or diploma at any university or other institution of tertiary education. Information derived from the published and unpublished work of others has been acknowledged in the text and a list of references given in this thesis.

Prativa Adhikari

_____ _____

Date Signature

CONTENTS

ACKNOWLEDGMENTS

First, I would like to express my sincere gratitude to my supervisor Prof. Ranabrata Mazumder for his unlimited guidance, insight and suggestions throughout the research. I thank him from the bottom of my heart for introducing me to the area of electroceramics. I thank him for his great patience, constructive criticism and myriad useful suggestions apart from invaluable guidance to me.

I am grateful to Prof. S.K Pratihar, Head of Department of Ceramic Engineering for his encouragement and help to carry out the thesis work.

I would also take this opportunity to express my gratitude and sincere thanks to Prof. S. Bhattacharyya, Prof. J. Bera, Prof. B.B. Nayak, Prof. S.K. Pal and Mr. A. Chowdhury, Prof. D. Sarkar, Prof. R. Sarkar, Prof. Sunipa Bhattacharyya, Prof. S. Dasgupta, Prof. S.K. Behera, Prof. A.Paul and Prof. P Saha for their invaluable advice, constant help, encouragement, inspiration and blessings.

I would take this opportunity to thank Mr. Subhabrata Chakroborty (Senior Technician) for FESEM pictures, Mr. Arvind Kumar (Technician) for various thermal and Mechanical measurements and all other Technical, Non-technical staff of ceramic engineering department.

I would also like to thank Prof. S. Panigrahi of Department of physics and Prof. G. Hota of Department of Chemistry for their invaluable time and cooperation during my entire M.Tech (R) work.

I am also indebted to my senior research colleagues Ganesh K. Sahoo, Subrat Mohanty, Nadiya B. Nayak, Geetanjali Parida, Abhisek Choudhary and G. Jayarao for their unconditional support and constant motivation whenever needed. I am very grateful to all my dear friends Sangeeta, Raju, Abhinay, Sowjanya and Soumya who have given me their friendship, put up with my odd hours, and provided me with lifts and practical help.

Last but not the least, I would like to thank my dear parents, my elder brother, my beloved husband and in-laws for their support.

PRATIVA ADHIKARI

Abstract

Piezoelectric ceramics are widely used as actuator, resonator, and spark igniter. Recently, much attention has been paid to prepare BZT-BCT piezoelectric ceramics because of its good dielectric, piezoelectric properties and environment friendly nature. However, piezoelectric ceramics based on $BaTiO_3$ suffer from low reliability and poor mechanical properties such as strength and toughness. A novel method has been used to improve the mechanical properties of ceramics by reinforcement of matrix with stronger oxide (Al_2O_3, MgO, ZrO_2, Stabilized-ZrO_2) or nonoxide (SiC) particles. It is well known that electrical properties of ferroelectric ceramics generally degrade with non-ferrolecric additives and decrease in sinterability usually encountered with these refractory oxide additives. Use of nano-oxide additives may drastically reduce the amount of additive and in effect electrical property may not degrade much.

The aim of this work is to study the densification, microstructure, electrical and mechanical properties of BZT–BCT with nano oxide additives (Al_2O_3, MgO, and stabilized-ZrO_2). BZT-BCT powders were prepared successfully by a conventional mixed-oxide method via planetary-milling technique. BZT–BCT composites were prepared by mixing high purity BZT–BCT powder and small amount (0.5-2.0 vol%) of oxides, i.e. Al_2O_3, MgO and ZrO_2(3Y) separately. The flexural strength and hardness of BZT–BCT composites were increased significantly for all the three nano-oxide addition. It was found that nano-oxides addition improves densification and significantly modifies the microstructure. Though the relative permittivity and piezoelectric constant of the composites were decreased with the addition of nano-oxide, the decrement was sharp for MgO whereas it was least for Al_2O_3. Change in grain size, distribution of oxide particle and formation of secondary phases were used to explain the properties. 1 vol% Al_2O_3 added BZT-BCT will be useful for devices like low power transducers, where extremely high dielectric constant and high "d" constant required.

List of figures

List of Tables

CHAPTER 1

INTRODUCTION

1.1 Piezoelectricity and Ferroelectricity

Piezoelectrics are a class of materials that can convert mechanical energy into electrical energy and vice-versa. The piezoelectric effect was first discovered in 1880 by the brothers Pierre and Jacques Curie. It was not until the 1940's that barium titanate was discovered to be a ferroelectric exhibiting an exceptionally high dielectric constant. [1] Polarisation requires a non-symmetric structure; therefore all the crystallographic point groups that have a center of symmetry can't show piezoelectricity. Furthermore, the cubic class 432, although lacking a center of symmetry, can't accommodate piezoelectricity. We are, therefore, left with 20 of the 32 crystallographic point groups that show piezoelectricity [2].Of these groups, 10 have a unique crystallographic axis and therefore can have an electric dipole even at zero applied field (electrical and mechanical). These materials are defined as pyroelectric and show a range of polarization due to a change in temperature.

The relationship between the different symmetry groups and the polarization properties are shown in figure 1.

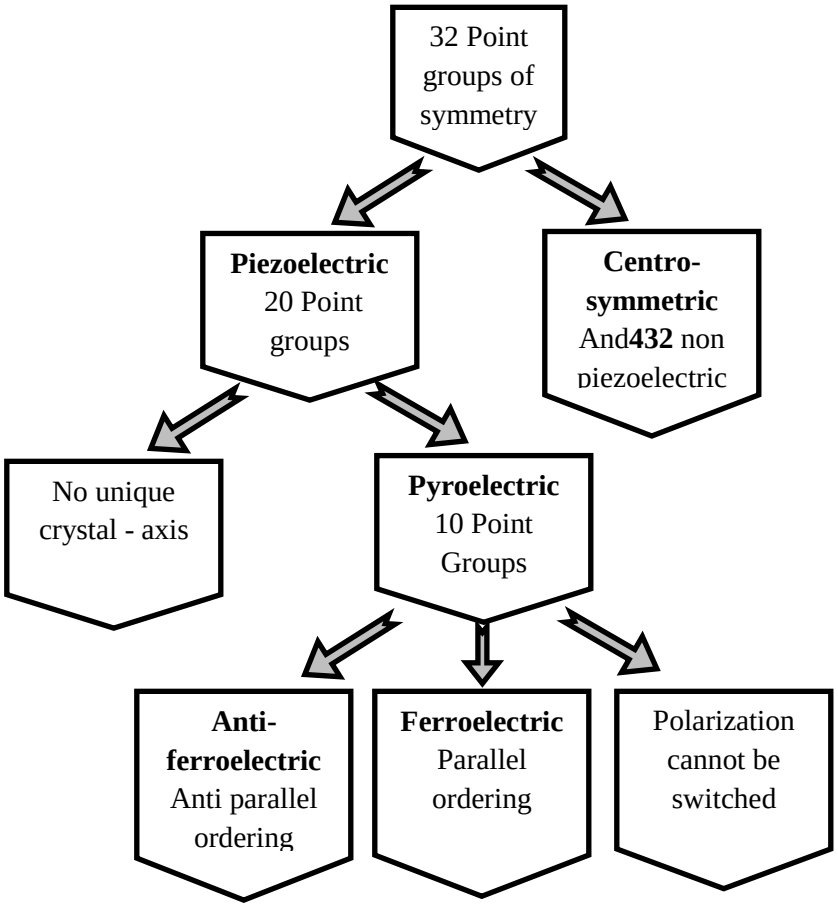

Figure 1.1: Crystallographic symmetry groups and polarized materials

Pyroelectric materials include a sub class of materials in which an applied external field can change the direction of polarization. These materials are referred to as ferroelectric. In ceramic form only ferroelectric materials show piezoelectricity.

1.2 Relative permittivity and dissipation factor

The relative permittivity (ε_r) is the ratio of the amount of charge that an element constructed from the ceramic material can store (absolute dielectric constant) to the charge that can be stored by the same electrodes when separated by a vacuum, at equal voltage (ε_o = 8.85 x 10^{-12} farad / meter).

ε_r may be measured at constant zero stress and is then called the "free" dielectric constant denoted by superscript T. Alternatively, it may be measured at constant strain, the so called (clamped) dielectric constant denoted by superscript S [3]. The free and clamped permittivity may differ greatly for piezoelectric materials and expressed as:-

$$\varepsilon^S = \varepsilon^T(1 - k^2) \qquad (1.1)$$

Where, k is the electromechanical coupling coefficient (to be discussed later).

With alternating voltages, the charge stored on a dielectric has both real (ε') and imaginary (ε'') components formed due to dielectric absorption. This loss is measured by ratio of phase component to in phase component. Dielectric loss is also called loss tangent denoted as tanδ which is written as

$$tan\delta = \frac{\varepsilon''}{\varepsilon'} \qquad (1.2)$$

Relative permittivity also depends on some extrinsic factors such as porosity of the sample, presence of secondary phases, defects, grain size and level of inhomogeneity.

1.3 Piezoelectric coefficients

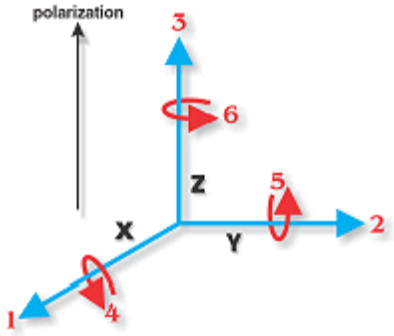

Figure 1.2: Directions of forces affecting a piezoelectric element

Figure 1.2 shows the direction of positive polarization coinciding with the Z-axis of a rectangular system of X, Y and Z axes. Direction X, Y, or Z is represented by numbers 1, 2, and 3 respectively and shear about one of these axes is represented by 4, 5, and 6 respectively [4].

1.3.1 Piezoelectric charge constant (d)

The polarization or strain induced in a piezoelectric material by a applied stress or an applied electric field is proportional to the input field (i.e. applied stress or applied electric field), where d is the proportionality constant. The piezoelectric charge constant (d) is the polarization generated per unit of mechanical stress (σ) applied to a piezoelectric material or the mechanical strain (*x*) experienced by a piezoelectric material per unit of electric field applied. Piezoelectric constant is an important indicator of materials for strain dependent (actuator) applications.

For direct piezoelectric effect,

$$P_i = d_{ijk}\sigma_{jk} \qquad (1.3)$$

Where P is the polarization, d_{ijk} is a 3rd rank tensor called as piezoelectric charge coefficient, σ is an applied stress (2nd rank tensor) and the subscripts i, j, k run from 1 to 3 using the Einstein convention.

For converse piezoelectric, d_{33} is written by

$$x_{ij} = d_{ijk}E_k \qquad (1.4)$$

Where *x* is the strain developed and E is an applied electric field. The piezoelectric coefficient, d, is numerically identical for both direct and converse piezoelectric effects for free boundary conditions [4].

It should be noted that the notation for the 3rd rank tensor d_{ijk} is often shortened to d_{ij}, where j = 1, 2, 3, 4, 5, 6 corresponds to jk = 11, 22, 33, 23 or 32, 13 or 31, 12 or 21, respectively (Example $d_{333=}$ $d_{33,}$ $d_{311=}$ d_{31}) [5].

The convention is to define the poling direction as the 3-axis, as illustrated in Figure 1.2.The shear planes are indicated by the subscripts 4,5 and 6 and are perpendicular to directions 1,2 and 3 respectively. For example, d_{31} is the coefficient relating the field along the polar axis to

the strain perpendicular to it, whilst d_{33} is the corresponding coefficient for both strain and field along the polar axis.

1.3.2 Electromechanical coupling factor

The electromechanical coupling factor (k_p) is probably the best single measurement of the efficiency of the piezoelectric materials in conversion of one energy into another. When an electric field is applied, it measures the fraction of the electrical energy converted into mechanical energy, or vice versa when stress is applied.

$$k^2 = \frac{electrical\ energy\ converted\ to\ mechanical\ energy}{Input\ electrical\ energy} \qquad (1.5)$$

or

$$k^2 = \frac{mechanical\ energy\ converted\ to\ electrical\ energy}{Input\ mechanical\ energy} \qquad (1.6)$$

The electromechanical coupling factor k_{eff} can be found out by determining resonance and anti-resonance frequencies in the impedance vs frequency plot of a poled piezoelectric ceramics by this equation:-

$$K_{eff} = \sqrt{\frac{f_a^{\,2} - f_s^{\,2}}{f_a^{\,2}}} \qquad (1.7)$$

Where f_s resonant frequency and f_a is the antiresonant frequency

The graph below shows the impedance of a piezoelectric transducer as a function of frequency. The minimum value at f_s corresponds to the resonance while the maximum value at f_a corresponds to anti-resonance.

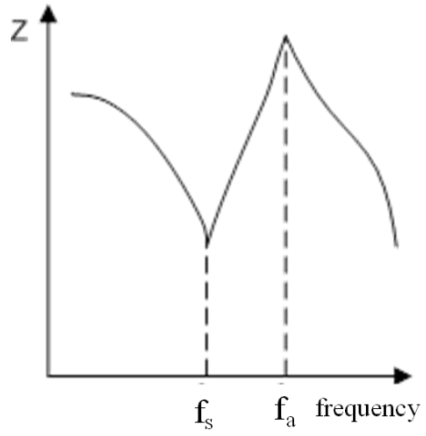

Figure 1.3: Impedance vs Frequency

1.3.3 Piezoelectric Voltage Constant

The piezoelectric voltage constant (g) is the electric field generated by a piezoelectric material in response to an applied physical stress. It is important for assessing a material's suitability for sensing (sensor) applications. The g constant is related to the d constant by the permittivity.

The constant d_{ij} and g_{ij} are related through the equation

$$g_{ij} = \frac{d_{ij}}{\varepsilon_0 \varepsilon_{ij}} \qquad (1.8)$$

Where ε_0 is the permittivity of the free space.

where g [mV/N] is the piezoelectric voltage constant, d is the piezoelectric charge constant, ε_r is the relative permittivity and ε_0 is the permittivity of free space (8.85×10-12 F/m).

The origin of the piezoelectric effect in ceramics is controlled by the intrinsic and extrinsic effect. Intrinsic effect arises due to the strain produced in crystal lattice. These intrinsic contributions are reversible and occur without loss [6]. In ferroelectric materials extrinsic effects are produced due to the motion of domain walls separating regions with different local polarization directions and phase boundary shifts [7]. This effect depends on frequency, time and applied field and irreversible in nature.

Piezoelectric coefficients such as piezoelectric charge constant, voltage constant and relative permittivity are temperature dependent.

1.3.4 Aging behavior

All ferroelectric materials suffer from aging phenomena. Aging is a process for a system to reach to an equilibrium state from a non-equilibrium state. More precisely aging can be defined as the spontaneous change of a material property with time under zero external stress and constant temperature. Like other characteristics of piezoelectric materials, aging depends on material type, processing and poling condition. Properties such as dielectric permittivity, dielectric loss, piezoelectric constants, and elastic compliance constants decrease with time and frequency constants increase with time.

Gotamare et al..[8] explained different mechanism for aging in ferroelectric ceramics: remnant polarization aging associated with the reversal of the poled domain structure to

random orientation; drift of charge carriers to the domain walls creating pinning centers and decreasing wall mobility; reorientation of the defect dipoles in bulk of the domains along the direction of local remnant polarization. The defect dipole reorientation model is predominant in the acceptor-doped ferroelectric materials which contain a significant concentration of oxygen vacancies and corresponding defect dipoles to provide a sufficient resistance to the domain wall motion. It has been reported that space charge formation and ionic drift mechanisms are significantly stronger than the dipole reorientation, mainly due to a much larger dimension of the space charge dipole (on the scale of the domain size) compared with the defect dipole dimension (on the order of the lattice parameter).

Aging can be characterized as thermally activated process as aging rate increases with increase in the temperature [9]. Degradation of piezoelectric properties due to loss of polarization is called thermally activated aging. In order to minimize the aging effect maximum applications of materials are restricted to $\frac{1}{2}T_C$ [10].

1.4 Curie temperature

Curie temperature in ferroelectrics is the temperature of phase transition between paraelectric phase and ferroelectric phase [11]. At this temperature, a piezoelectric ceramic will lose its polarized state. Therefore, piezoelectric devices should function much below the Curie temperature. Figure 1.5 shows the phase transition of $BaTiO_3$ crystal with temperature increasing though Curie point. Below the Curie point, the structure is tetragonal. The center of negative charge (O^{2-}ions) does not coincide with that of positive charge ($Ba^{2+}$and Ti^{4+} ions). Thereby, a dipole or spontaneous polarization is created in the crystal. When the temperature increases through the Curie point, the crystal undergoes a structural phase transition from ferroelectric phase to paraelectric phase. The crystal structure changes from tetragonal to cubic. The cations Ba^{2+} and Ti^{4+} displace relative to the anion O^{2-} and the centers of positive and negative charges coincide. Therefore, the dipole disappears and the material loses its piezoelectricity.

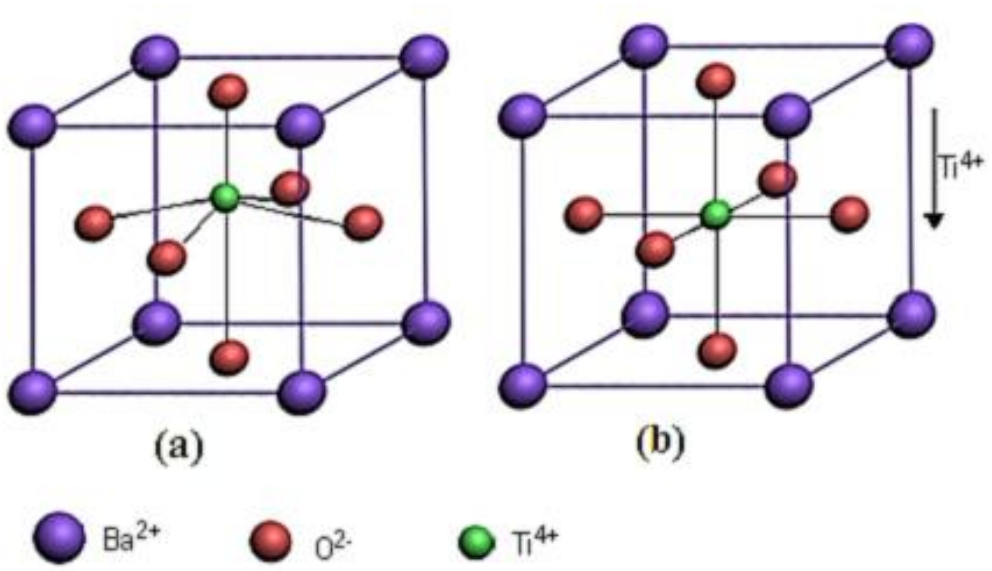

Figure 1.4: Crystal structure of $BaTiO_3$(a) Below the Curie point the structure is tetragonal; (b) Above the Curie point the structure is cubic

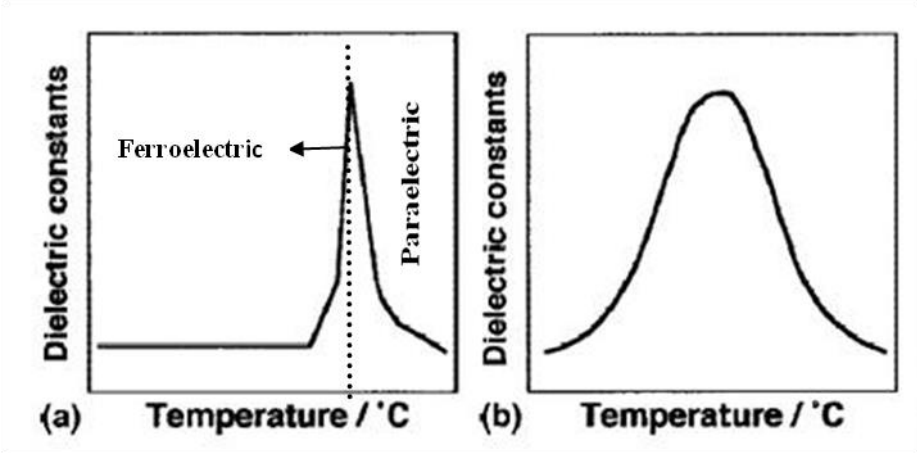

Figure 1.5: (a) Normal phase transition (b) Diffuse phase transition

Above, T_c, ferroelectric materials still show high dielectric constants, or relative permittivity, ε', and the relative permittivity follows the Curie-Weiss law:

$$\varepsilon' = \frac{C}{(T-\theta)} \qquad (1.9)$$

[12]Where C is the Curie constant and T is the Curie-Weiss temperature. The shape observed in Figure 1.5 (a) corresponds to a normal phase transition which is in agreement with Curie Weiss law. Figure 1.5 (b) describes about diffuse phase transition. These

materials show a frequency dependence and large broad peak. Relaxor materials show strong deviations from Curie Weiss law and show a weak remnant polarization.

1.5 Hysteresis behavior

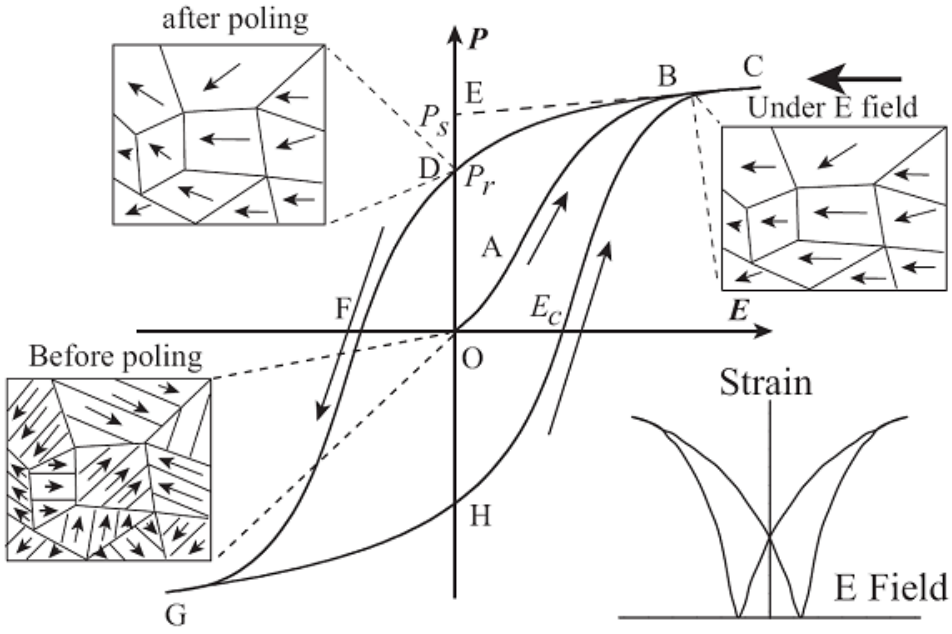

Figure 1.6: A typical hysteresis loop in ferroelectrics and corresponding domain reversal (polarization rotation) and strain–electric field curve [13]

Hysteresis loop, as a simple and effective tool, is the most generally accepted method to understand ferroelectric materials [14]. In principle, every ferroelectric material has its own unique hysteresis loop, as a fingerprint. Through the hysteresis loops, the ferroelectricity could be identified directly. Figure 1.6 is a typical ferroelectric hysteresis loop, through which the characteristic parameters, such as spontaneous polarization (Ps), remnant polarization (P_r) and coercive field (E_c) can be determined.

For ideal ferroelectric system, the observed hysteresis loops should be symmetric. The positive and negative Ec and Pr are equal. In reality, the shape of the ferroelectric hysteresis loops may be affected by many factors, such as thickness of the samples, material

composition, and thermal treatment, presence of the charged defects, mechanical stresses, and measurement conditions and so on.

1.6 Different Piezoelectric ceramics

1.6.1 Lead Zirconate Titanate (PZT)

During the last few decades or so, $PbTiO_3$–$PbZrO_3$(PZT)-based systems are the most widely used piezoelectric material [3].The steep increasing demand of PZT-based composition is a result of modern development such as passive to electrically active "smart" and "very smart" materials devices.

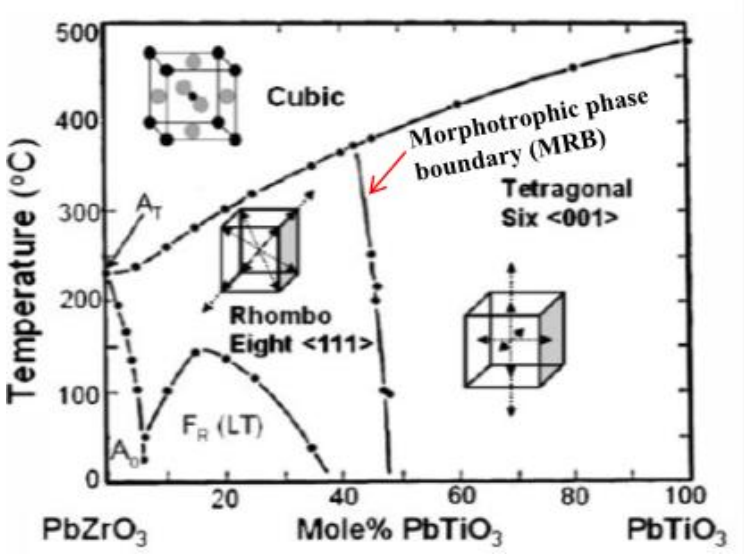

Figure 1.7: Phase diagram of $PbZrO_3$ -$PbTiO_3$

PZT has excellent piezoelectric properties in the vicinity of the morphotropic phase boundary (MPB) between rhombohedral and tetragonal phases [15].PZT based compositions has following advantages over other piezoelectric ceramics: (1) possess higher electromechanical coupling coefficients than other lead-free piezoelectrics, (2) have higher T_C values, which permit higher temperatures of operation, (3) can be easily poled, (4) possess a wide range of dielectric constant, (5) are relatively easy to sinter at lower temperatures than other leadfree piezoelectrics, (6) form solid-solution compositions with many different constituents, thus allowing a wide range of achievable properties. PZT ceramics are always used with a dopant or modifier to improve and optimize their basic properties for specific application[16].

PZT is now facing a global restriction because of its lead toxicity. Thus, there is worldwide focus on the development of lead free materials with electromechanical properties comparable with PZT [17].

1.6.2 Lead free piezoelectric ceramics

In past few decades various lead free systems extensively studied to find the alternative of PZT include $(Na_{0.5}K_{0.5})NbO_3$(NKN), $Bi_{0.5}Na_{0.5})TiO_3$(BNT), $BaTiO_3$ (BT) etc. [18-24].

1.6.2.1 Sodium Potassium Niobate (NKN) based materials

Sodium potassium niobate [(Na, K)NbO_3] is the solid solution of ferroelectric potassium niobate ($KNbO_3$ or KN) and antiferroelectric sodium niobate ($NaNbO_3$ or KN) [24]. Both have different orthorhombic structure at room temperature. KNN exhibits a MPB at around 50/50 composition separating two different orthorhombic phases and as for PZT, an increase in the properties for composition near this MPB is observed. NKN shows low piezoelectric properties (d_{33} ~ 80pC/N) due to difficulty in producing dense ceramics. Dense NKN ceramics are difficult to produce because of following two reasons:

1. According to phase diagram of $KNbO_3$-$NaNbO_3$[18], phase stability of NKN is limited to 1140^{o}C.So a high sintering temperature is not possible.
2. NKN system contains volatile elements like Na and K which result in poor densification.

Apart from above two reasons NKN systems are hygroscopic in nature which further degrade the properties and hinders its applications.

To improve the sinterability and properties of KNN ceramics, various solid solutions such as KNN–$BaTiO_3$, KNN–$LiNbO_3$, KNN–$SrTiO_3$, KNN–$LiTaO_3$, and KNN– Li(Nb,Ta,Sb)O_3, KNN–$LiSbO_3$, NKN-$CaTiO_3$, NKN-$BiFeO_3$,NKN-($Na_{.5}Bi_{.5}TiO_3$) etc. based composition at the MPB were used [16]. Saito et al.. [18] investigated MPB system between $(K_{0.5}Na_{0.5})NbO_3$, $LiTaO_3$ and $LiSbO_3$, and invented $(K_{0.44}Na_{0.52}Li_{0.04})(Nb_{0.84}Ta_{0.10}Sb_{0.06})O_3$[LF4] ceramics with an electric field-induced strain comparable with that of a typical actuator-grade PZT. The ceramic exhibited d_{33} of 300pC/N and the texturing of the material led to a peak $d_{33}$of 416 pC/N and Curie temperature was nearly 253°C.

1.6.2.2 Bismuth Sodium Titanate (BNT) based materials

Bismuth sodium titanate, $(Bi_{0.5}Na_{0.5})TiO_3$ (BNT) is another important lead free material which has a perovskite structure with strong ferroelectric properties (large remnant polarization (P_r~38 C/cm^2) and high Curie temperature (T_c ~ 320^{o}C). However, BNT-based ceramics undergo another phase transition below Tc that is known as depolarization temperature (T_d), which often occurs below 200°C.The piezoelectric properties of BNT ceramics are reduced below T_d due to depolarization. This depolarization in BNT ceramics is an important aspect from the application point of view. Fabrication of dense BNT ceramics is difficult as it requires higher sintering temperature above 1200^{o}C which results in loss of Bi from BNT based materials. High leakage currents and high coercive field (Ec=73kV/cm) negatively impact the poling process and polarization saturation is difficult to achieve in conventionally fabricated $(Bi_{0.5}Na_{0.5})TiO_3$ samples.

Moreover, to improve the piezoelectric properties of BNT, formation of solid solutions with other perovskite [$BaTiO_3$, $(Bi_{1/2}K_{1/2})TiO_3$, $NaNbO_3$,$BiFeO_3$,etc] to form an MPB was also studied. [25, 26].

1.6.2.3 Barium Titanate (BT) ceramics

BT ceramics also exhibit perovskite type structure. Perovskite oxides are a large family of ferroelectric oxides which include ABO_3 compounds. In ABO_3, 'A' and 'B' are cation elements or mixture of two or more cation elements. In the ideal perovskite crystal structure, if 'A' atom is taken at the corner of the cube, then 'B' atom resides in the body centre and a oxygen atom at each face centre of the cube.

For pure $BaTiO_3$, the permittivity passes through a maximum at 130^{o}C where the long-range domain structure characteristic of the tetragonal phase vanishes and it results in high permittivity. This transition temperature is called Curie temperature (T_C). Above Curie point (approximately 130^{o}C) the unit cell is cubic. Below the Curie point, the structure is slightly distorted to the tetragonal form with a dipole moment along c direction. Other transformations occur at temperatures close to 0^{o}C and -90^{o}C: below 5^{o}C the unit cell is orthorhombic with the polar axis parallel to a face diagonal and below -90^{o}C it is rhombohedral with the polar axis along a body diagonal. The various phases of $BaTiO_3$ are shown in figure 1.9 [27].

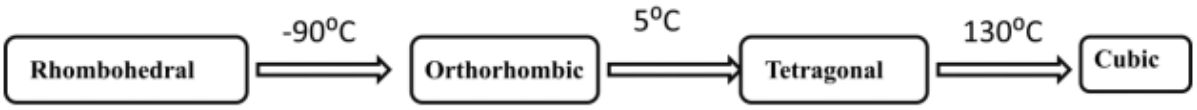

Figure 1.8: Various phases of $BaTiO_3$

$BaTiO_3$ shows phase transitions at -90°C (orthorhombicto rhombohedral), 5°C (tetragonal to orthorhombic), 130°C (cubic to tetragonal).These phase transitions result in higher relative permittivity near the phase transition temperatures in ε_r~T curve.

Though $BaTiO_3$ is the first piezoelectric transducer ceramic ever developed, its use in recent years has shifted away from transducers to an almost exclusive use as high-dielectric constant capacitors of the discrete and multilayer (MLC) types. The reasons for this are primarily twofold: (1) its relatively low Tc of 130°C, which limits its use as high-power transducers, and (2) its low electromechanical coupling factor in comparison to PZT (0.52 vs 0.48), which limits its operational output [15,16].

1.7 Modified $BaTiO_3$ for piezoelectric application

Incidentally, $BaTiO_3$ is not used in its true chemical form, but, rather, dopants or additives are used to modify and improve its basic properties. The electrical properties of $Ba(Zr_xTi_{1-x})O_3$ solid solutions have been studied extensively; however most of the work focuses on the nature of phase transition, the temperature dependence of the dielectric constant or the ferroelectric relaxor behavior of the systems with composition x usually higher than 0.15 [27]. Recently, the compositions $x<0.15$ found immense importance for possible application as lead-free piezoelectric [28, 29].

Recently, it is reported that $Ba(Ca_xTi_{1-x})O_3$ ceramics shows a large piezoelectric/electrostrictive strain [30,31]. Recently, high piezoelectric constants d_{33} = 200~600 pC/N, superior to PZT has been obtained in the Zr and Ca co-modified $BaTiO_3$ ceramics [32, 33]. The presence of morphotropic phase boundary is reported for these compositions.

1.8 Different techniques for improvement of mechanical properties of ceramics

Mechanical properties describe the way that a material responds to forces, loads, and impacts. They include strength of materials such as tensile strength, compressive strength,

shear strength, fracture toughness and hardness. Mechanical behavior is dependent on many factors such as temperature, composition and microstructure.

The ability to deform reversibly is measured by the elastic modulus. Materials with strong bonding require large forces to increase space between particles and have higher modulus of elasticity. Ceramics are generally inelastic and do not bend like metals. The compressive strength of a ceramic is usually much greater than their tensile strength. The fracture toughness is the ability to resist fracture when a crack is present. Ceramics generally have low fracture toughness.

The earliest studies of ceramics revealed the trend of decreasing strength with increased grain size or increased levels of porosity resulting in a maximum in strength as a function of sintering temperature [34].The grain size dependence of failure strength was based on the Griffith equation grain size d with flaw size c:

$$\sigma_f = \frac{YK_{Ic}}{d^{1/2}} \qquad (1.10)$$

Where σ_f is the tensile strength, Y is a constant determined by flaw size and specimen geometry and K_{Ic} is the critical stress intensity factor or toughness of the material.

Knudsen [35] generalized this to σ proportional to d^{-c} and was the first to attempt to combine it with a porosity dependence on strength

$$\sigma = \sigma_0 d^{-c} e^{-bV} \qquad (1.11)$$

Where σ_0 is the strength for a fully dense ceramic.

Carniglia [36] applied the Hall-petch equation to ceramics

$$\sigma = \sigma_c + Bd^{-\frac{1}{2}} \qquad (1.12)$$

Where σ_c is the stress required for activation of single crystal slip or twinning and B is a constant.

Hardness is usually defined as resistance to penetration and is a measure of the yield stress of ceramic. The unit of hardness is stress, usually given in GPa. It is generally measured by techniques which indent the surface. Typically hardness is determined from the size of impression left by applying a load to Vickers diamond square-based (pyramidal indenter in contact with sample. The ceramic response to the indenter and hence the characteristic hardness is a combination of plastic flow and cracking. It is affected by the intrinsic deformability of the ceramic (i.e the ease of slip and dislocation generation or twinning) and micro structural features such as multi-phase, grain size and orientation, porosity and grain boundary constitution [34]. Hardness decrease with porosity following the exponential law which also fits E, K_{Ic} , tensile and compressive strength

$$H = H_0\, e^{-bV} \qquad (1.13)$$

Where H is the hardness level at a given volume fraction porosity V, H_0 the hardness of a fully dense ceramic and b is a constant.

Hardness increases with decreasing grain size in ceramics although the mechanism by which the grain boundaries resist the indenter penetration is not clear.

In order to improve mechanical properties of ceramics great efforts have been made through detail micro structural design. The main objective is to increase strength and toughness. This can be achieved by the following mechanisms.

Crack deflection

It is well known that the fracture toughness of a polycrystalline material is appreciably high than a single crystal of same composition. Crack deflection can take place when there are local areas in a ceramic that have lower crack resistance to crack propagation than an average plane cutting through at right angles to the tensile stress. In a polycrystalline material as a crack is deflected along a weak grain boundary, the average stress intensity at its tip (K_{tip}) is reduced because the stress is no longer normal to the crack plane. [37]

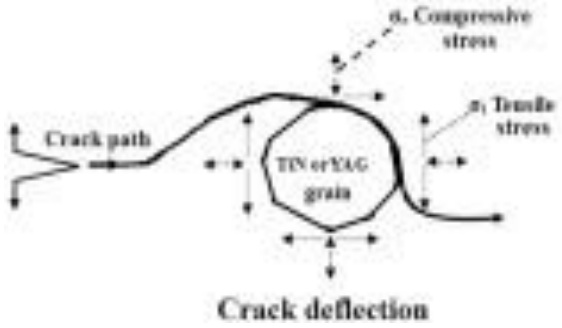

Figure 1.9: Crack deflection mechanism [37]

Crack impeding second phase

The crack propagating in a matrix containing the second dispersed phase forms loop between the particles increasing the crack propagation stress. As the ratio of the obstacles spacing (R_b) to obstacle diameter (R_d) decreases, the stress required for crack to propagate increases. However for higher values of the ratio (R_b/R_d), no further increase in strength and toughness values are observed. Thus, toughening can also occur by the inclusions of crack impeding second phase.

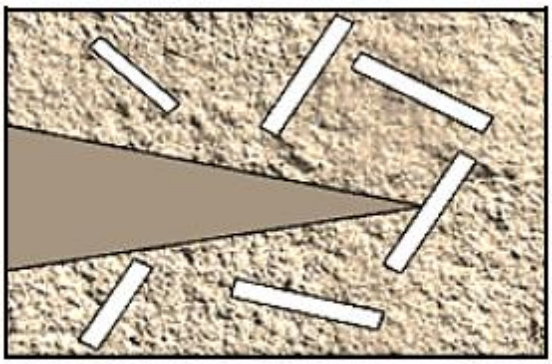

Figure 1.10: Crack Impeding Second Phase

Crack pinning

The propagation of a crack may be pinned by the nano-particles near the crack tip. Crack pinning leads to pull-out of a nano-particle. When a crack is pinned by a nano-particle as shown in figure 1.12, the crack cannot penetrate directly through the particle and an interfacial arc crack appears at $\theta = \pm \pi/4$[38].

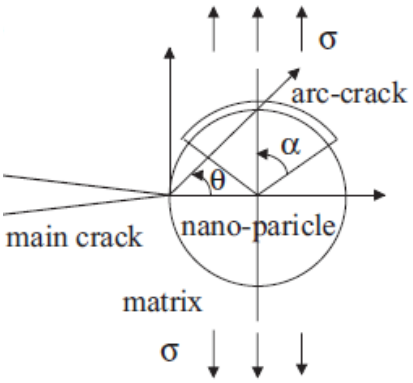

Figure 1.11: Crack Pinning Model [38]

Toughening by switching from intergranular to transgranular

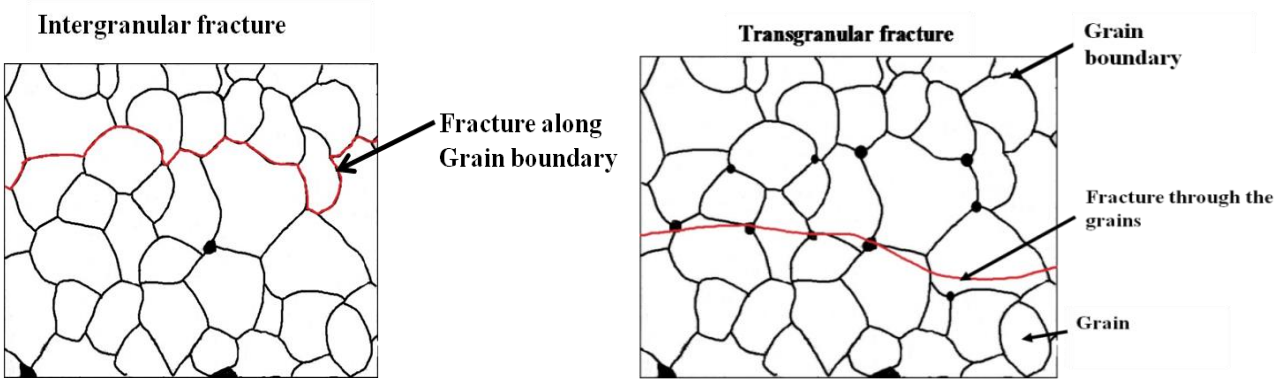

Figure 1.12: Switching from intergranular to transgranular fracture

In general, the fracture pattern in conventional ceramics is mostly intergranular. A. K. Soh et al.. [39] observed that with the increase of the volume fraction of nanoparticles transgranular fracture increases. The presence of nanoparticles along the grain boundary enhances the fracture resistance thereby producing tougher nano-composites. Nihara and Zhao et al.. [40, 41] suggested that the presence of nanoparticles along the grain boundary changes the

fracture pattern from inergranular to transgranular which is responsible for toughening. Pezzotti et al.. [42, 43] pointed out that the bridging of nanoparticles near the crack tip is the main toughening mechanism in nanocomposite. Tan and Yang [44] did some theoretical investigations on the following toughening mechanisms:

(a) switching from intergranular to transgranular fracture;

(b) fracture surface roughening by zigzag crack path; and

(c) shielding by clinched rough surfaces near the crack tip

Crack bridging

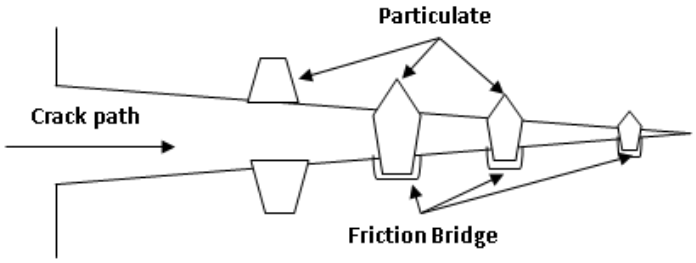

Figure 1.13: Crack Bridging Model

This type of mechanism occurs in fibre/particulate reinforced composites in which crack bridging occurs due to fibre-crack interactions. The average crack tip intensity is reduced due to the presence of particulates on the crack path. The particulates acts as two ends of the crack bridge and thus toughens the material [45, 46].

Transformation Toughening

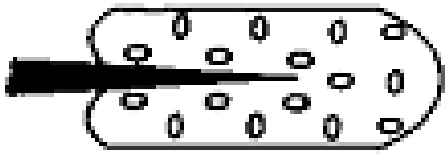

Figure 1.14: Crack shielding in transformation toughening [37]

The transformation toughening is also known as crack shielding mechanism which is related to the process of zone development. It has been observed that maximum toughness occurs when the transformation zone fully extends over the crack surface.

Thus, the presence of a second phase constituent which undergoes a stress induced martensitic transformation has been observed to toughen structural ceramics. For e.g in case of zirconia toughened Alumina (ZTA) ceramics the transformation from tetragonal to monoclinic (t → m-ZrO_2) results in the lowering of crack tip stress intensity. This helps in increment of toughness.

It is to be mentioned that the electrical and mechanical properties, both are important for ferroelectric and piezoelectric applications. For example, multilayer actuators (MLA) at the time of operation generate stress around 50MPa [16], during end termination process of Multilayer capacitor or actuator also generates stress of 30-50MPa.

As stated above, the breakthrough made by Liu and Ren et al.. in $BaTiO_3$-based ceramics with co-dopants of Zr, and Ca,[$Ba(Zr_{0.2}Ti_{0.8})O_3$-$0.5(Ba_{0.7}Ca_{0.3})TiO_3$ (BZT- 0.5BCT)]has offered a significant impact on the development of lead-free piezoceramics [32]. The piezoelectric coefficient (d_{33})wasreported more than 500 pCN^{-1}, comparable to that of soft PZT ceramics. However, there are very few reports available on the study of mechanical properties of BZT-0.5BCT and no reports on its improvement with different techniques.

Present thesis attempts to study the densification, microstructure, electrical and mechanical properties of BZT–BCT with different nano-oxide additives [Al_2O_3, MgO, ZrO_2(3Y)].

In next chapter, a through literature review focused on synthesis of BZT-BCT by the different method, its sintering, structural, dielectric and piezoelectric properties of BZT-BCT, and improvement of mechanical properties of $BaTiO_3$ and PZT was presented.

References

[1] A.Von Hippel, R.G.Breckenridge, F.G.Chesley and L.Tisza , Ind. Eng. Chem. **38** 107 (1946)

[2] H.L.Tuller and Y. Avrahami, Electroceramics. In “Encyclopedia of Smart materials”; edited by Schwartz, M.M (John Wiley and sons, New York, (2002)

[3] B. Jaffe, W. R. Cook Jr. and H. Jaffe, Piezoelectric Ceramics, Academic Press, New York (1971)

[4] A.J. Moulson, J.M. Herbert, Electroceramics—Materials, Properties, Applications Chapman & Hall, London, (1990)

[5] R. E. Newnham, Properties of materials Anisotropy, Symmetry, Structure, Oxford University Press Inc. New York (2005)

[6] D. Damjanovic, M. Demartin, J. Phys. Condens. Mat. **9** 4943 (1997)

[7] G. Arlt, H. Dederichs, R. Herbiet, Ferroelectrics **74** 37 (1987)

[8] Sunil W. Gotmare, Serhiy O. Leontsev, and Richard E. Eitel, J. Am. Ceram. Soc. **93** {7} 1965 (2010)

[9] A. Barzegar, R. Bagheri, and A. K. Taheri, "Aging of piezoelectric composite transducers," J Appl Phys. 89 (2001)

[10] W. A. Schulze, "Review of literature on aging of dielectrics," Ferroelectrics **87** (1988)

[11] A.Von Hippel, R.G.Breckenridge, F.G.Chesley and L.Tisza , Ind. Eng. Chem. **38** 107 (1946)

[12] https://explorermaterials.files.wordpress.com/2014/09/equationcurie‑weiss.jpg

[13] L. Jin, F. Li, S.Zhang, J. Am. Ceram. Soc. **97** 1 (2014)

[14] D. Damjanovic, Rep. Prog. Phys. **61** 1267 (1998)

[15] A.J. Moulson, J.M. Herbert, Electroceramics—Materials, Properties, Applications Chapman & Hall, London, (1990)

[16] G. H. Haertling Ferroelectric Ceramics: History and Technology J. Am. Ceram. Soc. **82** {4} 797 (1999)

[17] Wei Li, Zhijun Xu,w Ruiqing Chu, Peng Fu, and Guozhong Zang, J. Am. Ceram. Soc. **93** {10} 2942 (2010)

[18] Y. Saito, H. Takao, T. Tani, T. Nonoyama, K. Takatori, T. Homma, T.Nagaya, and M. Nakamura, Nature **432** 84 (2004)

[19] M. E. Rogers, C. M. Fancher, and J. E. Blendell, J. Appl. Phys. **112** 052014 (2012)

[20] D. Y. Wang, N. Y. Chan, S. Li, S. H. Choy, H. Y. Tian, and H. L. W.Chan, Appl. Phys. Lett. **97** 212901 (2010)

[21] K.-I. Park, S. Xu, Y. Liu, G.-T.Hwang, S.-J. L. Kang, Z. L. Wang, and K.J. Lee,Nano Lett.**10** 4939 (2010)

[22] Y. C. Yang, C. Song, X. H. Wang, F. Zeng, and F. Pan,Appl. Phys. Lett.**92** 012907 (2008)

[23] D. M. Lin, D. Q. Xiao, J. G. Zhu, and P. Yu,Appl. Phys. Lett. **88** 062901(2006)

[24] L. Egerton, D. M. Dillon, J. Am. Ceram. Soc. **42** 438 (1959)

[25] T. Takenaka, K. Maruyama, K. Sakata, Jpn. J. Appl. Phys. **30** 2236 (1991)

[26] V.A. Shuvaeva, D. Zekria, A.M. Glazer, Jiang Q, S.M. Weber, P. Bhattacharya, P.A. Thomas, Phys. Rev. B. **71** 174114 (2005)

[27] T. Maiti, R. Guo, A. S. Bhalla, J. Am. Ceram. Soc. **91** 1769 (2008)

[28] Z. Yu, C. Ang, R. Guo, A.S. Bhalla, J. Appl. Phys. **92** 1489 (2002)

[29] L. Dong, D.S. Stone, R.S. Lakes, J. Appl. Phys. **111** 084107 (2012)

[30] L.L. Zhang, X.S. Wang, H. Liu, X. Yao, J. Am. Ceram. Soc. **93** 1049 (2010)

[31] X. Wang, C.N. Xu, H. Yamada, K. Nishikubo, X.G. Zheng, Adv. Mater. **17** 1254 (2005)

[32] W. Liu, X. Ren, Phys. Rev. Lett. **103** 257602 (2009)

[33] I. Coondoo, N. Panwar, H. Amor, M. Alguero, A.L. Kholkin, J. Appl. Phys., **113**, 214107, (2013)

[34] Ceramic Microstructures, W. Lee, Kluwer Academic Publishers 89-96,(1994)

[35] F.P. Knudsen, J. Am. Ceram. Soc. **42**{8} 376 (1959)

[36] S. C. Carniglia, J. Am. Ceram. Soc. **48** {11} 580 (1965)

[37] Ritchie, R. O., Mat. Sci. Engg., **A103** 15(1988)

[38] M. Toya, J. Mech. Phys. Solids **22** P325 (1972)

[39] A.K Soh, D-N. Fang, Z-Xu. Dong, J. Comp. Mater. **38** 227 (2004)

[40] K. Niihara, J.Ceram. Soc. Jpn. **99** {10} 962 (1991)

[41] J. Zhao, , L.C. Stearns, M. P. Harmer, H.M. Chan, and G.A. Miller, J. Am. Ceram. Soc., **76** {2} 225 (1993)

[42] Pezzotti, G., Nishida, T. and Sakai, M., J. Ceramic Soc. of Jpn.**103** 889 (1996)

[43] Pezzotti, G., Nishida, T. and Sakai, M.,J. Ceramic Soc. of Jpn. **104** 557 (1997)

[44] H.L. Tan, and W.Yang, Mechanics of Materials **30** 111 (1998)

[45] W- Y. Mai and B.R. Lawn, J. Am. Ceram. Soc. **70** 289 (1987)

[46] M.V. Swain, J. Mater. Sci.Lett. **5** 1313 (1986)

CHAPTER 2

LITERATURE REVIEW

2.1 Ca and Zr co-modified $BaTiO_3$ ceramics

$BaTiO_3$ (BT) based ceramics have received a great deal of attention from the scientific community in searching for environment friendly lead free piezoelectric materials. Chemical substitutions at the Ba^{2+} and Ti^{4+} sites are made to tailor the properties to meet a variety of device and performance requirements. $BaZr_xTi_{1-x}O_3$ (BZT,$x \leq 0.1$) has become a good piezoelectric material due to its larger piezoelectric coefficients, electromechanical coupling coefficients and more stable structure [1]. Similarly, Ca doping in BT ceramics increases the phase transition temperature of BCT ceramics.

Ca,Zr co-doped i.e.$(Ba,Ca)(Ti,Zr)O_3$ ceramics are used for capacitor application to generate permittivity values as high as ~18000 for Y5V serials [2,3]. Few work has been performed on the dielectric properties and tunabilities of $(Ba_{1-x}Ca_x)(Zr_yTi_{1-y})O_3$ ceramics and only a few works have focused on the studies of piezoelectric properties of $(Ba_{1-x}Ca_x)(Zr_yTi_{1-y})O_3$ materials [4].

Recently, Liu and Ren [5] have reported that Pb-free $Ba(Zr_{0.2}Ti_{0.8})O_3$-$(Ba_{0.7}Ca_{0.3})TiO_3$ (BZT-BCT) solid solution exhibits an MPB between rhombohedral and tetragonal phase. The high piezoelectric coefficient d_{33} ~300-600pC/N was reported in ceramic samples which is comparable to high-end PZT ceramics. This finding led to a surge of worldwide investigation on BT- based ceramics possessing a good potential for replacement of lead containing PZT material.

The phase diagram of pseudo-binary $Ba(Zr_{0.2}Ti_{0.8})O_3$-$x(Ba_{0.7}Ca_{0.3})TiO_3$ ceramics is shown in Fig 2.1. There are three typical compositions in BZT–xBCT solid solutions which are x=0.14, 0.32, and 0.50 respectively corresponding to the cubic phase at room temperature, cubic–rhombohedral–tetragonal (C–R–T) triple point near 57 °C and tetragonal phase at room temperature, with a very high piezoelectric coefficient [6]. The piezoelectricity is enhanced at MPB composition due to low polarization anisotropy. This low polarization anisotropy leads to a low energy barrier between two ferroelectric phases and facilitates the rotation between the coexisting rhombohedral (P_S [111]) and tetragonal (P_S [100]) phases. The enhanced piezoelectric performance has been attributed to the vanishing polarization anisotropy and the polarization rotation in the presence of a tricritical point. On the other hand, polymorphic phase transition (PPT) plays an important role to improve the dielectric and piezoelectric properties. However, the crystal structure for MPB composition of BZT-

xBCT piezoceramic is still under debate. Previous crystallographic studies suggest that the two binary phases in the phase diagram, tetragonal and rhombohedral phases, coexist in the high-property MPB composition. On the contrary, an intermediate orthorhombic phase (Amm2) has been reported within a narrow composition/temperature regime in the BZT-xBCT system and the phase diagram has been modified as shown in Fig 2.2. The authors used high-resolution synchrotron x-ray diffraction techniques to prove the presence of intermediate orthorhombic phase [7].

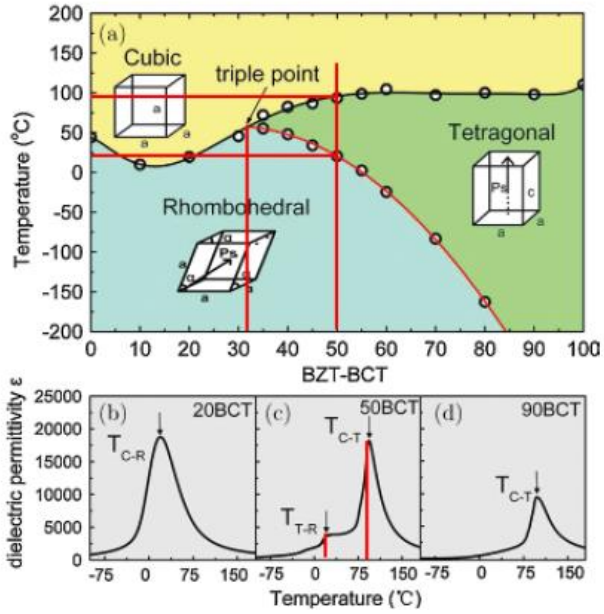

Figure 2.1 (a) The phase diagram of pseudo-binary ferroelectric $Ba(Zr_{0.2}Ti_{0.8})O_3$-$(Ba_{0.7}Ca_{0.3})TiO_3$ [BZT-xBCT] ceramics(b)-(d) Dielectric permittivity curves for 20BCT, 50BCT and 90BCT, respectively.

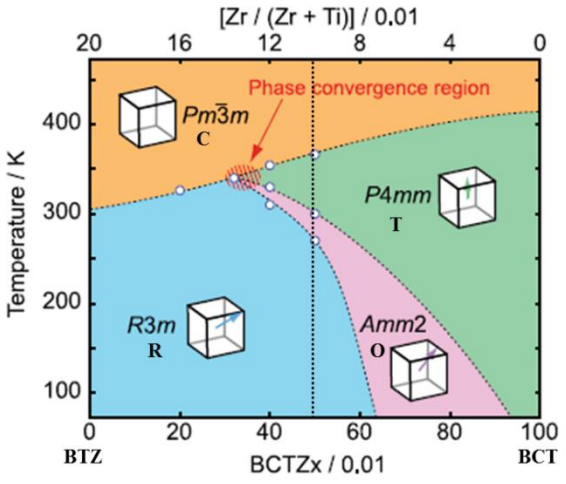

Figure 2.2 Modified phase diagram of pseudo-binary ferroelectric $Ba(Zr_{0.2}Ti_{0.8})O_3$-$(Ba_{0.7}Ca_{0.3})TiO_3$ ceramic.

Li et al.. [8] had reported a low d_{33} of 328pC/ N and high dielectric constant of 4800 in $(Ba_{0.84}Ca_{0.16})(Ti_{0.9}Zr_{0.1})O_3$ ceramics (near around MPB) with a coexistence of rhombohedral and orthorhombic phases. They also reported a d_{33} of 365 pC/N in $(Ba_{0.92}Ca_{0.08})(Ti_{0.95}Zr_{0.05})O_3$ ceramics with an MPB between orthorhombic and tetragonal phases at optimal sintering temperature. They also further reported a d_{33} of 387pC/N in $(Ba_{0.99}Ca_{0.01})(Ti_{0.98}Zr_{0.02})O_3$ ceramics with relatively high Curie temperature Tc =115°C. They also varied Ca and Zr simultaneously in $(Ba_{1-x}Ca_x)(Ti_{1-y}Zr_y)O_3$and found piezoelectric coefficient in between 325-387pC/N using optimal sintering temperature [9,10,11].

Benabdallah et al.. [12] have found transverse piezoelectric coefficients, d_{31}, as high as 200 pC/N and 120 pC/N for BZT-0.5BCT and $0.68Ba(Zr_{0.2}Ti_{0.8})O_3$-$0.32(Ba_{0.7}Ca_{0.3})TiO_3$[BCTZ32], respectively at room temperature which is comparable to soft and hard PZT. They obtained density of 90% for pure BZT-0.5BCT ceramic (without TiO_2 excess) and density improved up to 96% for 1mol% TiO_2 addition in BZT-0.5BCT ceramic.

Wang et al.. [13] obtained high piezoelectric properties of d_{33} ~ 650 and dielectric constant of 4500 for BZT-0.5BCT ceramics using optimum calcination (1300°C) and sintering temperature (1540°C).The ceramic forms at MPB between rhombohedral and tetragonal phase at room temperature having phase transition temperature (Tc)=85°C. Su et al.. [14] investigated the poling dependence and stability of electrical properties of BZT-0.5BCT ceramics. The huge piezoelectric coefficient d_{33}~630pC/N and 56% of planar electromechanical coupling factor for BZT-0.5BCT ceramics was obtained by using the optimized poling condition (2.5Ec and 40°C for poling field and temperature, respectively).They also reported that these materials exhibit strong temperature and time dependence owing to a rather low depolarization temperature (below 80–90°C) and extremely high aging rate (30% and 25% loss for d_{33} and kp, respectively, 10^4 min after poling).

Hao et al.. [15] studied the correlation between microstructure and electrical properties of BZT-0.5BCT ceramic. They have used three different sintering methods such as spark plasma sintering, two step sintering and normal sintering of BZT-0.5BCT ceramic to obtain grain size in the range of 0.4 to 32μm. The optimum piezoelectric properties for ceramics with grain size more than 10 μm are d_{33}>472 pC/ N, K_p> 0.48 for BZT-0.5BCT.

Tian et al.. [16, 17] studied the phase transition behavior and electrical properties of BZT-0.5BCT ceramics. The maximum piezoelectric, electromechanical coupling coefficient and dielectric constant (d_{33}=572, K_p=0.57, ε_r=4821) were observed near MPB region.

2.2 Different methods for preparation of BCT-BZT (BCZT) powders

Yang et al.. [18] have prepared $(Ba_{0.88}Ca_{0.12})(Zr_{0.12}Ti_{0.88})O_3$ ceramics via sol-gel method using tetrabutyl orthotitanate and zirconium oxynitrate as the precursors. The phase pure powder was obtained at 800^{o}C for 2h and the crystallite size was ~37nm. These ceramics were sintered at 1280°C/2h. The Curie temperature, dielectric constant and piezoelectric coefficient d_{33} (calculated from the slope of the piezoelectric displacement curve) were 95°C, 2588 at room temperature and 215pm/V respectively.

Tan et al.. [19] also reported the synthesis of $(1-x)BaTi_{0.8}Zr_{0.2}O_3$-$xBa_{0.7}Ca_{0.3}TiO_3$ (x=0.2-0.4) powder by sol gel method at temperature of 900°C for 2 h .These pellets were sintered at 1250℃ for 3h with heating rate of 10°C/min. The piezoelectric coefficient (d_{33}) ~391pm/V and highest dielectric constant (~9000) at x=0.3 composition was observed which is near the C-R-T triple point in the phase diagram.

Puli et al.. [20] prepared high dielectric constant and low loss of $[(BaZr_{0.2}Ti_{0.8})O_3]1-x-[(Ba_{0.7}Ca_{0.3})TiO_3]$ (x = 0.10, 0.15, 0.20) (BZT–BCT)ceramics by sol-gel method. The phase pure powder was obtained at 800°C for 2 h. The pellets were sintered at 1280°C for 2h in carbolite furnace and the densities were in between 5.32 to 5.49 gm/cc with the average grains size of 0.5 µm to 2µm. The average grain size decreases with increase in calcium content. Dielectric constant and Curie temperature (Tc) values decreased with increase in Ca content. They found the piezoelectric coefficient d_{33} of the BZT–BCT ceramics are independent of Ca content and the values lie in between 174pC/N and 177pC/N. These materials have practical applications in the development of Y5V capacitors.

Praven et al.. [21] have synthesized BZT –0.5BCT by sol–gel method using barium acetate, zirconium oxychloride, calcium nitrate tetrahydrate and titanium isopropoxide as raw materials. As-synthesized powders were calcined at 1000°C and the particle size was found to be 35–50 nm. XRD patterns of the calcined powders contain a few unreacted peaks which were removed after sintering. They showed a complete formation of single-phase perovskite for BZT–0.5BCT ceramics and the density was found to be ~93 % of the theoretical density,

obtained at 1550°C. The grain size of BZT-0.5BCT ceramic was found to be 10–20μm. They observed the phase transition temperature at 72°C with highest value of dielectric constant 11,768. High piezoelectric coefficient of d_{33} ~ 490pC/N was obtained by this method. Praven et al.. also observed remnant polarization (P_r) of 11.55 μC/cm^2 and relative permittivity of 20,020 at the Curie temperature of 95°C, high d_{33} ~530pC/N large electromechanical coupling coefficient.

Wang et al.. [22] synthesized 0.5Ba $(Zr_{0.2}Ti_{0.8})O_3$-0.5$(Ba_{0.7}Ca_{0.3})TiO_3$ (BZT-0.5BCT) nanocrystallites via a citrate precursor method at a low temperature of 700°C [22]. They obtained phase pure perovskite with particle size in the range of 30nm to 60 nm by using appropriate calcination temperatures. But they have not studied sintering and electrical properties of the synthesized powders.

Montero et al.. [23] prepared $Ba_{0.9}Ca_{0.1}Ti_{0.9}Zr_{0.1}O_3$ powder by Pechini polymeric precursor method at 700°C for 1h. Dense ceramics were obtained from these reactive precursors using sintering temperatures below 1300°C. They found that ceramics sintered at 1275°C/5h exhibited the best ferro–piezoelectric properties d_{33} = 390 pC/N, d_{31} = ~143 pC/N, kp = 50% , dielectric constant 2253 and tanδ = 0.06 (100 kHz), at room temperature. T_C was found to be 112°C. Relative density of 97% with having average grain size 5μm was observed at 1250°C with high Tc = 115°C and d_{33}~240pC/N.

2.3 Different approaches for improvement of mechanical properties of PZT and its effects on electrical property

Lead zirconate titanate (PZT) and related materials are widely used as actuators, sensors etc because of their excellent piezoelectric properties. Many of the applications involve electrically or thermal induced stresses, mechanical loads induced due to vibration that may result in mechanical failure and subsequently breakdown of the devices. Moreover, PZT ceramics suffer from poor mechanical properties (fracture toughness, strength etc.). Various authors have reported the enhancement of mechanical properties of PZT ceramics by nano-particulate addition. Some of the literatures have been discussed below.

Puchmark et al.. [24] studied the effect of Al_2O_3 addition on hardness of PZT ceramics. Volume fraction of alumina was varied from 0 – 2 %. The maximum hardness (4.3 GPa) was obtained with 1 vol% Alumina addition and at higher alumina content (2 vol%) hardness value decreases due to lower sinterability and lower density of the samples.

Xiang et al.. [25] fabricated oxides (Y_2O_3, MoO_3,WO_3) doped PZT ceramics by conventional sintering method. They studied the effect of oxides on electrical and mechanical properties of PZT ceramics. Weight % of various oxides was varied from0.1-1. It was observed that above optimal concentration of oxide content (0.1wt %), fracture strength and toughness decreases due to decrease in density. The electrical properties deteriorated with concentration of dopants >0.1 wt%.

Jiansirisomboon et al.. [26] studied the effect of NiO on mechanical, electrical and microstructural properties of PZT ceramics. They evaluated fracture toughness and young's modulus for different amount (0 – 1 wt%) of nano NiO addition on PZT. With increase in NiO addition, relative density increased from 88% to 97%.The densification improvement observed in this study was believed to be caused by a creation of oxygen vacancies due to substitution of Ni^{2+}ion into $Zr^{4+}$and Ti^{4+}ions in the system which could help improve densification rate. Addition of NiO was found to inhibit grain growth and enhance hardness of PZT ceramics. Although fracture toughness slightly degraded by NiO addition in PZT. It was suggested that optimal composition of PZT/NiO system would be <0.1 wt% NiO.

Zhang et al.. [27] incorporated Ag into PZT piezoelectric ceramics. He found that fracture strength increased from 69 MPa to 130 MPa when concentration of Ag was increased from 0 to 15 vol%. The enhancement of fracture strength in PZT/Ag composite was due to good PZT/Ag interface bonding, higher strength of Ag phase and the particle-dispersion-strengthening effect. Fracture toughness also increased about 2.5 times in PZT/Ag composite compared to PZT monolith. Increment in fracture toughness values was due to crack deflection technique.

Tajima et al.. [28] studied the effect of Al_2O_3, MgO and ZrO_2on the mechanical and electrical properties of PZT ceramics. All oxides were varied from 0.1 – 1 vol% in PZT/oxide nano-composite. The average grain size of nanocomposite reduced with oxide addition which was the reason for enhanced mechanical properties. Kp of the Al_2O_3added composite was less than that of the MgO-added composites.

In the past few years, the novel design idea has been applied in the field of functional ceramics. In $BaTiO_3$/SiC [29] and PZT/Ag systems, the second phases have obviously improved the fracture strength and fracture toughness of ceramic matrix. However the

problem of property trade-off, i.e. a deterioration of electrical properties, in particular, electromechanical coupling factor, still remains unsolved [25].

Mechanical properties of some PZT ceramics [30] could be improved by addition of 1 vol% WO_3. However further increase in the content of WO_3 affected the dielectric properties of PZT ceramics.

Zeng et al.. [31] fabricated SiC reinforced PZT ceramics by diffusing SiC at different times. Fracture strength and Young's modulus increased with diffusion of SiC. The increment could be attributed to the diffusion of SiC into the microscopic pores, cracks and grain boundary of PZT ceramics.

Wang et al.. [32] observed microstructure, electrical and mechanical properties of MgO nanoparticles reinforced porous PZT95/5 ferroelectric ceramics. PZT/MgO ceramics possess enhanced mechanical properties as compared to porous PZT ceramics (fracture toughness and hardness is improved 31.3% and 19.8% respectively). Addition of MgO reduces grain size. According to the Hall–Petch relationship, the smaller grain size can exhibit better hardness and fracture toughness because fine grains cause higher density of grain boundaries to retard crack propagation.

2.4 Different approaches for improvement of mechanical properties of $BaTiO_3$ and its effects on electrical properties

Jiansirisomboon et al.. [33] studied effect of alumina nano particulates addition on electrical and mechanical properties of barium titanate ceramics. He has investigated mechanical properties such as Knoop hardness and Young's modulus of $BaTiO_3$and was found to be improved with only 0.5 vol% of Al_2O_3addition. The hardening of the nano-composites may be partly associated with the grain size reduction due to the Al_2O_3 addition as well as the dissolution of Al_2O_3 in $BaTiO_3$ at grain boundaries. The sample having a smaller grain size contained more grain boundaries which provided more obstacles to dislocation pile-up in the adjacent grains, leading to harder materials. An increase in 'E' with increasing content of additive was also probably due to the high modulus of Al-rich phase.

Ali et al.. [34] investigated enhancement of piezoelectric and ferroelectric properties of $BaTiO_3$ ceramics by aluminum doping. He found that 1 mol% alumina doped barium titanate

samples exhibit enhanced dielectric constant, piezoelectric constant (d_{33}) and remnant polarization whereas dielectric loss factor and leakage current and coercive field (E_c) decreased than those of pure $BaTiO_3$and T_c slightly shifted to a lower temperature for the Al-doped sample.

Zhan et al.. [35] studied fracture toughness and toughening mechanism in BT/Al_2O_3 nanocomposites. It was observed that more than 1.6 times increase in fracture toughness over the pure nano-crystalline alumina had achieved in the 7.5vol.% BT/Al_2O_3 nanocomposite. The authors suggested that contribution to toughening may be due to stress induced domain switching of the ferroelectric phase.

Jiansirisomboon et al.. [36] studied microstructural and knoop hardness of $BaTiO_3$/xAl_2O_3nanocomposite ceramics (where x = 0, 3, 5, 10 and 15 mol%). Three factors were responsible for the hardness in $BaTiO_3$/xAl_2O_3*viz.*Al_2O_3content, grain size and porosity. It was observed that with increase in Al_2O_3 content Knoop hardness increases (3.63 GPa in pure BT to 5.42GPa in BT/15mol% Al_2O_3). The addition of Al_2O_3nanoparticulates could effectively reduce the grain size. Needle like grains found in BT matrix contained some amount of Al which resided at the grain boundary. One of the possible explanations for the increase in hardness values was that the addition of nanoparticles reinforces the grain boundary and acts as effective pins against crack propagation.

Ren et al.. [37] studied the effect of MgO content on tunable dielectric properties of BZT/MgO composite. 10 wt% - 40 wt% MgO was varied in the BZT/MgO composite. All samples reached a maximum of ~95% of the theoretical density (TD) after sintering at 1350^{o}C/4h. It was found that addition of MgO led to decrease in dielectric permittivity and Curie temperature to below 100^{o}C as trace amount of Mg^{2+} ions dissolved in BZT grains. However addition of MgO helped in the increase in tunability by about 30%.

Nagai et al.. [38] studied the effect of MgO doping on the phase transformation of $BaTiO_3$ (BT). MgO concentration was varied from 0.2 mol% to 5 mol% in BT. 96% of TD was achieved at the sintering temperature of 1350^{o}C/2h. There was a decrease in the value of T_c(ΔT_c = 42^{o}C) with increase in MgO content from 0.2 mol% to 2 mol%. Raman spectra revealed that orthorhombic phase is the stable phase at room temperature for 0.5mol% MgO

addition. However orthorhombic and rhombohedral phase seemed to exist at higher temperature in MgO doped BT.

Yoon et al.. [39] studied the effect of liquid phase (MgO in the acceptor site of BT) characteristics on the microstructure and dielectric properties of BT. 0.5mol% MgO and Nb in acceptor site and donor site of BT was done respectively. The compacts were sintered from 1270 -1400/2h. Sintered density of about ~95% and 92% of TD were obtained with doping at acceptor and donor site respectively. It was observed that grain growth is critically affected by the liquid phase that gets formed during heat treatment.

Vittayakorn et al.. [40] studied the effect of nano sized MgO particles on the phase formation, microstructural characterization and electrical properties of BT. 0 -1 vol % of MgO were added in BT and the BT/MgO nanocomposite was prepared by conventional mixed oxide approach. Green compacts were sintered between 1300-1450^{o}C for 2 hrs. The average grain size decreased from ~75µm in pure BT to 0.4 µm in BT/MgO composite. MgO addition leads to grain growth suppression and poor densification. The dielectric constant decreased from ~5776 in pure dense BT to ~1956 in 1vol% MgO content in BT/MgO nanocomposite.

Cai et al.. [41] studied the dielectric and microstructural properties of pure and MgO doped BT ceramics. Pure and MgO doped BT were prepared by following the conventional solid state synthesis. It is found that addition of MgO (<1.5 at%) in BT does not produce any secondary phase. However at higher MgO content (>1.5 at%) , small peaks of MgO are found which indicate that the solubility limit of MgO in BT lies in between 1-1.5 at%. Curie temperature falls from 120^{o}C to 95^{o}C when MgO content is increased from 0 – 2 at% in BT ceramics. Average grain size drastically reduced from ~ 60µm to ~5µm with increase in MgO from 0 – 2 at% in BT ceramics. This reduction in grain size may be due to the fact that MgO acts as grain growth inhibitor. Dielectric constant also decreases with increase in MgO content.

Namsar et al.. [42] observed the Structure–property relations of ferroelectric $BaTiO_3$ ceramics containing nano-sized Si_3N_4 particulates. He found that the addition of small amount of Si_3N_4 caused an apparent increase in both grain size and density due to liquid

phase sintering. In these samples, both low density and the presence of secondary phase seemed to play a role in this reduced ferroelectric behavior.

Fisher et al.. [43] studied the abnormal grain growth in BT ceramics by addition upto 1 mol% Al_2O_3. Addition of Al_2O_3content sharply increased the abnormal grain number density. Al_2O_3 is incorporated into the BT lattice by substitution for TiO_2.TiO_2 leaves the BT lattice and segregates at the grain boundaries. The presence of excess TiO_2 could be one of the reasons to promote abnormal grain growth. Abnormal grain growth could also be caused by inhomogeneity in the green compact microstructure such as agglomerate formation.

Recently, Kaushal et al.. [44] reported hardness values of 543 MPa for BZT–BCT ceramics prepared by traditional dry pressing technique and measured using nano indentation. They also found that hardness values can be improved when complex freeze drying technique was used for powder preparation. However, there is no report on improvement of mechanical properties using oxide additives.

Table 2.1 Table showing mechanical properties of Al_2O_3, MgO, PSZ and Barium titanate

2.5 Mechanical properties of Al_2O_3, MgO, PSZ, Barium titanate, and BZT-BCT

Oxide additives	Density at RT ($g/cm^{3)}$	Hardness (GPa)	Fracture toughness at RT ($MPam^{1/2}$)	Young's modulus (GPa)	MOR (MPa)	Ref.
Al_2O_3	3.98	19.3	3.8-4.5	400-410	550-600	[45]
MgO	3.58	5-7	2.7-2.8	270-330	100-200	[45]
PSZ	5.7-5.75	10-11	8	205	700	[45]
$BaTiO_3$	5.6	3.1	1.1-1.6	99	65-82	[46]
BZT-BCT	5.78	0.54	-	-	-	[44]

Summary of literature review and scope of the work

- The newly discovered BZT- 0.5BCT have attracted great attention due to its excellent dielectric and piezoelectric properties. The electrical properties of BZT- 0.5BCTsolid solutions have been studied extensively; however most of the work focuses on the nature of phase transition, structure, powder synthesis, effect of processing conditions on dielectric and piezoelectric properties and the temperature dependence of the dielectric and piezoelectric properties.
- It is to be mentioned that the electrical and mechanical properties, both are important for use of piezoceramics in device applications. However, there are very few reports available on the study of mechanical properties of BZT-0.5BCT and no reports on its improvement with different techniques.
- In ceramic system there is common practice for enhancement of the mechanical properties by reinforcement of oxide (Al_2O_3, MgO, ZrO_2, and Stabilized-ZrO_2) or nonoxide (SiC) particles which have better mechanical properties than the matrix.
- The same method can be used to improve the mechanical properties of ferroelectric ceramics by reinforcement with mechanically stronger particles.
- It is well known that electrical properties of ferroelectric ceramics generally degrade with non-ferroelectric additives and decrease in sinterability usually encountered with these refractory oxide additives. Use of nano-oxide additives may drastically reduce the amount of additive due to high surface area and in effect electrical property may not degrade much.
- It was reported that $BaTiO_3$-(BT) based piezoelectric ceramics suffer from low mechanical strength and poor reliability under loading conditions which limits their applications as transducers, sensors and actuators where high fracture toughness and fracture strength are required.
- Nano-particulates incorporated BT-based composites, including Al_2O_3, ZrO_2, MoO_3, NiO, SiC, Ag and Ni, were studied in order to improve their mechanical properties. It was found that both oxide and metal additives could improve the mechanical properties of the BT-based composite ceramics. However, there are only a few studies on their electrical properties and in particular their piezoelectric properties.

In this context, it will be interesting to study whether some nano sized mechanically stronger particle incorporation can improve the strength and hardness of BZT-BCT without much degrading the electrical properties.

2.6 Objective of the work

The objectives of the present work have been defined on the basis of the existing problems, challenges and current status in the field of lead free piezoceramics. The objective of the present thesis was "To optimize the amount of different nano oxides additives and sintering temperature to get suitable dielectric, piezoelectric and mechanical properties"

2.7 Organization of the Thesis

The thesis has been divided into five chapters:

Chapter–I presents a brief introduction on basics of ferroelectric, piezoelectric properties, different mechanism for improvement of mechanical properties and important lead based and lead free ferroelectric materials

Chapter–II deals with the detailed literature review of structural, dielectric and piezoelectric properties of BZT-BCT, synthesis of BZT-BCT by different methods and its sintering. Effect of different oxide additives on mechanical and electrical properties of PZT and $BaTiO_3$was also reviewed in details.

Chapter–III deals with the detailed experimental process related to this research work.

Chapter–IV describes the results and discussion, which has been divided into 4 sections, where, **Section 1** describes the fabrication and characterization of BZT-0.5BCT ceramics, **Section 2**describes the effect of nano-Al_2O_3 addition on phase evolution, densification, microstructure, dielectric, piezoelectric and mechanical properties of BZT-0.5BCT,**Section 3** describes the effect of nano-MgO addition on phase evolution, densification, microstructure, dielectric, piezoelectric and mechanical properties of BZT-0.5BCT **Section 4** describes the effect of nano-ZrO_2 addition on phase evolution, densification, microstructure, dielectric, piezoelectric and mechanical properties of BZT-0.5BCT

Chapter–V contains the concluding remarks and the scope of future work.

References

[1] T. Maiti, R. Guo, A. S. Bhalla, J. Am. Ceram. Soc. **91** 1769 (2008)

[2] D.F.K. Hennings, H. Schreinemacher, J. Eur. Ceram. Soc. **15** 795 (1995)

[3] H. Kishi, Y. Mizuno, H. Chazono, Jpn. J. Appl. Phys. **42** 1 (2003)

[4] D. Hennings, H. Schreinemacher, Mat. Res. Bull. **12** 1221 (1977)

[5] W. Liu, X. Ren, Phys. Rev. Lett. **103** 257602 (2009)

[6] J. Wu, D. Xiao, W. Wu, J. Zhu, J. Wang, J. Alloys Compd. **509** L359 (2011)

[7] D.S. Keeble, F. Benabdallah, P. A. Thomas, M. Maglione, J. Kreisel, Appl. Phys. Lett., **102** 092903 (2013)

[8] W. Li, Z. Xun, R. Chu, P. Fu, G. Zang, Physica B. **405** 4513 (2010)

[9] W. Li, Z. Xu, R. Chu, P. Fu, G. Zang, J. Am. Ceram. Soc. **93** 2942 (2010)

[10] W. Li, Z. Xu, R. Chu, P. Fu, G. Zang, Mater. Sci. Eng. B. **176** 65 (2011)

[11] W. Li, Z. Xu, R. Chu, P. Fu, G. Zang, Mater. Lett. **64** 2325 (2010)

[12] F. Benabdallah, A. Simon, H. Khemakhem, C. Elissalde, M. Maglione, J. Appl. Phys., **109** 124116 (2011)

[13] P Wang, Y. Li, Y. Lu, J. Eur. Ceram. Soc. **31** 2005 (2011)

[14] S. Su , R. Zuo, S. Lu, Z. Xu, X. Wang, L. Li, Curr. App. Phys. **11** S120 (2011)

[15] J. Hao, W. Bai, W. Li, J. Zhai, J.Am.Ceram. Soc. **95** 1998 (2013)

[16] Y. Tian, L. Wei, X. Chao, Z. Liu, Z. Yang, J. Am. Ceram. Soc. **96** 496 (2013)

[17] Y. Tian, L. Wei, X. Chao, Z. Liu, Z. Yang, J. Appl. Phys. **113** 184107 (2013)

[18] R. Yang, X. Fu. W. Deng, Z. Tan, Y. Zhang, L. Han, C. Lu, X. Guan, Adv. Mater. Res. **148-149** 1062 (2011)

[19] Z. Tan, W. Fu, X. Deng, R. Yang, X. Guan, C. Lu, Y. Zhang, L. Han, Adv. Mater. Res. **148-149** 1480 (2011)

[20] V. S. Puli, A. Kumar, D. B. Chrisey, M. Tomozawa, J. F. Scott, R. S.Katiyar, J. Phys. D: Appl. Phys. **44** 395403 (2011)

[21] J. P. Praveen, K. Kumar, A.R. James, T. Karthik, S. Asthana, D. Das, Curr. Appl. Phys. **14** 396 (2014)

[22] M. Wang, R. Zuo, S. Qi, L. Liu, J. Mater. Sci: Mater Electron. **23** 753 (2012)

[23] A. R. Montero, L. Pardo, R. L. Juárez, A.M. González , M.P. Cruz, M.E. Castrejón, J. Alloys Compd. **584** 28 (2014)

[24] C. Puchmark, G. Rujijanagul, S. Jiansirisomboon, T. Tunkasiri, N. Vittayakorn, T. Comyn, S.J. Milne Current Applied Physics **6** 323 (2006)

[25] P. Xiang, X. Dong, H. Chen, Z. Zhang, J. Guo Ceram. Inter. **29** 499 (2003)

[26] S. Jiansirisomboon, M. Promsawat, O. Namsar, A. Watcharapasorn, Mater. Chem. Phys. **117** 80 (2009)

[27] H.L. Zhang, J.-F.Li, B.-P. Zhang, W. Jiang, Mater. Sci. Engg. **A 498** 272 (2008)

[28] K. Tajima, H. J. Hwang,M. Sando and K. Niihara J. Euro.Ceram. Soc.**19** 1179 (1999)

[29] H.J.Hwang, K. Niihara, J.Mater.Sci. **33** 549 (1998)

[30] S. Jiansirisomboon, T. Sreesattabud, A. Watcharapasorn, Ceram. Inter. **34** 719 (2008)

[31] T. Zeng, X. Dong, H. Yang, C. Mao and H. Chen, Scripta Mater. **55** 923 (2006)

[32] J.Wang, HNie, CLan, G Wang, X Dong, X Chen, Fei Cao, He Hongliang,Ceram. Inter. **39** 3915 (2013)

[33] S. Jiansirisomboon, A. Watcharapasorn, Current Appl. Phys. **8** 48 (2008)

[34] A. I. Ali, C. W. Ahn, Y. S. Kim, Ceram Inter. **39** 6623 (2013)

[35] G-D Zhan, J. Kuntz, J. Wan, J. Garay, A. K. Mukherjee, Mater. Sci. Engg. **A356** 443 (2003)

[36] S. Jiansirisomboon, A. Watcharapasorn and T. Tunkasiri, Chiang Mai J. Sci. **33** {2} 175 (2006)

[37] P. Ren, H. Fan, X. Wang, X. Tan, Mater. Res. Bull. **46** 2308 (2011)

[38] T. Nagai,K. Iijim, H. HwangM. Sando,T. Sekino and K. Niihara, J. Am. Ceram. Soc. **83**{1} 107 (2000)

[39] S. Yoon, J. Lee, D. Kim and N. M. Hwang, J. Am. Ceram. Soc. **86** {1} 88 (2003)

[40] W.C. Vittayakorn, D. Bunjong, R. Muanghlua and N. Vittayakorn, J. Ceram. Process. Res. **12** {5} 493 (2011)

[41] W. Cai, ,C.L.Fu, J. C. Gao and C. X. Zhao, J. Adv. Appl. Ceram. **110** {3} 181 (2011)

[42] O. Namsar, A. Watcharapasorn, S. Jiansirisomboon, Ceram Inter. **38S** S95 (2012)

[43] J. G. Fisher, B-Ki Lee, A. Brancquart, S-Y Choi, S-J. L. Kang, J. Euro. Ceram Soc. **25** 2033 (2005)

[44] A. Kaushal, S. M. Olhero, B. Singh, R. Zamiri, V. Saravanam and J. M. F. Ferreira, RSC Adv. **4** 26993 (2014)

[45] Cowley, J.D. and Lee, W.E. Mater. Sci.Tech Chapter **2** {11} 87 (2005)

[46] J.M. Blamey, T.V. Parry, J. Mater. Sci. **28** 4988 (1993)

CHAPTER 3

EXPERIMENTAL WORK

Introduction

3.1 Powder synthesis, sintering and characterization

In batch formulation, the raw materials (metal oxide or carbonate) were weighed according to the stoichiometric formula. All raw materials were preserved prior to batch formulation in a clean, dry and moisture free desiccator. High purity raw materials were used for batch synthesis. For our work, $Ba(Zr_{0.2}Ti_{0.8})O_3$-0.5$(Ba_{0.7}Ca_{0.3})TiO_3$[BZT- 0.5BCT] will be synthesized by solid state mixing method via planetary milling. BZT-0.5BCT can also be represented by the formula $(Ba_{0.85}Ca_{0.15})(Zr_{0.1}Ti_{0.9})O_3$.

Different characterization techniques to study the physical properties of powder and sintered ceramics were also described.

Planetary milling

The planetary ball mill owes its name to the planet-like movement of its vials. These are arranged on a rotating support disk and a special drive mechanism causes them to rotate around their own axes. The centrifugal force produced by the vials rotating around their own axes and that produced by the rotating support disk both act on the vial contents consisting of the material to be ground and the grinding balls. The superimposition of the centrifugal forces produces grinding ball movements with high pulverization energy. The centrifugal forces acting on the grinding jar wall initially carry the grinding balls in the direction in which the grinding jar is rotating. Differences occur between the speed of the grinding jar wall and the balls; this results in strong frictional forces acting on the sample. The schematic configuration of planetary mill is shown in Figure 4.1 As the rotational movement increases, Coriolis forces act on the balls to displace them from the grinding jar walls. The balls fly through the grinding jar interior and impact against the sample on the opposite grinding jar wall. This releases considerable dynamic impact energy. The combination of the frictional forces and impact forces causes the high degree of size reduction of planetary ball mills [1,2]

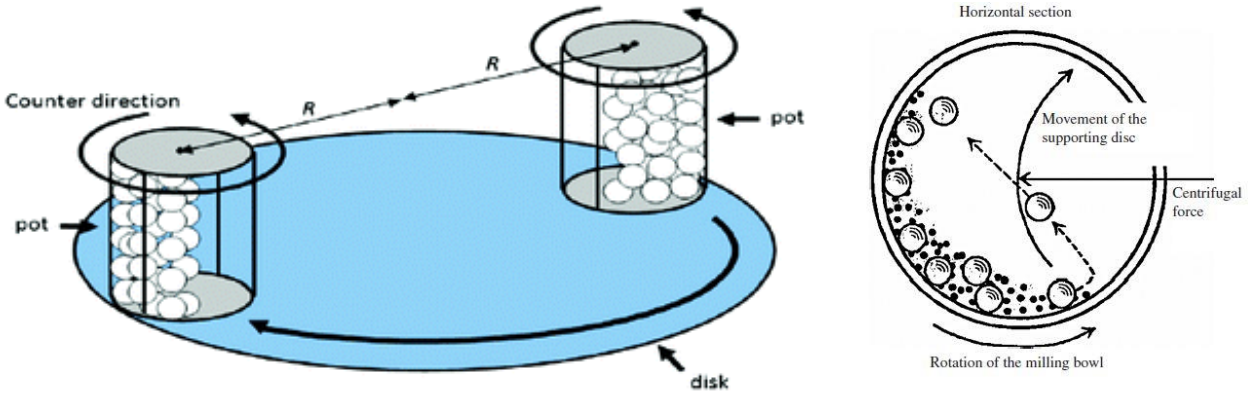

Figure 3.1 Schematic diagram of the planetary ball mill and the movement of a ball in the pot

The BZT- 0.5BCT powder was prepared by planetary milling method. Reagent grade of barium carbonate [$BaCO_3$ (Sigma Aldrich, 99%)], calcium carbonate [$CaCO_3$ (Sigma Aldrich,99%)], zirconium dioxide [ZrO_2 (Sigma Aldrich, 99.9%)] and TiO_2 (Sigma Aldrich, 99.0%) were used as the starting materials. Stoichiometric amount of powders were mixed by planetary mill (Fritizsch Pulveriser) for 10h (RPM 300) with zirconia ball using isopropyl alcohol as the media. The mixture was dried at 100°C overnight in an oven. The mixture was placed in alumina crucible, which was subsequently inserted into furnace and heated in the temperature range of 1200°C, at 3°C/min in air. Figure 3.1 shows the flow chart for the preparation of BZT-0.5BCT ceramics. Al_2O_3(99.8%, REINSTE, Nano Ventures), MgO (Sigma Aldrich Chemie, GmbH) and ZrO_2 (Sigma Aldrich Chemie, GmbH) nanopowders were mixed (after dispersing in acetone) with pure BZT-0.5BCT in mortar pestle.Pellets from the synthesized powders were prepared using uniaxial pressing at a pressure of 350 MPa.

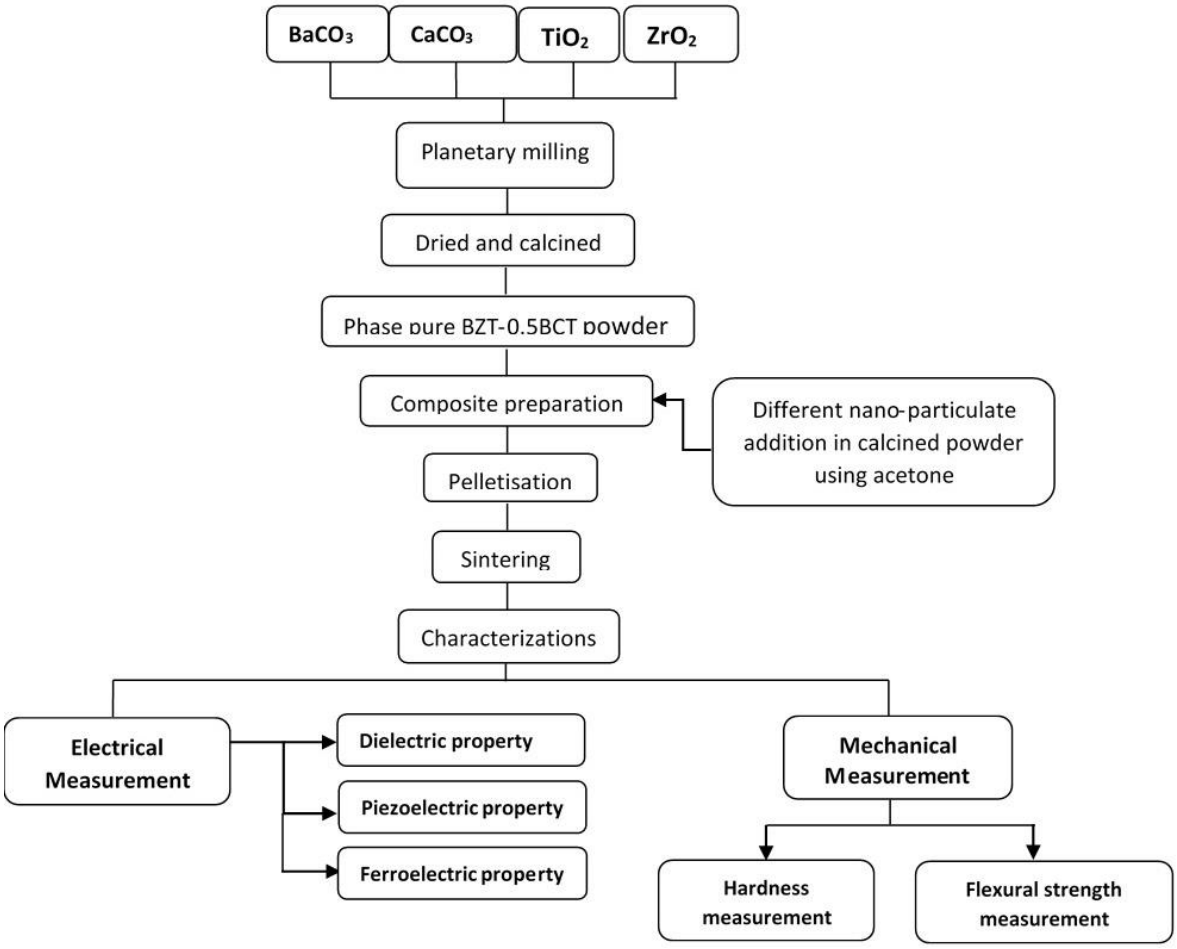

Figure 3.2: Flowchart for the preparation and characterization of different nano oxides [Al_2O_3, MgO and ZrO_2 (3Y)] added BZT-BCT composite ceramics

The pellets were sintered at 1300°C, 1350°C, 1400°C and 1500°C for different soaking time and cooled inside the furnace.

3.1.1 DSC-TG

The milled powder was ground and characterized by differential scanning calorimeter (DSC) and thermo gravimetric analysis (TGA) using NETZSCH STA (Model No 409C). DSC is the more recent technique and was developed for quantitative calorimetric measurements. The signal from the differential scanning calorimeter will be regarded as proportional to the difference in thermal power between the sample and reference, $d\Delta q/dt$. Differential scanning calorimeters make use of acrucible to contain the sample. The reference is either an inert material in a crucible of the same type as that used for the sample

or simply the empty crucible. Crucibles commonly measure 5 -6 mm in diameter made up of alumina. This technique is excellent for determining the chemical kinetics, enthalpy transitions and transformation, presence and quantity of hydrated water, decomposition behavior of gel, phase transitions, crystallization temperature and formation of products, etc. of precursor powders synthesized through different chemical route. Thermal analysis of powder was carried out in air atmosphere with the heating rate of 10^{o}C/min from RT to 1400^{o}C. When a material undergoes physical or chemical change it absorbs or releases thermal energy. The temperature difference of the sample with respect to the reference inert material (α-Al_2O_3) during heating or cooling is plotted in a DSC curve as the deviation from zero base line. Exothermic or endothermic changes are shown in opposite directions of the baseline.

Theory of DSC:

The aim was to derive an expression for the instrument signal in response to the evolution of heat from a sample as represented by dh/dt. The sample and its crucible were considered as one with a total heat capacity C_P. A similar assumption was made regarding the reference material and its crucible, which together had a total heat capacity C_R. It was assumed that there was a source of thermal energy at temperature T_p and a single thermal impedance R between the sample and the source of thermal energy and between the reference and the source of thermal energy. The heat flow between the thermal energy source and the sample was represented as dq/dt as measured by the instrument. The heating rate was represented by dT,/dt = p and assumed to be linear. Gray obtained the equation,

$$dh/dt = - dq/dt + (C_S - C_R)\, dT_P/dt - RC_S\, d^2q/dt^2 \qquad (3.1)$$

Thus the heat evolution from the sample is given by the instrument signal measured from zero (term 1), a heat capacity displacement (term 2) and a third term whichincludes the product RC. This product has units of time so that (term 3) represents a thermal lag. Included in the publication was a recipe for obtaining dh/dt from the experimental curve by making allowance for thermal lag. For inert samples dh/dt = 0 and the displacement (term 2) provides a route to the determination of heat capacity.

Theory of TGA:

TGA is basically an analytical technique in which the mass change of a substance is measured as a function of temperature whilst the substance is subjected to a controlled temperature programme. The temperature programme must be taken to include holding the sample at a constant temperature other than ambient, when the mass change is measured against time. Mass loss is only seen if a process occurs where a volatile component is lost. There are, of course, reactions that may take place with no mass loss. As materials were heated, they lose weight due to drying, or from chemical reactions that liberate gasses. Some materials can gain weight by reacting with the atmosphere in the testing environment. The results may be reported directly as mass of the sample varying with temperature or time, i.e. as m versus T. Thus a mass loss appears as a downwards curve. Instead of mass in mg, the scale may be converted into percent of the original mass. An alternative is to convert the results into a percentage mass loss.

3.1.2. Dilatometric and sintering study of powder compact

Shrinkage behavior of the green compact bar shaped samples was investigated by NETZSCH dilatometer model DIL 402 C. In the dilatometer the specimen was kept in a specimen holder in the centre of the furnace. The linear dimensional change i.e. shrinkage or expansion of the specimen was transmitted through the push rod (pressed against the sample inside the furnace) to the measuring head.

Samples in the form of bar having a dimensions 15x 5 x 5 mm (l x b x h) for dilatometry experiment. The heating rate was maintained at 10^{o}C/min. The measurement was carried out from room temperature to 1400^{o}C in Argon atmosphere.

Sintering of green compacts was carried out `in a chamber furnace (45R5Y) by heating it from room temperature to 650^{o}C at a heating rate of 3^{o}C/minute with a holding time of 1 hour at 650^{o}C for binder removal.Thereafter, the heating was continued at the rate of 3^{o}C/minute till the final sintering temperature was attained. A holding time of 4 hours was provided at the peak sintering temperature. Following the sintering, the samples were furnace cooled to room temperature. All sintering experiments were done on a platinum sheet kept on top of inverted cylindrical alumina crucible.

3.1.3. X-ray diffraction (XRD)

X-Ray Diffraction (XRD) has proven to be a powerful and versatile tool for analysis of many aspects of fabricated barium titanate based material. This non-destructive method measures constructively interfered monochromatic x-rays diffracted at specific angles by crystal planes internal to the sample [4]. The phase evolution of the calcined powder as well as that of the sintered samples was studied by X-ray diffraction technique (Philips PAN analytical, The Netherland) using Cu $K_\alpha$radiation. The instrument was run at power settings of 35 kv and 25 mA. The samples were scanned in 2θ ranges from 15 to 80° with the step size of 0.02° and a count time of 4s per step.

Phases present in the sample was identified with the search match facility available with Philips X'pert high score plus software.

The crystallite size of the calcined powders was determined from X-ray line broadening using the Scherer's equation as follows:

$$t = \frac{0.9\lambda}{\beta \cos\theta} \qquad (3.2)$$

Where, t = crystallite size, λ = wavelength of the radiation, θ = Bragg's angle and β = full width at half maximum (FWHM) peak. Line broadening due to instrument was subtracted from the peak width before calculating the crystallite size using the following formula:

$$\beta^2 = \beta^2_{meas} - \beta^2_{equi} \qquad (3.3)$$

where,β_{meas} = measured full width at half maximum from peak, β_{equi}= instrumental broadening [Standard Silicon sample was used, whose β value was 0.09821 at 2θ = 29° with (hkl) value (111)].

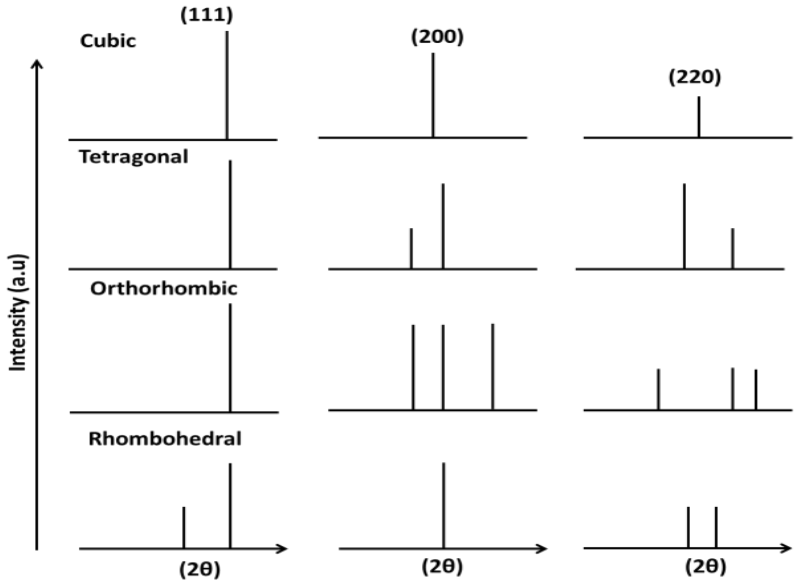

Figure 3.3 Characteristic X-ray diffraction patterns for various symmetries showing the corresponding splitting with respect to the cubic (111), (200) and (220) reflections.

X-ray diffraction patterns can be used to monitor structural properties such as phase purity and change of symmetry (phase transition). If a crystal structure changes from cubic to tetragonal, the interaxial angles remain same ($\alpha, \beta, \gamma, = 90°$) where the edges of the unit cell are different ($a = b \neq c$). This will affect the d-spacing of the lattice that results in the splitting or merging of peaks as shown in Figure 3.3. This characteristic X-ray diffraction pattern can be used to identify the symmetry and phase components of the materials [5].

3.1.4 Field Emission Scanning Electron Microscopy (FESEM)

Powder morphology, grain shape and size were observed by SEM (JEOL JSM 6480LV) and FESEM (Nova Nano SEM 450) equipped with an energy dispersive X-ray spectrometer (EDX). As-sintered and fracture surface of the samples were cleaned with acetone in an ultrasonic bath to remove foreign particles and then oven dried for 1 hour. The samples were gold coated for 2 minutes using a sputter coater for FESEM analysis.

3.1.5 Density measurements

The bulk density of the samples was measured by Archimedes principle. The formula for the calculation of bulk density is as follows.

$$Bulk\,density = \frac{W_d}{W_s - W_{su}} \times Density_{liquid}$$

$$Relative\ density = \frac{bulk\ density}{Theoritical\ density} X\ 100$$

Where W_d, W_s and W_{su} are the dry weight, soaked weight and suspended weight of the sample, respectively. The liquid used for calculation was kerosene of density 0.81 g/cc.

3.2 Dielectric and piezoelectric properties

3.2.1 Dielectric properties measurements

For electrical measurements, both the surfaces of pellets were painted uniformly with silver conductive paste (Alfa Aesar) and cured at 500^{o}C for half an hour. Thus a pellet with two parallel electrodes acts as a single layer capacitor.

The dielectric constant or relative permittivity (ε_r) is defined as the ratio of the permittivity of the material to the permittivity of free space. The dissipation factor is defined as the tangent of the loss angle (tan δ). It is a measure of the amount of electrical energy which is lost through conduction when a voltage is applied across the piezoelectric element. The dielectric constant (ε_r) and dielectric loss factor (tan δ) was measured using HIOKI 3532-50 LCR Hitester. Measurements are generally carried out in the frequency range of 42 Hz to 1MHz. Dielectric behavior has also been studied as a function of temperature with the temperature ranging from room temperature to 200^{o}C depending on the composition. The samples were placed in between two platinum sheets each of which is connected to a platinum wire. The whole arrangement was covered with an alumina tube. A small force was applied by a spring to ensure good contact to the sample electrodes. The temperature of the specimen was controlled using a carbolite furnace at a heating rate of 2^{o}C/min.

The relative permittivity (ε_r) is calculated from the measured values of capacitance and physical dimension of the specimen. The relations are expressed as:

$$C = \frac{\varepsilon_0 \varepsilon_r A}{t} \qquad (3.4)$$

Where ε_r the relative permittivity of the piezoelectric material, ε_0 is the relative permittivity of free space (8.854×10^{-12} F/m), t is the distance between electrodes (m), A is the area of the electrodes (m^2).

In an alternating electric field the dielectric permittivity or relative permittivity is a complex quantity and can be written as

$$\varepsilon_r^* = \varepsilon' + \varepsilon'' \qquad (3.5)$$

Where ε' is the real part of the dielectric permittivity and ε'' is the imaginary part of permittivity and related to the energy loss in the system.

When dielectric is subjected to the ac voltage, the electrical energy is absorbed by the material and is dissipated in the form of heat. The dissipation is called dielectric loss. In this case, current leads the voltage by (90-δ), where δ is called the loss angle and tanδ is the electrical loss, better known as tangent loss as shown in Fig 3.4.

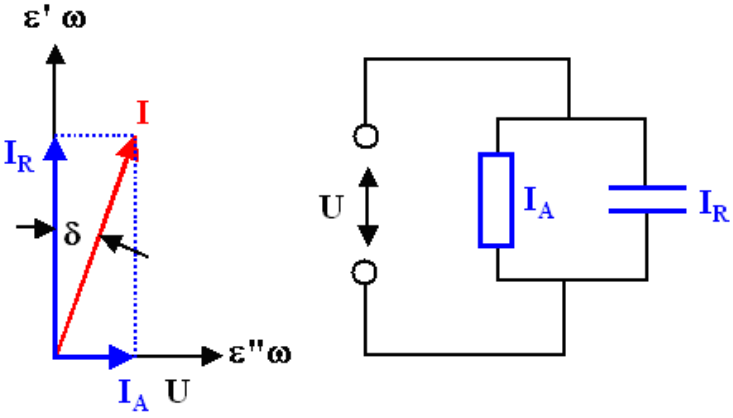

Figure 3.4 Phasor diagram between current and voltage.

The loss tangent can be expressed [6] as

$$\tan\delta = \frac{\varepsilon''}{\varepsilon'} \qquad (3.6)$$

Curie temperature (Tc): It is the temperature above which the spontaneous polarization (Ps) of the ferroelectric materials vanishes and it goes to paraelectric state.

3.2.2 Ferroelectric Measurements: Hysteresis loops

The Polarization hysteresis measurement was carried out by an automatic P-E loop tracer (Marine India, Electronics). For these measurements, the thickness of the pellets was reduced to ~1mm. The pellets were electroded with silver paste and cured at 500^{o}C for 30min. All the measurements were carried out at room temperature.

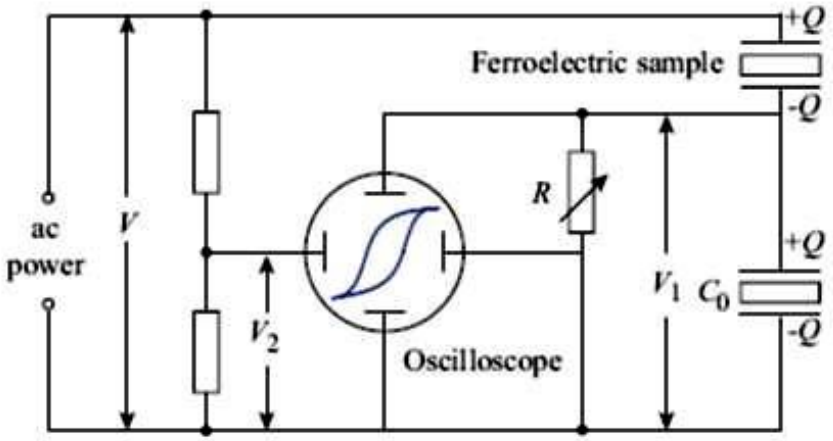

Figure 3.5 Schematic circuit of the Sawyer–Tower Bridge for measuring the P–E characteristics of ferroelectrics [7].

The polarization hysteresis measurements based on standard Sawyer- Tower circuit is shown in Figure 3.5. In order to avoid dielectric breakdown in air, silicon oil with a high dielectric strength was used to cover the sample. An approximate value of the electric field strength in the sample is obtained with the input voltage and the sample thickness.

3.2.3 Poling

For piezoelectric properties, the specimens were poled in silicon oil at room temperature for 20 min by applying electric field of 2.5kV/mm. Poling was an essential step before ferroelectric ceramics exhibiting piezoelectric properties. Poling was a process of domain reorientation and domain wall movement by external driven electric field. The ability of poling is depended on the temperature, electric field, time and thickness of samples. In ferroelectric ceramics, adjoining dipoles form regions of local alignment called domains. The alignment gives a net dipole moment to the domain, and thus a net polarization. The direction

of polarization among neighboring domains is random. So, the ceramic element has no overall polarization.

Poling is a process during which a high electric field is applied on the ferroelectric samples to force the domains to reorient the direction of the applied electric field. The poling is possible in the ferroelectric ceramics and poling steps are shown in fig 3.6.

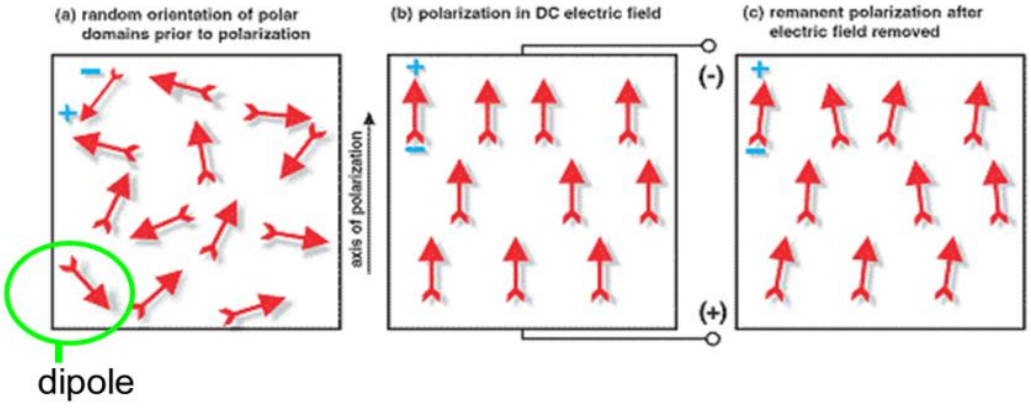

Figure 3.6 Poling of ferroelectric material

3.2.4 Piezoelectric measurements

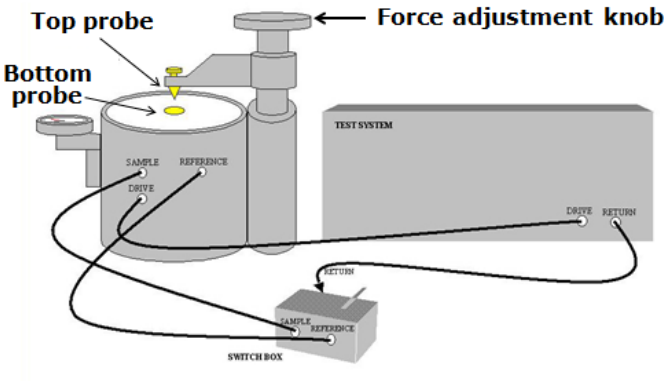

Figure 3.7 Schematic of piezoelectric constant (d_{33}) measurement

The d_{33} coefficients of the poled samples were measured after 24h with a d_{33} meter (YE2730A d_{33} Meter, APC International Ltd.). A force of 0.25N is applied to the sample and the corresponding d_{33} coefficient is measured.

3.3.5 Electromechanical coupling factor

Electromechanical coupling factor (k) is used to measure the conversion efficiency between the electrical and mechanical energy in piezoelectric material. It can be determined by

measuring impedance of the electrically poled samples in a frequency range 10kHz to 5 MHz using HIOKI 3532-50 LCR Hitester.

The electromechanical coefficient is calculated using the formula mentioned below:

$$K_{eff} = \sqrt{\frac{f_a^{\,2} - f_s^{\,2}}{f_a^{\,2}}} \qquad (3.7)$$

Where f_s resonant frequency and f_a is the anti-resonant frequency

3.2.6 Aging behavior

Sets of 5 pellets for each composition were prepared for aging study. Poled pellets were characterized for piezoelectric constant d_{33}, and electromechanical coupling coefficient k_P for piezoelectric and dielectric response. For piezoelectric materials, aging of the piezoelectric property (d_{33}) can be described as a function of time (t). It shows the linear relation with time on logarithmic scale which can be describing with the general equation 3.8.

$$p(t) = p(t_0) + A \log(t) \qquad (3.8)$$

Where p is the material property, t_0 is the starting time for the measurements, and A is the aging rate (constant) which can be either positive or negative.

3.3 Mechanical property Measurement

Depending on the loading force value and the indentation dimensions, hardness is divided into three types: -

I. **Macro-hardness tests (Rockwell, Brinell, and Vickers)** are the most widely used methods for rapid routine hardness measurements. The indenting forces in macro-hardness tests are in the range of 50N to 30000N.

II. **Micro-hardness tests (micro-Vickers, Knoop)** are applicable when hardness of coatings surface hardness or hardness of different phases in the multi-phase material is measured. Small diamond pyramid is used as indenter loaded with a small force of 10 to 1000gf.

III. **Nano-hardness** test uses minor loads of about 1 nano-Newton followed by precise measuring depth of indentation.

3.3.1 Vickers hardness

Hardness is defined as the resistance to permanent deformation which is caused by indentation. It is measured by making indentation on flat polished surfaces. Vickers hardness test uses a square base diamond pyramid as the indenter with the included angle between opposite faces of the pyramid of 136^{o}.The indenter size, shape and the load applied may all affect the hardness measured and should be defined. The Vickers hardness number (H_V) is defined as the load divided by the surface area of the indentation.

Mathematical formula to measure hardness is given by

$$\mathbf{H_v = 1.854(P/d^2)} \qquad (3.9)$$

Where Hv is Vickers hardness, P is the applied load and d is the average length of two diagonals.

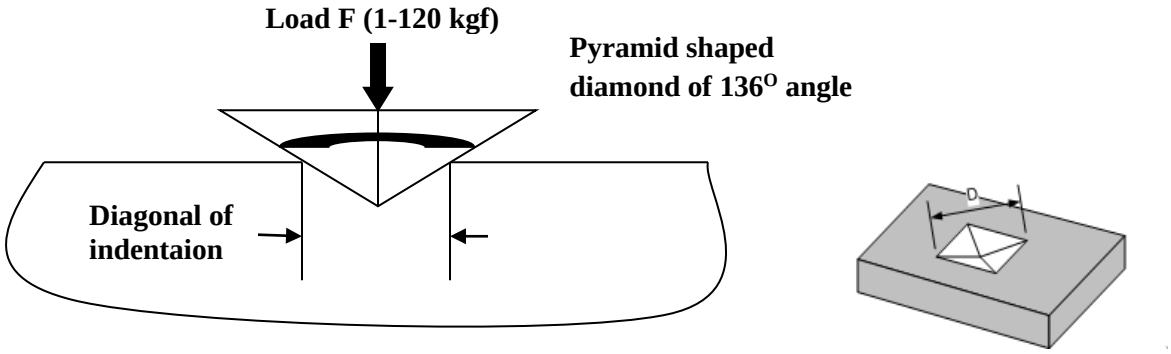

Figure 3.8: Vickers Hardness arrangement

The mechanism behind Vickers hardness test is to measure the dimension of the indentation (depth or actual surface area of the indentation) during the application of load into the sample. Hardness is not fundamental property and its value depends on the combination of yield strength, tensile strength and modulus of elasticity.

Hardness was measured by the indentation technique using Vickers diamond indenter. The indentation load of 0.5kg was applied for 10s.

3.3.2 Flexural Strength

Flexural strength is defined as the materials ability to resist deformation under load. It is measured at the moment of rupture where the highest stress is experienced within the material.

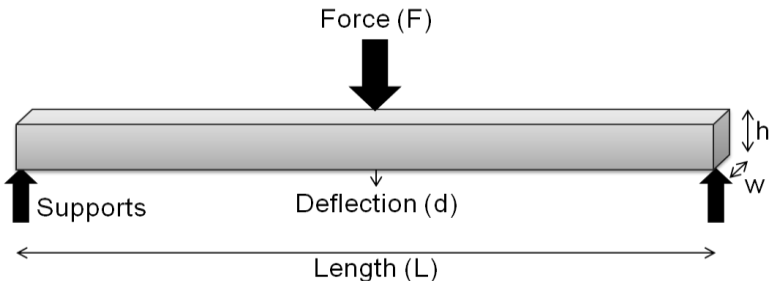

Figure 3.9: Three point bending setup

Above figure shows 3 point bending setup. For a rectangular sample under a load (F) in a three-point bending setup strength is measured by following equation.

$$\sigma_f = \frac{3\,F\,L}{2bd^2} \qquad (3.10)$$

Where, F is the load (force) at the fracture point (N), L is the length of the support span (mm), b is width (mm) and d is thickness (mm)

Flexural test is of two types such as three point flexural test and four point bending test. In three point bending the applied force produces its peak stress at the specimen mid-point with reduced stress elsewhere. This stress localization is ideal for testing for specific dislocation of stress on a component or material. While in case of 4 point bending test load produces peak stresses along an extended region of the specimen hence exposing a larger length of the specimen with more potential for defects and flaws to be highlighted.

The Flexural strength was measured on the rectangular bars (40 mm length) by three point bending method. The span was 40 mm and the rate of loading was 0.5 mm/min.

References

[1] M.N. Rahaman, Ceramic Processing and Sintering, (CRC Press, Taylor & Francis Group) (2007)

[2] H. Mio, J. Kano, F. Saito, Chem. Eng. Sci., 59, 5909-5916, (2004)

[3] H. Mio, J. Kano, F. Saito, Chem. Eng. Sci., 59, 5909-5916, (2004)

[4] B. D. Cullity, Elements of X-Ray diffraction Second edition ed., (1978)

[5] L. E. Smart, E. A. Moore, Solid State Chemistry, (Taylor & Francis, London, (2005)

[6] M.W. Barsoum, Fundamentals of Ceramics, McGraw–Hill, Boston, (1997),

[7] A. J. Mouson, J. M. Herbert. Electroceramics-Materials properties, applications. Chapman and Hall, London, (1990)

CHAPTER 4

RESULT AND DISCUSSIONS

Section 1: Fabrication and characterization of BZT-0.5BCT ceramics

Introduction

From literature review (chapter 2) it is found that BZT–BCT may be a prospective alternative of lead-based piezoelectric. Present thesis attempts to study the densification, microstructure, electrical and mechanical properties of BZT–BCT with different nano oxide additives (Al_2O_3, MgO, and stabilized-ZrO_2). Before studying the effect of different nano oxide addition in BZT-BCT, it is important to discuss the preparation of phase pure BZT-BCT powder, to find out suitable sintering temperature to get best dielectric and piezoelectric property.

The present section deals with the optimization of calcinations temperature to get phase pure BZT-BCT powder and to study densification behavior and microstructure to get best dielectric and piezoelectric properties.

4.1 BZT- 0.5 BCT powder synthesis

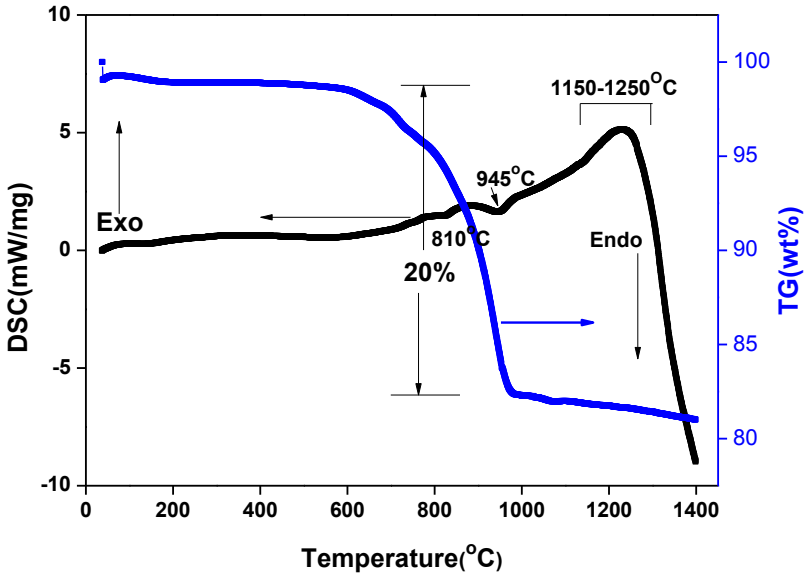

Figure 4.1: DSC and TG plots of the stoichiometric mixture of oxides after planetary milling for preparation of BZT-0.5BCT

Figure 4.1 shows the thermal analysis of un-calcined oxide mixture obtained after planetary milling. According to the TG plot, an overall weight loss of 20% is observed. The total weight loss can be divided into three steps. In the first step (room temperature – 200^{o}C), minor weight loss of about ~2% is observed that could be due to removal of absorbed moisture and isopropyl alcohol. In the second step, the sample shows a major weight loss of about 18% in the temperature range 610^{o}C – 1000^{o}C. Two small endothermic peaks can be observed in the corresponding DSC curve at 810^{o}C and 945^{o}C. These endothermic peaks could be attributed to the decomposition of carbonates [1]. A further weight loss of 2% occurs around 1000^{o}C - 1400^{o}C, which could be ascribed to the removal of residual carbonates. In the corresponding DSC curve, a broad exothermic peak is seen which could be attributed to the crystallization of perovskite phase [1].

4.2 Powder characteristics and Phase analysis of BZT- 0.5BCTpowder

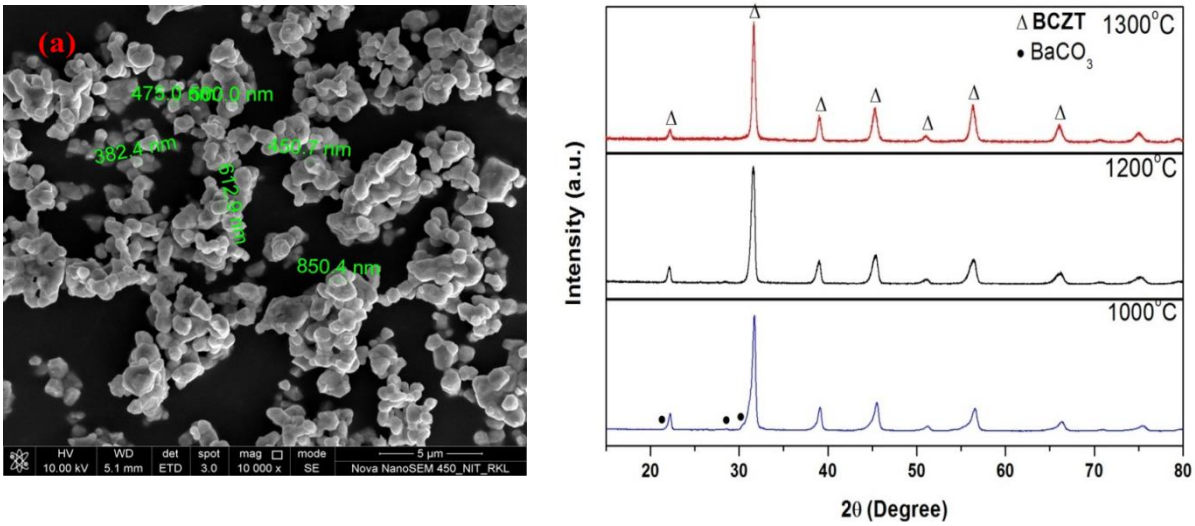

Figure 4.2: (a) FESEM micrograph of BZT-0.5 BCT powder (b) XRD patterns of BZT-0.5BCT powder calcined at different temperatures.

Figure 4.2 (a) shows FESEM micrograph of the BZT-0.5BCT powder calcined at 1200°C. BZT-0.5BCT powders are almost non-agglomerated and spherical to irregular in shape with average particle size of 0.4-0.8µm.Figure 4.2(b) shows the X-ray diffraction patterns of the0.5BCZT powder prepared by the solid state route via planetary milling and calcined at three different temperatures (1000°C 1200^{o}C and 1300^{o}C). It is observed that the perovskite phase is formed along with the impurity phases of $BaZrO_3$ (JCPDS No.74-1299) and $CaTiO_3$ after calcination at 1000^{o}C. As the temperature increased to 1200^{o}C, the impurity peaks are

completely removed. It can be concluded that the pure perovskite phase is formed via formation of the different intermediate compounds like $BaZrO_3$,$CaTiO_3$. Wang et al.. observed a trace of impurity phases in the powders of similar composition calcined at 1300°C [2].The pure BZT-0.5BCT showing both tetragonal and rhombohedral (T+R) phase whose XRD data can be matched with the JCPDS No. 89-1428 and 85-1796 respectively [3,4].

4.3 Densification and Microstructure of BZT- 0.5BCT

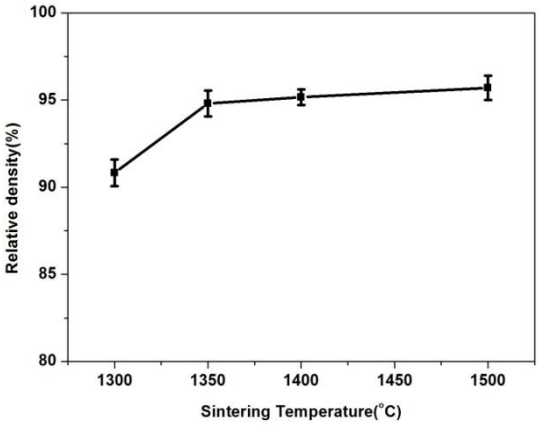

Figure 4.3: Bulk density of BZT-0.5BCT sintered at different temperatures

Figure 4.3 depicts the effect of sintering temperature on the sintered density of the BZT-BCT pellets. It is evident that the bulk density of the pellets [measured with respect to the true density of BZT-BCT (5.78g cm^{-3})] increases with increasing sintering temperature but beyond 1350^{o}C no significant change of density was observed.

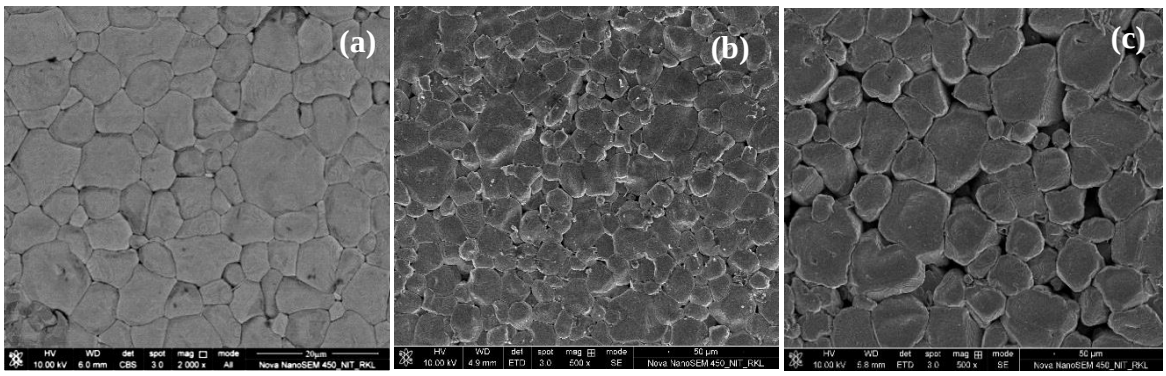

Figure 4.4: FESEM micrograph of BZT-0.5BCT ceramic sintered at (a) 1350°C, (b) 1400°Cand (c) 1500°C /4h

From the microstructures [figure 4. 4] it is clear that increase in sintering temperature leads to increase in the grain size of BZT-0.5BCT ceramic. The average grain size of 6.5 µm, 14 µm and 18µm are obtained for the samples sintered at 1350^{o}C, 1400^{o}C and 1500^{o}C respectively. Wang et al.. [2] observed that calcination temperature and sintering temperature have an important effect on the density and microstructure of the final ceramics. They achieved sintered density of 96% and found grain size of 15 µm at a sintering temperature of 1540^{o}C. In our case, realization of similar density at low temperature (1350^{o}C) may be attributed to the fine particle size of the BZT-0.5BCT powder.

4.4 Dielectric and piezoelectric property measurement of BZT- 0.5BCT

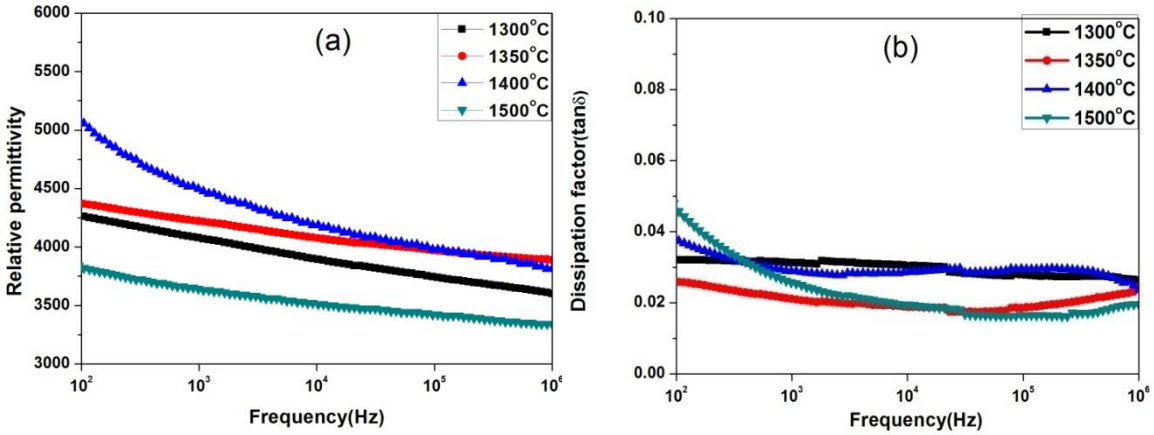

Figure 4.5 (a) Relative permittivity and (b) dissipation factor as the function of frequency for BZT-0.5BCT ceramic sintered at 1300°C, 1350°C, 1400°C, and 1500°C /4h.

Figure 4.5 (a) and (b) shows the relative permittivity and loss factor as a function of frequency (100Hz to 1MHz) for BZT-BCT ceramic sintered at 1350°C, 1400°C, 1450°C and 1500°C for 4hr measured at room temperature. The room temperature relative permittivity of BZT-BCT ceramics increased with increasing sintering temperature upto 1400^{o}C. The loss factor of all BZT-BCT ceramics was less than 4% at 1kHz.Dielectric permittivity value of BZT-BCT samples decreases with increase in frequency. This decrease of ε_r is due to the decrease in polarization with the increase in frequency. Sample sintered at 1400^{o}C and 1450^{o}C shows higher low frequency dispersion in dissipation factor. The relative permittivity of 0.5BCZT ceramics in all compositions in this study is more than that reported in the literature [5-9]. The enhancement of dielectric and piezoelectric properties can be explained

by the existence of Morphotropic Phase Boundary (MPB) in 0.5BCZT composition. The coexistence of tetragonal and orthorhombic phase facilitates more number of polarization directions and polarization rotation and polarization extension/contraction. It is observed that d_{33} and ε_r both are dependent on the grain size of the sintered ceramics. Higher grain size (18µm, 1500^{o}C sintered) samples have low d_{33}. Only increase in grain size cannot explain the reduction of piezoelectric property of the sintered BZT-BCT ceramics. It may be that atomic arrangement at the grain boundaries is much more similar to that in the grains for low temperature sintered sample (1350^{o}C), due to a lower concentration of oxygen vacancies and trapped electrons in grain boundaries. This can be explained as; the creation of oxygen vacancies and other charge carriers (e.g. electrons and holes) are related to sintering at high temperatures. While sintering at high temperature, oxygen loss increases leading to the formation of oxygen vacancies, accompanied by partial reduction in Ti^{4+} to Ti^{3+} ions by the following reactions using Kroger-Vink notations

$$2O_O^x \leftrightarrow 2V_O^{\cdot\cdot} + O_2(g) + 4e^-$$

$$Ti^{4+} + e' \leftrightarrow Ti^{3+}.$$

However, when the temperature is slowly cooled to room temperature in air, oxidation process occurs as $2V_O^{\cdot\cdot} + O_2(g) + 4e^- \leftrightarrow 2O_O^x$. The occurrence of this re-oxidation process at the grain boundaries leads to the formation an insulating grain boundary and conductive oxygen deficient grains [10,11]. Therefore, 1500^{o}C sample may have higher concentration of defects in the grain grain boundary region and degrades the dielectric and piezoelectric properties.

Table 1 summarizes the density, relative permittivity, dissipation factor and piezoelectric constant of BZT-0.5BCT ceramics sintered at different temperatures.

Thus it can be concluded that the optimum calcination temperature for BZT-0.5BCT powder was 1200^{o}C/2h.We obtained smaller grain size of 6.5 µm for BZT-0.5BCT ceramic sintered at 1350^{o}C/4h. The results show that the ceramics sintered at 1350°C exhibit the optimum electrical properties: d_{33} = 450pC/N, kp = 41%, ε_r= 4215, and tanδ>= 2 %, respectively. Thus for subsequent studies i.e. addition of different nano-oxide in BZT-BCT, sintering temperature will be upto 1350^{o}C.

Table 4.1 Table showing the variation of density and electrical properties of BZT-0.5BCT ceramic with the sintering temperature

Sintering Temperature(^oC)	**Relative Density (%)**	**Dielectric permittivity(ε_r)**	**Dielectric loss($\tan\delta$)**	**d_{33}**
1300	91.5	4069	0.0312	350
1350	95.4	4215	0.0205	450
1400	95.6	4475	0.0285	320
1500	96.4	3630	0.0255	310

Section 2: Effect of Al_2O_3addition on phase evolution, densification, electrical and mechanical properties of BZT-0.5BCT

Introduction

In the previous section the preparation of BZT-0.5BCT by solid state mixing method via planetary milling was described, where 95.5% sintered density could be achieved at 1350^{o}C. Increasing sintering temperature (> 1400^{o}C) promotes grain growth and degrades piezoelectric properties.

It is to be mentioned that the electrical and mechanical properties, both are important for ferroelectric and piezoelectric applications. For example, multilayer actuators (MLA) at the time of operation generate stress around 50MPa (described in chapter 1). BZT-0.5BCT is a prospective lead-free piezoelectric material. Additions of different nano-oxides to improve the mechanical properties of PZT and $BaTiO_3$ have been studied extensively.

To the best of our knowledge there is no report available on the electrical and mechanical properties of BZT-0.5BCT ceramics with addition of nano-sized Al_2O_3 with an aim to improve the mechanical property without degrading much the piezoelectric properties. The present section describes the densification, microstructure, dielectric, piezoelectric and mechanical properties of BZT–0.5BCT with nano-Al_2O_3 oxide additions

4.5 Powder characteristics

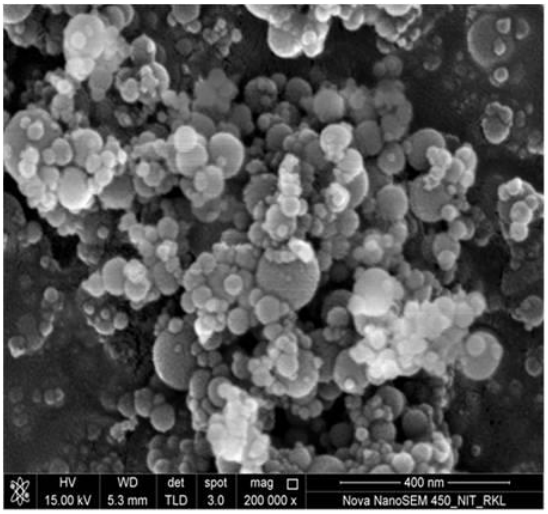

Figure 4.6 FESEM micrograph of nano Al_2O_3 powder.

Figure 4.6 shows the FESEM micrograph of Al_2O_3 nano-powder. It is clear from the figure that Al_2O_3 particles are spherical in shape with average particle size of ~60nm.

4.6 Phase Analysis of sintered samples

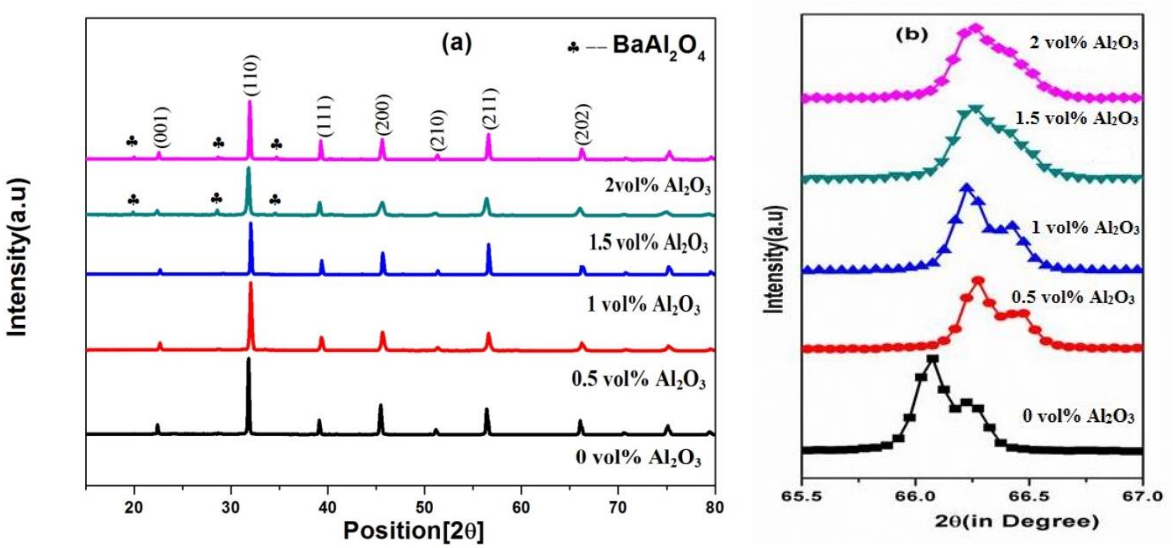

Figure 4.7 (a)X-ray diffraction patterns of different vol. % of nano oxide Al_2O_3 added BZT-0.5BCT ceramics sintered at 1350^{o}C/4hrs(b) magnified X-ray diffraction patterns in the range of 65.5-67^{o}C.

Figure 4.7(a) shows the X-ray diffraction patterns of nano-Al_2O_3 (0 to 2 vol %) added BZT-0.5BCT ceramics sintered at 1350^{o}C /4h.It can be observed that all the compositions exhibit the pure perovskite structure. The secondary phase of barium aluminate ($BaAl_2O_4$) can be observed at higher vol% of Al_2O_3 (~1.5vol %). This secondary phase was also reported to be observed in Al_2O_3added $BaTiO_3$ ceramics [12]. No trace of added $Al_2O_3$was detected for low concentration of addition, possibly because its amount was less than the XRD detection limit. Moreover, it is clear from the magnified X-ray pattern in the range of 65-67^{o}C [figure 4.7(b)] that the position of the diffraction peaks shift towards the higher diffraction angles with small addition of Al_2O_3 (< 1vol %), but for higher amount of addition further shifting of the peak positions were not observed. The pure BZT-0.5BCT shows both tetragonal and rhombohedral (T+R**)** phase which can be matched with the JCPDS No. 89-1428 and 85-1796 respectively [3,4]. Small addition of Al_2O_3 in BZT-BCT can incorporate Al^{3+} in B-site as an acceptor dopant and which promotes oxygen vacancies in the structure. As Al^{3+}(0.54Å) has

less ionic radius compared to Zr^{4+}(0.72Å) and Ti^{4+}(0.605Å), promotes reduction in lattice parameter which is demonstrated in peak shifting to higher angle. Moreover, higher amount of Al_2O_3addition (>1 vol%) resulted in higher symmetry perovskite phase. It may be due to small solid solubility of Al_2O_3 in $BaTiO_3$.The secondary phase of $BaAl_2O_4$ could be attributed to the chemical reactions between BZT-0.5BCT and Al_2O_3 occurring during sintering process, resulting in the formation of intermediate new compound [12].

4.7 Thermal Shrinkage behavior, Density Measurement and Microstructure

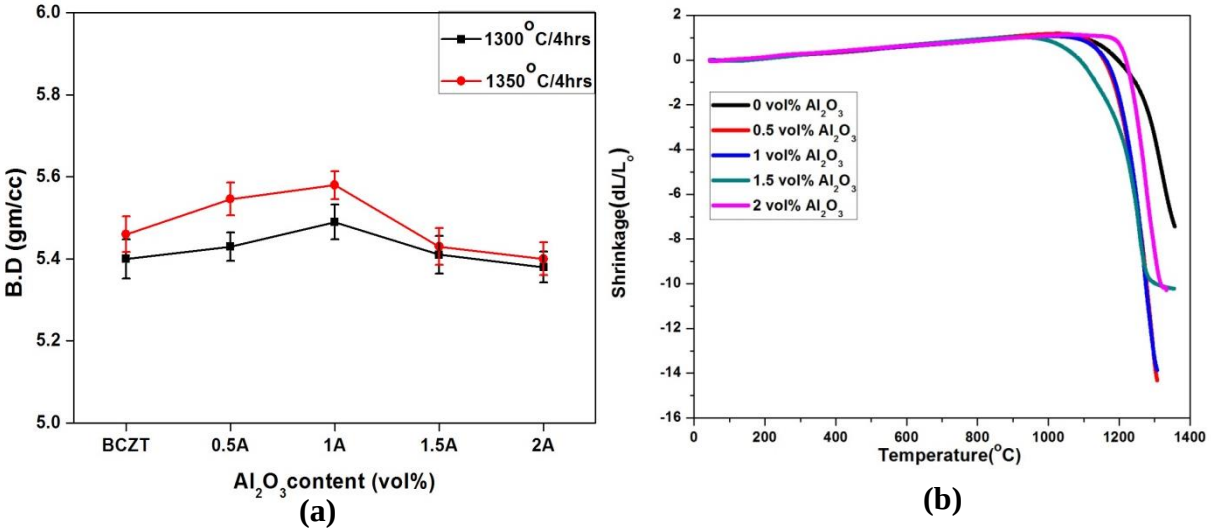

Figure 4.8: (a) Bulk density of nano-Al_2O_3 added BZT-0.5BCT sintered at two different temperatures (b) Thermal shrinkage behavior of different vol. % of nano- oxide Al_2O_3 added BZT-0.5BCT green compact

Figure 4.8 (a) depicts the effect of Al_2O_3 addition on the sintered density of the BZT-0.5BCT at two sintering temperatures, viz., 1300°C and 1350°C. From the figure, it is evident that the bulk density of the pellets [true density of BZT-0.5BCT is 5.78 g/cm^3] increased with an increasein Al_2O_3 addition up to 1vol% followed by a decrease with further addition of Al_2O_3.It may be that small Al_2O_3 addition modifies the grain boundary region or produces small amount of liquid phase which enhances density. Above the optimum amount of Al_2O_3 addition (~1vol %), the densification decreases, this may be due to the presence of higher amount of refractory oxide and generation of impurity phases. The presence of secondary

phase is also confirmed from X-ray diffraction pattern. Jiansirisomboon et al.. [12] observed thatAl_2O_3 addition in $BaTiO_3$ beyond 1 vol% reduces the bulk density to 89% .

Figure 4.8 (b) represents the thermal shrinkage behavior of pure and different volume % of nano-Al_2O_3 added BZT-0.5BCT in a temperature range of room temperature to 1400^oC. Al_2O_3 incorporation enhances the thermal shrinkage upto 1 vol% addition. Higher addition reduces the shrinkage due to the refractory nature of Al_2O_3.

Microstructural Analysis of BCZT + Al_2O_3 sintered specimens

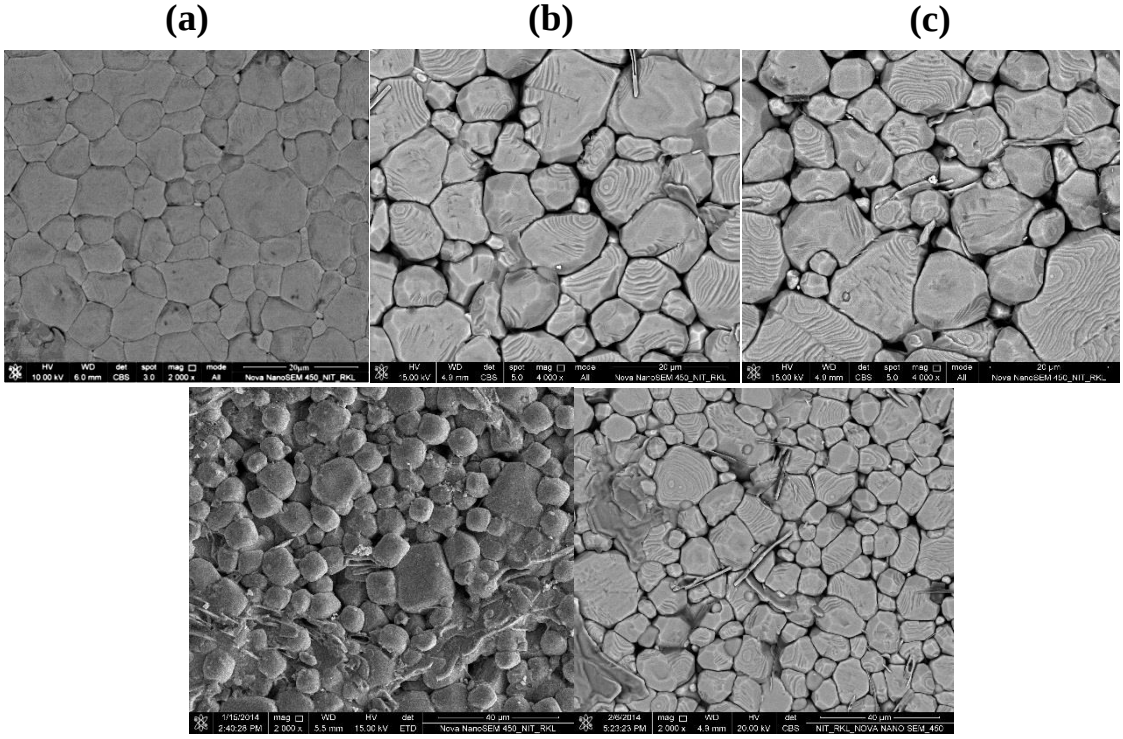

Figure 4.9: FESEM micrographs of (a) x=0 (b) x=0.5 (c) x=1.0 (d) x=1.5 (e) x=2 vol % nano Al_2O_3 added BZT-0.5 BCT ceramic sintered at 1350^oC

Figure 4.9(a-e) shows the FESEM micrographs of nano-Al_2O_3 added BZT-0.5BCT ceramics sintered at 1350^oC for 4h.All the compositions show dense microstructures and average grain size increases with increase in Al_2O_3 content. The grain size is in the range of 2.85-12µm, 6-9 µm, 4.1-12.8 µm, 7.5-13.2µm and 8.1-18µm for 0 -2vol% Al_2O_3 addition BZT-0.5BCT ceramics respectively. Wu et al. [13] reported that the ZnO addition in BZT-0.5BCT ceramics significantly increases the grain size. Cui et al. [14] also reported that CuO modified BZT-0.5BCT ceramics significantly showed increased grain size. Fisher et al. [15]

reported that Al_2O_3 modifications in $BaTiO_3$ promote abnormal grain growth during sintering. Thus, it is believed that a small amount of Al_2O_3 addition to BZT-0.5BCT ceramics can modify the microstructure and the grain size of the BZT-0.5BCT ceramics. A second phase is visible at the grain boundaries region for higher concentration of Al_2O_3 (Figure 6 (d, e)). This second phase was also observed by other researchers [15, 16].

4.8 Dielectric properties

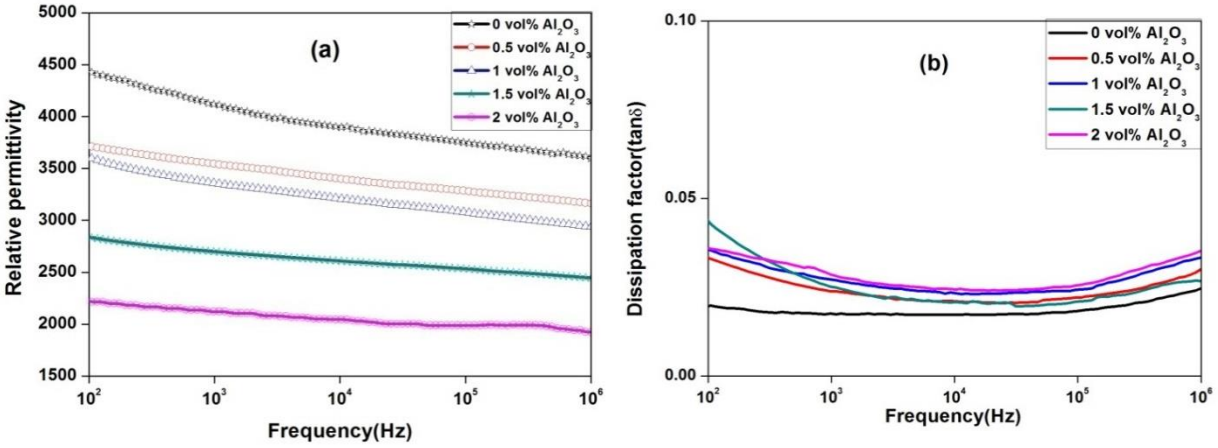

Figure 4.10 (a) Relative permittivity and (b) dissipation factor as the function of frequency for nano-Al_2O_3 added BZT-0.5BCT ceramic sintered at 1350°C/4h.

Figure 4.10 (a) and (b) shows the room temperature relative permittivity and dissipation factor as a function of frequency for nano-Al_2O_3 added BZT-0.5BCT ceramic sintered at 1350°C/4h.The addition of nano-Al_2O_3 reduced the relative permittivity of BZT-0.5BCT ceramic without any major change in loss tangent. Pure BZT-0.5BCT sample has higher relative permittivity (4215) with dissipation factor (2%) sintered at 1350°C, these values are better than those reported in the literature [3, 4,17]. The relative permittivity of all the compositions was very stable in the frequency range 1 kHz to about 1 MHz.

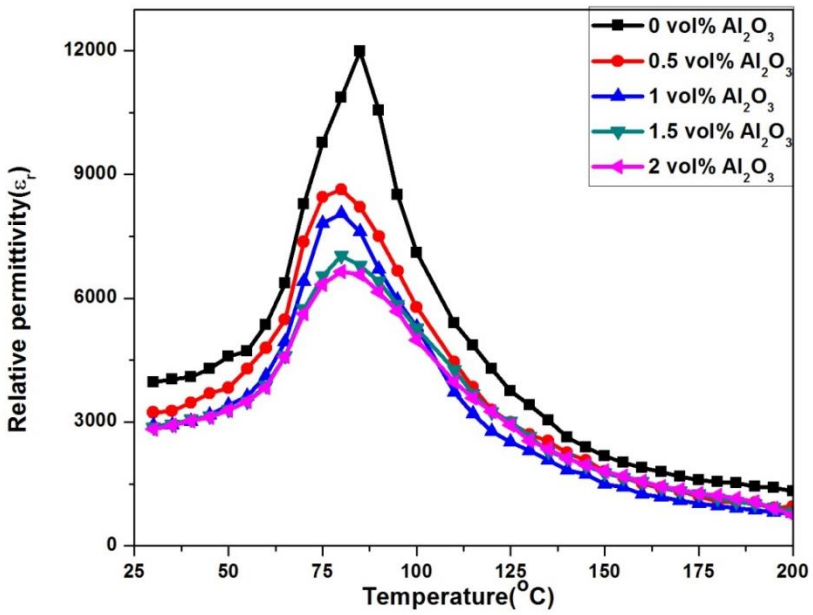

Figure 4.10 (c) Temperature dependence of relative permittivity of Al_2O_3 added BZT-0.5BCT ceramics.

Figure 4.10 (c) shows the relative permittivity versus temperature dependence curves for Al_2O_3added BZT-0.5BCT ceramics. It can be observed that the pure BZT-0.5BCT ceramics exhibit the tetragonal–cubic (T_c) phase transition temperature at around 85°C. These results are well consistent with reported result [18,19]. It also shows no significant change in the phase transition temperature (T_c) for all Al_2O_3 added samples. The decrease in permittivity for Al_2O_3 addition may be understood by considering the formation of non-ferroelectric low-ε Al_2O_3 rich phase. Al^{3+} ions could act as acceptor dopants in B-site of BZT-0.5BCT and may produce oxygen vacancies, which could also cause domain clamping in BZT-0.5BCT ceramics [20, 21]. These results on dielectric measurement were in agreement with a previous report on Al_2O_3 addition on $BaTiO_3$ system [12]. It may be that Al_2O_3 has a small solubility in BZT-0.5BCT, the slight change in Curie temperature, therefore, came from lattice modification. Beyond a certain concentration of added Al_2O_3, the Al-rich non-ferroelectric grain boundary phase should only affect the value of dielectric constant and dielectric loss without affecting the Curie temperature as observed in Figure 4.10 (c). The invariance of T_C was also observed in PZT/Al_2O_3 and $BaTiO_3$/Al_2O_3 system [12, 20].

4.9 Ferroelectric and piezoelectric properties

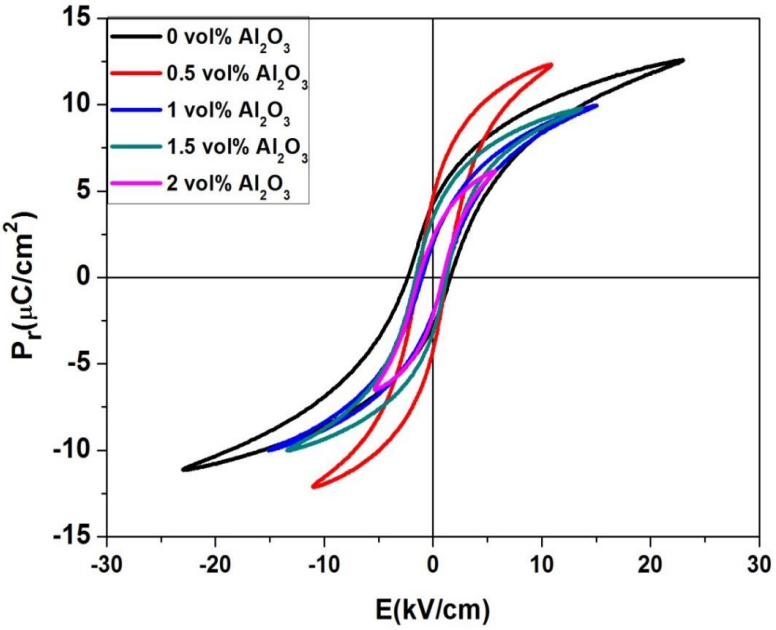

Figure 4.11: P-E hysteresis loops of Al_2O_3 added BZT-0.5BCT ceramics at room temperature.

Figure 4.11 shows the polarization-electric field characterization of the Al_2O_3 added BZT-0.5BCT ceramics at room temperature. The pure BZT-0.5BCT ceramics are typically soft, with a very low coercive field E_c and a relatively high remnant polarization P_r. It is found that the remnant polarization (P_r) and coercive fields (E_c) decreases with increasing Al_2O_3 content. Decrease in remnant polarization can be attributed to the formation of non-ferroelectric Al_2O_3 rich phase.

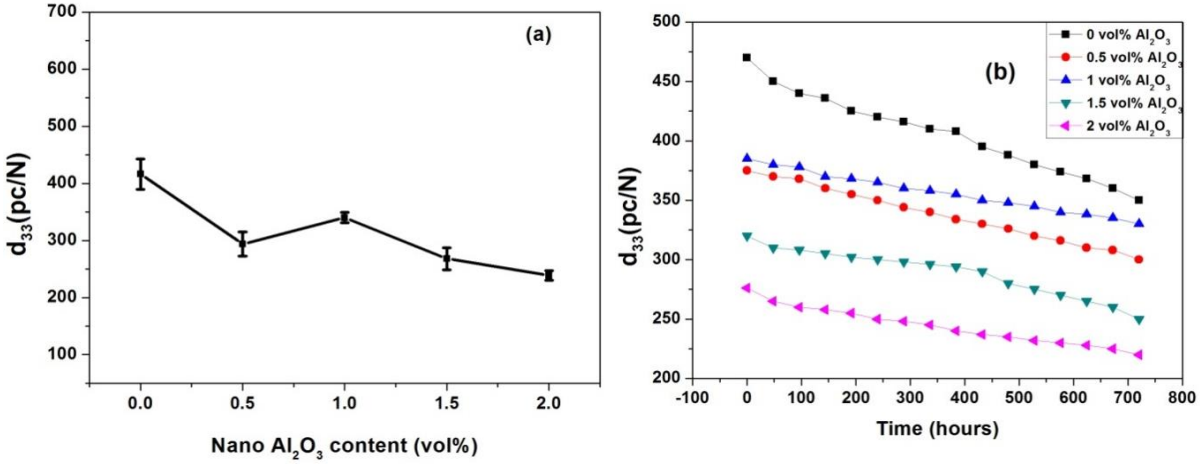

Figure 4.12 (a) Piezoelectric coefficient (d_{33}) as the function of different vol% of Al_2O_3 added BZT-0.5BCT sintered at 1350°C/4h. (b) Piezoelectric coefficient (d_{33}) vs time (hours)

Value of piezoelectric coefficient (d_{33}) of Al_2O_3 added BZT-0.5BCT ceramics are shown in Figure 4.12(a). d_{33} of pure BZT-05BCT ceramic is 450pC/N quite close to the values reported in literature [21], higher than that reported by Li et.al [18, 22] and lower than that reported by Lue et.al and Wang et.al [2, 3]. The d_{33} value gradually decreases with increase in Al_2O_3 addition. The d_{33} of 350pC/N was obtained at 1vol% addition of Al_2O_3, which is 22% less than that of BZT-0.5BCT (450pC/N). For higher concentration of Al_2O_3 content (beyond 1vol %), piezoelectric constant degrades rapidly and that because of excessive amount of non-piezoelectric Al-rich phase in the matrix. The d_{33} value decreases with increase in time (hours) as shown in figure 4.12 (b).The aging rate observed for BZT-0.5BCT is 14%/decade. Addition of Al_2O_3 reduces the ageing rate. For 1 vol% Al_2O_3 added BZT-0.5BCT shows aging rate of 7%/decade. The rapid decline in the piezoelectric response of BZT-0.5BCT is believed to be the result of loss of polarization due to back switching of the ferroelectric domains [23]. It may be that presence of Al_2O_3 rich grain boundaries reduces the rate of gradual reversal of the domain configuration to the random state. Su et al.. [17] observed the extremely high aging rate in BZT-0.5BCT ceramics, 30% and 25% loss for d_{33} and kp, respectively, 10^4 min after poling. However, in the present case, further studies are required to understand the exact aging mechanism in Al_2O_3 added BZT-0.5BCT.

4.10 Mechanical properties

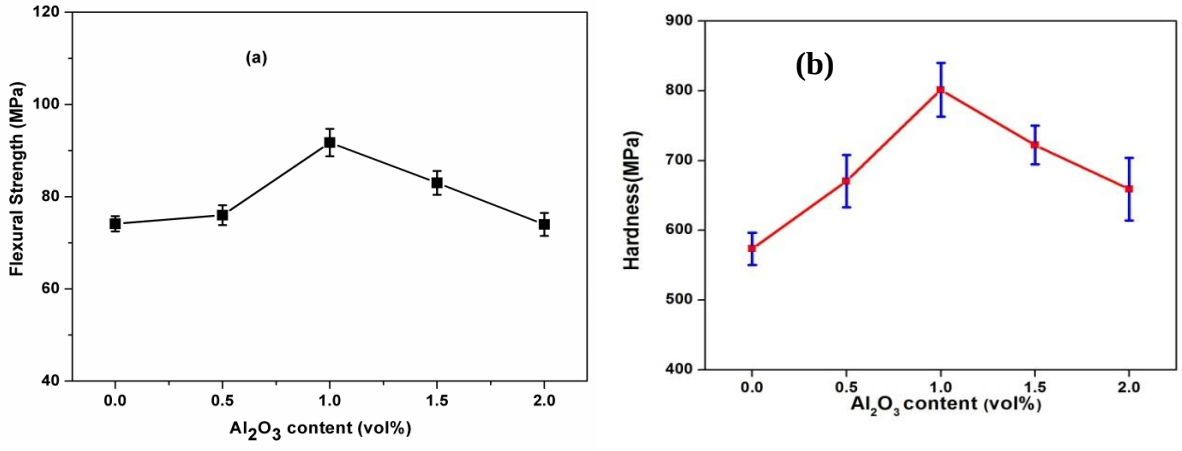

Figure 4.13: (a) Flexural Strength and (b) Hardness of Al_2O_3 added BZT-0.5BCT ceramics.

The measured flexural strength and Vicker's hardness (H_v) are shown in Figure4.13 (a) &(b). It can be observed that both H_v and flexural strength increases with an increasing amount of Al_2O_3 addition upto 1vol% followed by a decrease with further addition of Al_2O_3.The maximum hardness (741.5MPa) and flexural strength (92MPa) was obtained at 1 vol% of Al_2O_3 addition, which is higher than that of pure BZT-0.5BCT ceramic (Hv~573.5 MPa, Flexural strength~74MPa).It is to be mentioned that there is no report available on the strength measurement of BZT-0.5BCT ceramic for comparison. Recently, Kaushal et al.. [24] reported hardness values of 543 MPa for BZT–BCT ceramics prepared by traditional dry pressing technique and measured using nano indentation. In our case, the improved density [Figure4.8 (a)] is helpful for enhancing the strength and hardness of the BZT-BCT composite ceramics. Secondly, the Al_2O_3-rich grain boundary phase may form obstacles between the primary phases for crack propagation and increasing the crack propagation stress and that contributing to the strengthening [25].EDAX mapping of fracture surface of 1vol% Al_2O_3 added sample, figure 4.13, shows concentration of Al in the grain boundary region. Different physical properties of Al_2O_3 added BZT-0.5BCT is summarized in Table 4.2. Nevertheless, the results from this study indicated that enhancement of mechanical properties of BZT-0.5BCT while maintaining its electrical properties could be achieved by small addition of Al_2O_3 nano-particulates in agreement with other nano-composite material systems.

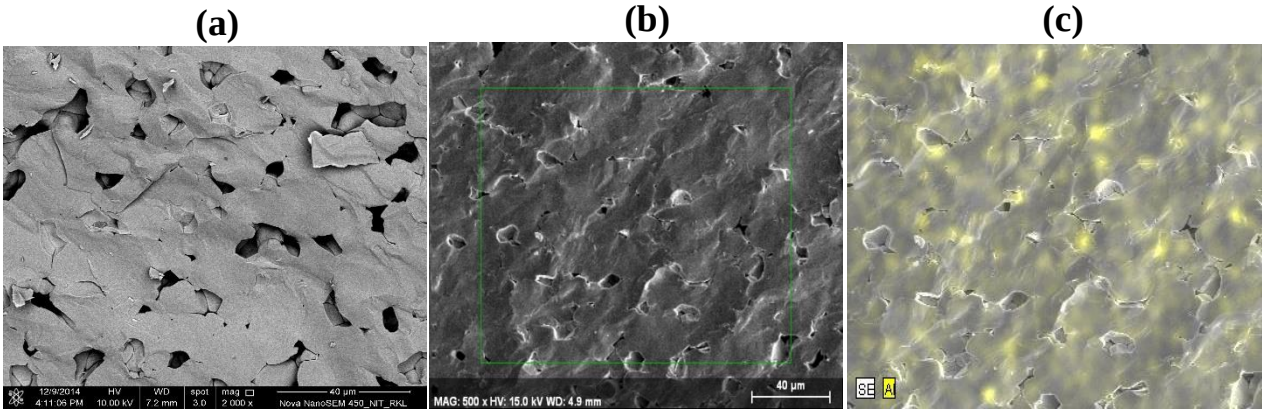

Figure 4.14: Fracture surface of sintered specimen with different volume fraction (a) V_f= 0 %,(b) V_f= 1% (c) Xray spectra for 1 vol% Al containing BCZT ceramic.

Table 4.2: Table showing various mechanical and electrical properties of BCZT + Al_2O_3 sintered specimens

Al_2O_3 content Volume %	**Relative density (%)**	**Average grain size(Min. - Max.) (Avg.) (µm)**	**H_v (MPa)**	**Flexural strength (MPa)**	**Loss (tanδ)**	**ε_r**	**d_{33} (pC/N)**	**g_{33} (Vm/N)**	**Kp (%)**
0	95.45	2.85-12 (6.5)	561	73.5	0.0205	4215	450	11.61	41.23
0.5	96.95	6-9(7.8)	620.5	76	0.0262	3740	300	9.37	41.42
1	97.55	4.1-12.8(10)	741.5	92	0.0227	3630	350	11.45	41.57
1.5	94.93	7.5-13.2(12.5)	722.5	83	0.031	2936	268	11.24	44
2	94.4	8.1-18(16)	659	74	0.0245	2530	238	10.78	45

Section 3: Effect of MgO addition on phase evolution, densification, electrical and mechanical properties of BZT-0.5BCT

Introduction

In previous section effect of nano-Al_2O_3 addition in BZT-0.5BCT was described where flexural strength and hardness of the composite was increased upto certain addition. High piezoelectric constant was retained in the composite ceramics. No major shift in Curie peak was also observed. However, the change in permittivity around the phase transition temperature is still high and which may restricts application of composite ceramics above room temperature. It is discussed in chapter 2 that MgO addition in PZT reduces the grain size and improves the strength and hardness of the composite ceramics without much degrading the piezoelectric property. MgO doping in $BaTiO_3$ modifies the different phase transition temperature, reduces grain size and make Curie temperature peak broader.

To the best of our knowledge there is no report available on electrical and mechanical properties of BZT-0.5BCT ceramics with addition of nano-sized MgO with an aim to improve the mechanical property with suppression of permittivity peak height around the phase transition temperature.The present section describes the densification, microstructure, dielectric, piezoelectric and mechanical properties of BZT–0.5BCT with nano-MgO additions.

4.11 Powder characteristics

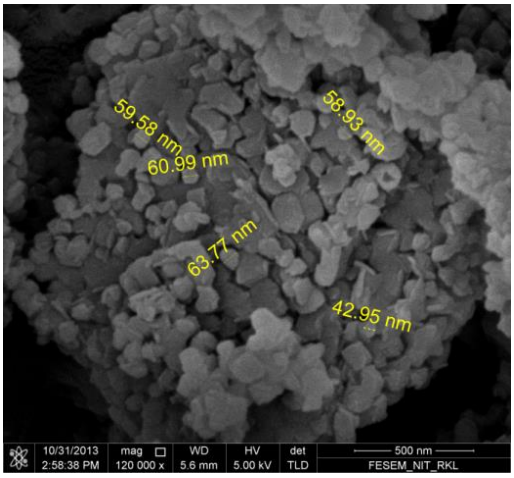

Figure 4.15: FESEM micrograph of nano MgO powder.

The FESEM micrograph (figure 4.15) depicts the particle size of MgO powder, which is in the range of 42-120 nm.

4.12 Phase Analysis of sintered sample

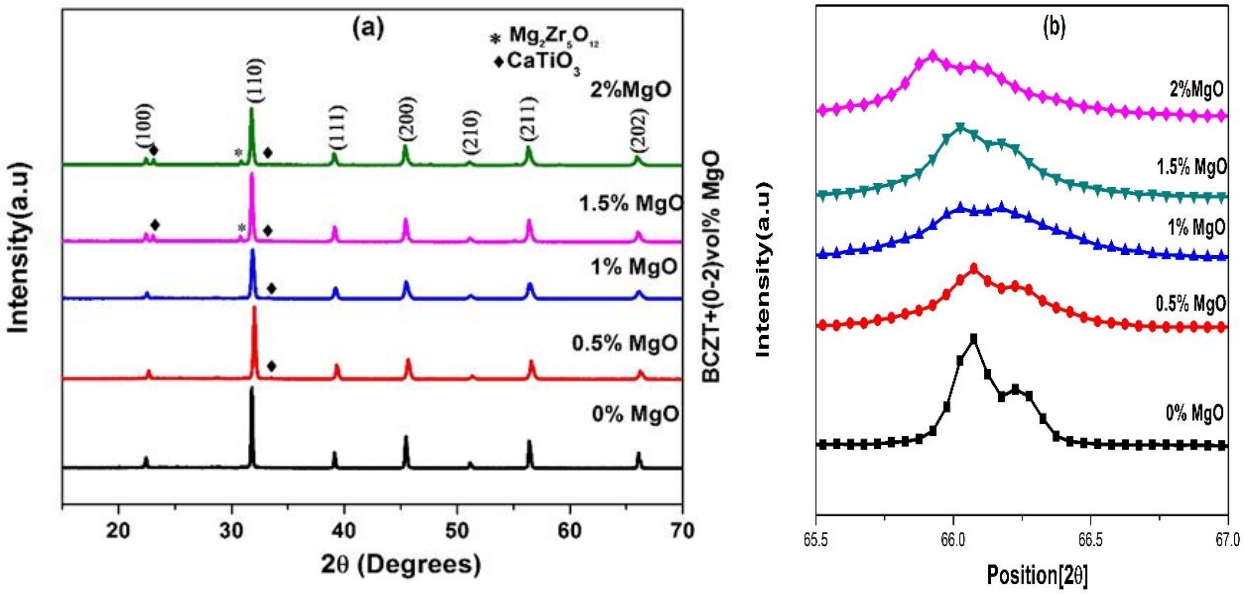

Figure 4.16 (a)X-ray diffraction patterns of pure BZT-0.5BCT and different vol. % of nano-MgO added sample sintered at 1350°C/4hrs (b) magnified X-ray diffraction patterns in the range of 65-67°C.

Figure 4.16 (a) shows the X-ray diffraction patterns of nano-MgO (0-2 vol %) added BZT-0.5BCT ceramics sintered at 1350°C /4h. It can be observed that all compositions exhibit the perovskite structure. The diffraction pattern of pure BZT-0.5BCT ceramic (0% MgO) matches with tetragonal perovskite $BaTiO_3$ (JCPDS file no. 75-0460), with lattice parameters a= 3.9945 Å and c= 4.0335 Å and space group P4/mmm. It is to be noted that $CaTiO_3$ secondary phase was generated for small addition of MgO (0.5 vol%). The secondary phase of $Mg_2Zr_5O_{12}$ (JCPDS file no. 80-0967) can be observed at higher vol% of MgO (x>1 vol %). No trace of MgO was detected, possibly because its amount was less than the XRD detection limit. Moreover, it is clear from the magnified X-ray pattern in the range of 65.5-67° that the position of the diffraction peaks shift towards the lower diffraction angles with addition of MgO indicating higher lattice volume. It is interesting to mention that (202) peak splitting did not disappear with MgO addition but X-ray diffraction peaks are broadened. From the broadened X-ray profile, it is hard to acquire further information on the structural change of the composite upon MgO addition. For small addition of MgO in BZT-0.5BCT,

Mg^{2+}incorporates into the B-site as acceptor dopant and this can promote oxygen vacancies in the structure. As Mg^{2+}(0.72Å) [26] have higher ionic radius compared to Ti^{4+}(0.605Å), it increases the lattice parameter which is demonstrated in peak shifting to lower angle. Probably, incorporation of Mg^{2+} in BZT-BCT destabilizes the structure and also expelles out less soluble Ca^{2+} ion which reacts with TiO_2 to form $CaTiO_3$. It may also create compositional inhomogeneity in the structure. That is also demonstrated later in the ε_r~T plot. For higher addition, Zr comes out from the structure and it reacts with excess MgO to form $Mg_2Zr_5O_{12}$ as MgO has only 1 atom% solubility in $BaTiO_3$ [27].

4.13 Thermal Shrinkage behavior, Density Measurement and Microstructure

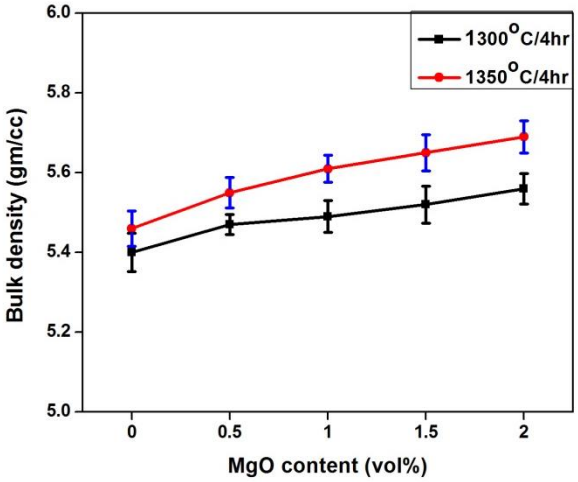

Figure 4.17 (a) Bulk density of nano-MgO added BZT-0.5BCT sintered at two different temperatures

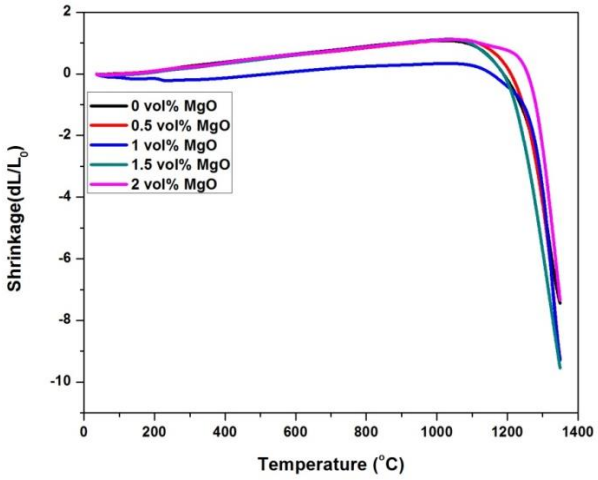

Figure 4.17 (b) Thermal shrinkage of nano-MgO added BZT-0.5BCT from room temperature to 1400°C

Figure 4.17(a) depicts the effect of MgO addition on the sintered density of the BZT-0.5BCT at two sintering temperatures, viz., 1300°C and 1350°C. From the figure, it is evident that the bulk density increased marginally with an increase in MgO addition. Thermal shrinkage increases with increase in MgO addition (Figure4.17 (b)), indicating that MgO incorporation effectively modifies the grain surfaces and promotes densification.

Microstructural Analysis of BZT-0.5BCT + MgO sintered specimens

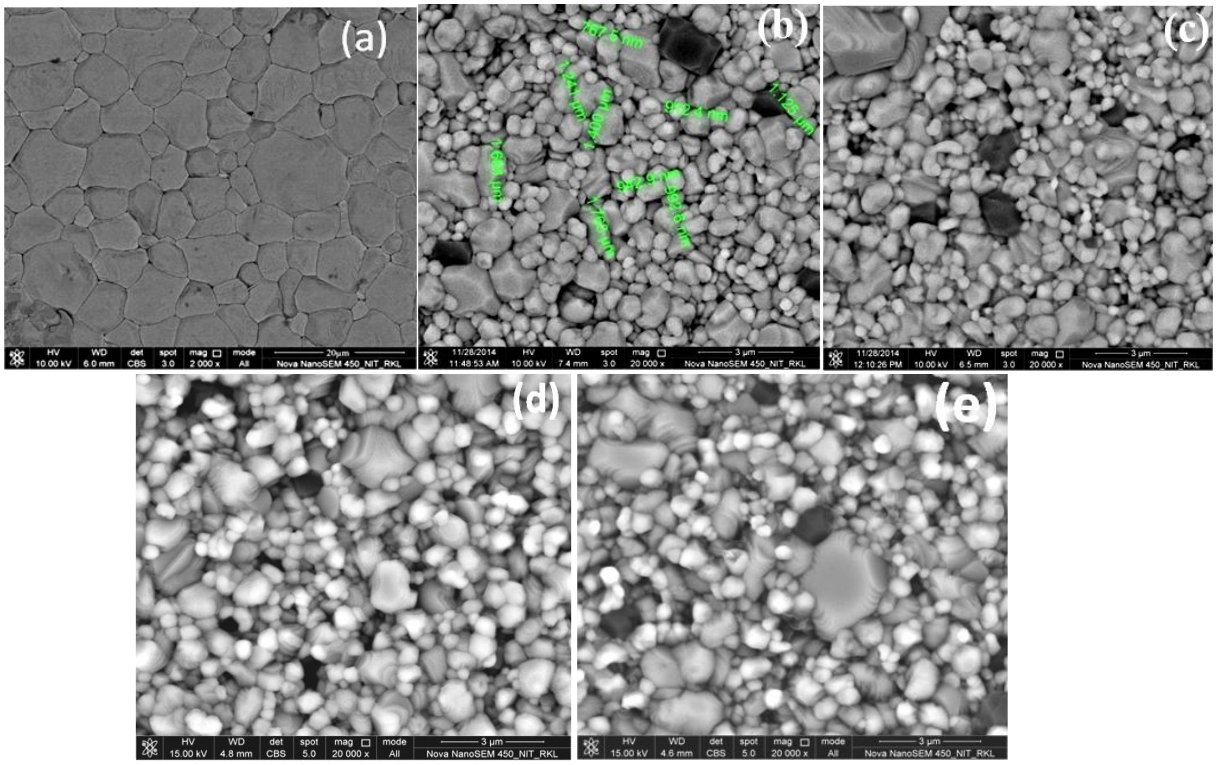

Figure 4.18: FESEM micrographs of nano MgO added BZT-0.5BCT ceramic sintered at 1350^{o}C/4hr (a) x=0 (b)x=0. 5 (c) x=1.0 (d) x=1.5 (e) 2 vol %

Figure 4.18(a-e) shows the microstructure of different vol% MgO added BZT-0.5BCT ceramic sintered at 1350^{o}C for a dwelling time of 4 hr. The grain size was evaluated from the FESEM images using the line intercept method in which a minimum of 30 grains were considered for calculating the average grain size. The values are listed in Table 2. In the SEM image for the BZT-0.5BCT, Figure4.18 (a), the contrasts of the grains are almost same. A considerable homogeneity of the microstructure is observed. A typical dense microstructure of pure BZT-0.5BCT ceramic with grain to grain contact is revealed in microstructure. Average grain size of ~4μm is observed for pure BZT-0.5BCT ceramic. Interestingly, with MgO addition the grain size decreases drasticallyFigure4.18 (b-e). Probably, MgO addition, up to a certain level, inhibits grain growth and helps in densification. Sakabe et al.. and Park et al.. observed grain size reduction in MgO doped $BaTiO_3$ [27, 28].In addition, extra phases with dark contrast are observed in the FESEM image for MgO added sample. EDX mapping,

figure 4.24 (f) , shows that the additional phases have a higher concentration of Ca. Mg distribution in the sample was homogeneous as seen in Figure4.24 (d) .In the XRD profile, small peaks of $CaTiO_3$ appeared. Thus, the additional phase was assigned as $CaTiO_3$ for lower amount of MgO addition (0.5-1 vol %).EDX mapping (Figure24 (e) and (g)) shows that for higher amount of addition (1.5-2 vol% MgO) some additional Mg- rich phases have also been generated along with $CaTiO_3$.

4.14 Dielectric properties

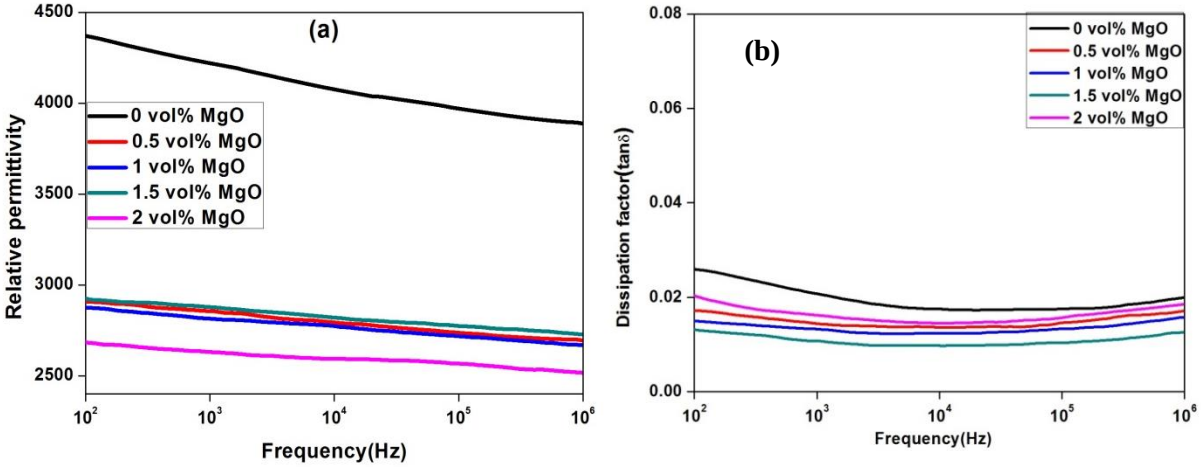

Figure 4.19 (a) Relative permittivity and (b) dissipation factor as the function of frequency for nano-MgO added BZT-0.5BCT ceramic sintered at 1350°C/4h.

Figure 4.19 shows the (a) relative permittivity and (b) dissipation factor vs. frequency for different MgO added BZT-0.5BCT samples (at room temperature). It can be observed that the room temperature relative permittivity values for MgO added BCZT samples 0, 0.5, 1, 1.5, 2 are 4215, 2842, 2821, 2865 and 2640 respectively at 1 kHz. The loss factor of all BCZT ceramics are less than 2.5% at 1 kHz and it decreases with MgO addition. It is to be mentioned that domain wall mobility allows domains to align with an external applied field, yielding extrinsic permittivity contributions. If domains are immobile or less mobile, they cannot contribute or cannot contribute as greatly and thus permittivity is decreased. The most interesting aspect of MgO added samples is its relative permittivity vs temperature response (Figure20).It is clear that MgO additions effectively suppress the relative permittivity around phase transition temperature. The phase transformations of $BaTiO_3$ were reported to be changed by the grain size. When the grain size of $BaTiO_3$ is reduced below 1 μm, the

tetragonality (*c/a*) of the $BaTiO_3$ phase starts to decrease, and the phase transformations are affected by the "size effect."[29] In our case reduction in permittivity and flattened phase transition peak could be attributed to the significant reduction in grain size and generation of non-ferroelectric phase in the matrix.

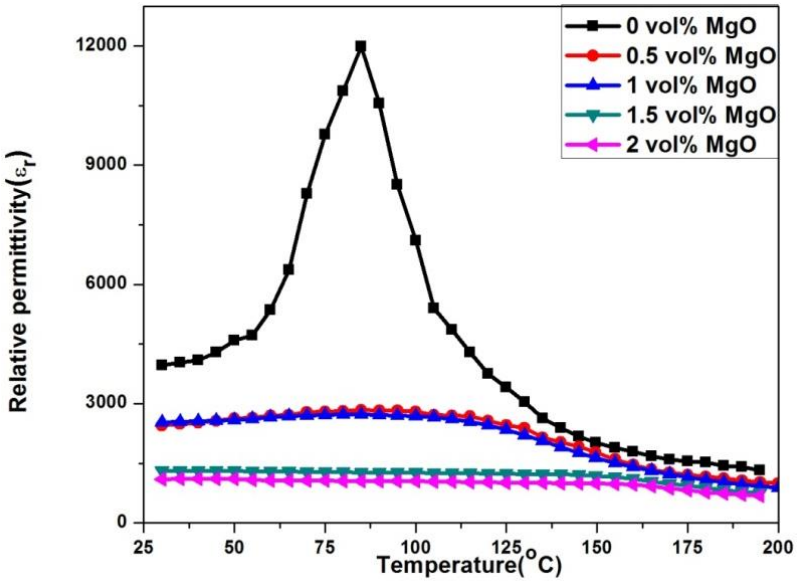

Figure 4.20 Temperature dependence of relative permittivity of MgO added BZT-0.5BCT ceramics

4.15 Ferroelectric and piezoelectric properties

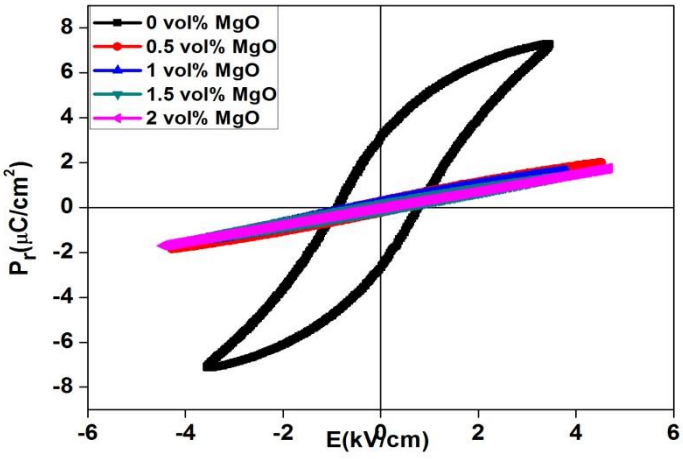

Figure 4.21 P-E hysteresis loops of MgO added BZT-0.5BCT ceramics at room temperature.

Figure 4.21 shows the polarization-electric field characterization of the MgO added BZT-0.5BCT ceramics at room temperature. Pure BZT-0.5BCT ceramics are typically soft, with a very low coercive field E_c= 1.2 kV/cm and a relatively high remnant polarization P_r= 4μC/cm^2.It is found that the remnant polarization (P_r) and coercive fields (E_c) decreases rapidly with increasing MgO content. With the increasing MgO content, the ferroelectric behavior almost disappears. Decrease in remnant polarization can be attributed to the formation of non-ferroelectric MgO rich phase and decrease in grain size.

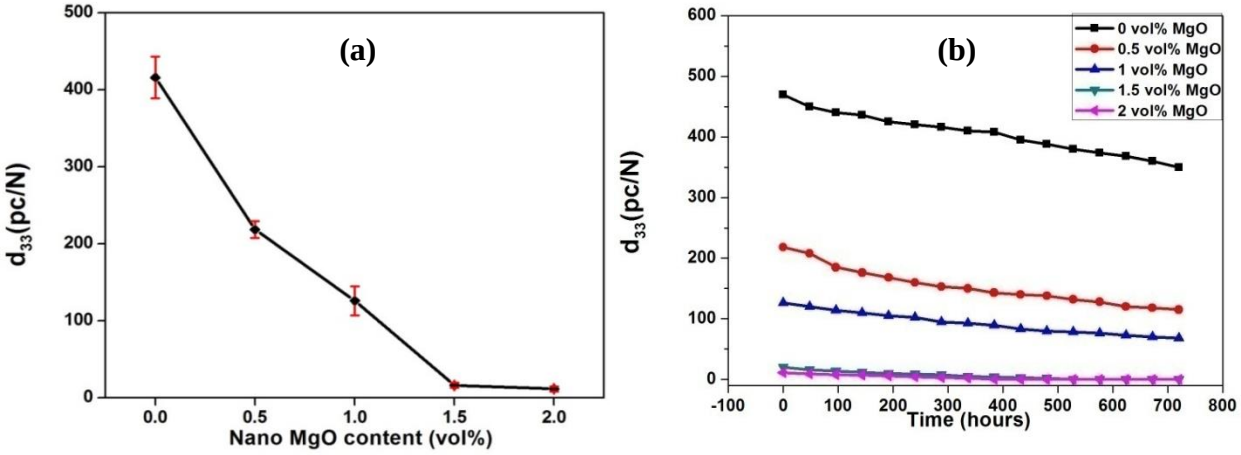

Figure 4.22 Variation of piezoelectric coefficient (d_{33}) of sintered BZT-0.5BCT ceramics with (a) different vol% of nano oxide (MgO) addition (b)time(hours)

Piezoelectric coefficient (d_{33}) value of MgO added BZT-0.5BCT ceramics are shown in figure 4.22(a). The d_{33} value sharply decreases with increase in MgO addition. The $d_{33}$of 150 pC/N was obtained for 1vol% of MgO addition, which was 66% less than that of BZT-0.5BCT (450pC/N).For higher concentration of MgO content (beyond 1vol %), piezoelectric constant degrades rapidly and this is because of excessive amount of non-piezoelectric MgO-rich phase in the matrix. It is generally accepted that grain size is the main influence on the piezoelectric properties of PZT or $BaTiO_3$–based ceramics. Therefore, in our case it is likely that the reduction in the piezoelectric properties was mainly due to the reduction in grain size and introduction of non-piezoelectric $CaTiO_3$/Mg_2ZrO_4 phase in the composite ceramics.

The d_{33} value decreases with increase in time (no of hours) as shown in figure 4.22 (b).The aging rate observed for BZT-BCT is 14%/decade. MgO addition reduces the ageing rate. For 1 and 2 vol% MgO added, BZT-0.5BCT shows aging rate of 3% and 1.5%/decade. The defect dipole reorientation model is predominant in the acceptor-doped ferroelectric materials, which contain a significant concentration of oxygen vacancies and corresponding defect dipoles to provide a sufficient resistance to the domain wall motion. It is also known that drift of charge carriers to the domain walls creating pinning centers and decreasing wall mobility; reorientation of the defect dipoles in bulk of the domains along the direction of local remnant polarization [30]. This may be the possible reason for reduction of aging rate in BZT-BCT/MgO composite ceramic.

4.16 Mechanical properties

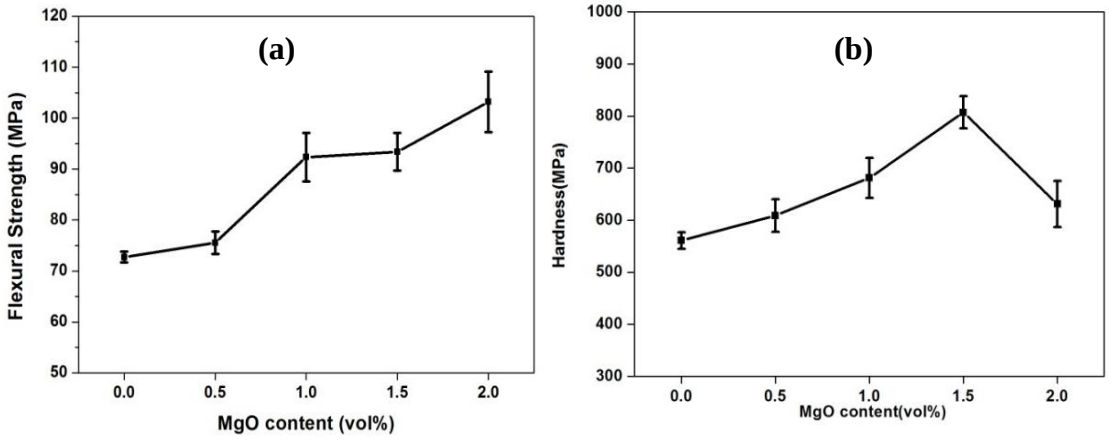

Figure 4.23: (a) Flexural Strength and (b) Hardness of MgO added BZT-0.5BCT ceramics.

Figure 4.23 (a) and (b) shows flexural strength and hardness of MgO added BZT-0.5BCT ceramics, respectively. It was found that the hardness and flexural strength, both increases with increase in MgO concentration. In particular, the value of flexural strength of 1 vol. % MgO added BZT-0.5BCT was 93MPa, which is almost 25% higher than that of monolithic BZT-0.5BCT (73 MPa).Firstly the improved density (Figure 4.17(a)) is helpful for enhancing the hardness of the MgO-BZT-BCT composite ceramics. Secondly, non-primary particles precipitated from a supersaturated solid solution may be partly contributing to the strengthening. Classically, high values of H_v are considered to be related to the effect of

increased grain boundaries [34] which are found in samples with smaller grain sizes, providing additional obstacles to the crack propagation, thus leading to harder materials. Further studies are required to understand the decrement of hardness at 2vol% addition.

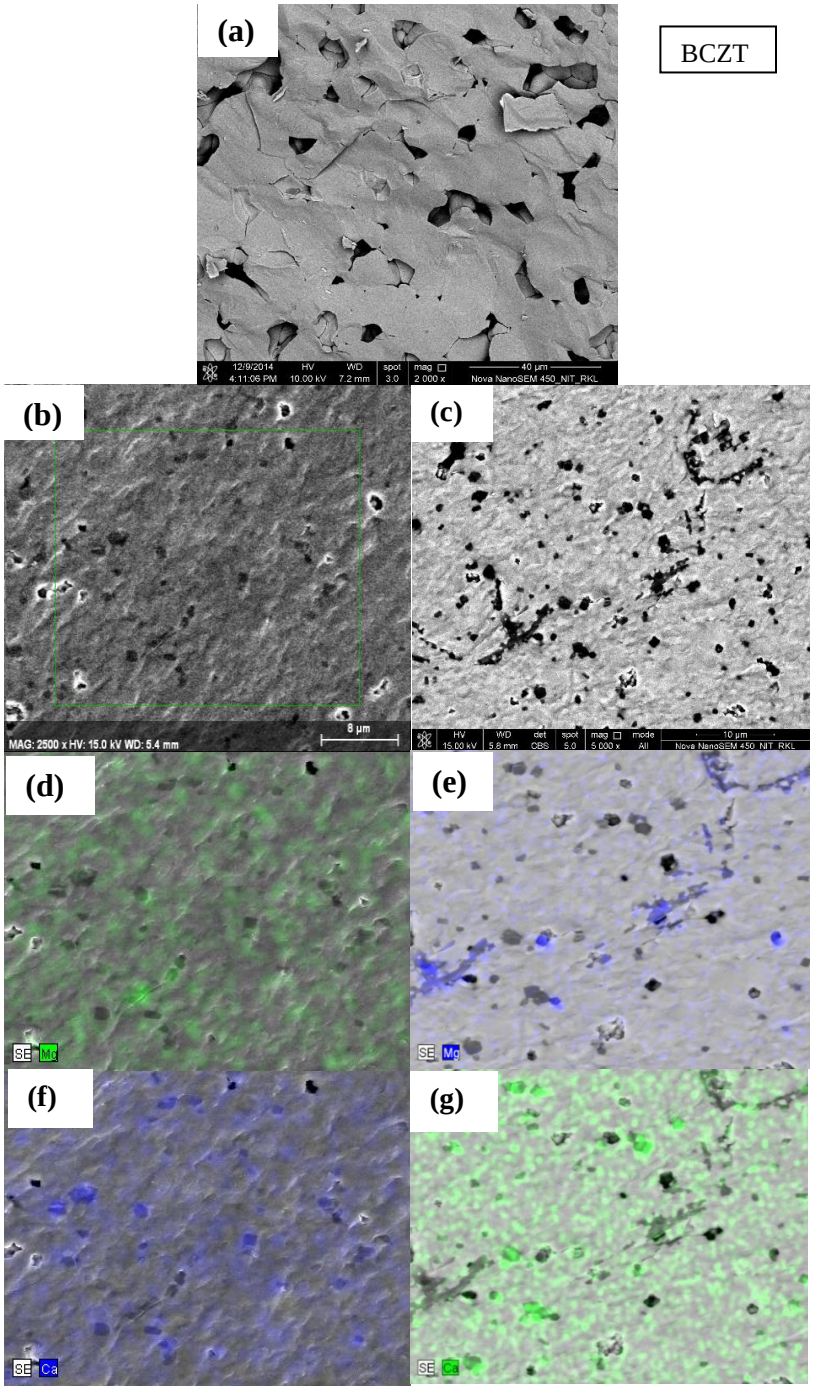

Figure 4.24: Fracture surface of BZT-BCT/MgO sintered specimen with different volume fraction MgO (a) V_f= 0 %,(b) V_f= 1% (c) 2 vol% EDAX mapping of Mg and Ca (d) and (e) 1 vol% (f) and (g) 2 Vol% MgO addition

The BZT-0.5BCT with flat surface and no clear grain boundaries revealed that the fracture mode was mainly intra-granular (Figure4.24 (a)). While in MgO added BZT-BCT sample it was inter-granular i.e. crack has propagated through the grain boundary (a three dimensional effect is there).(Figure4.24 (b)& (c)).MgO addition significantly reduces the grain size, and the fracture mode also modifies. In addition, similar results were reported in PZT/MgO, PZT/ZrO_2 and Al_2O_3/SiC, composite systems by other researchers [31, 32, and 33].In summary, the grain size reduction with increasing MgO content (Figure 4.18), observed in our BZT-BCT/MgO composite ceramics, is believed to be the major factor influencing the hardening and increase in strength of the composite ceramics.

1 vol% of MgO added sample may be suitable for capacitor application due to flat permittivity-temperature response with reasonably high permittivity (~2500) and improved mechanical strength.

Table 4.3: Table showing various mechanical and electrical properties of BCZT + MgO sintered specimens

MgO content	**Relative density (%)**	**Average grain size (Min. - Max.)(Avg.) (μm)**	**H_v (MPa)**	**Flexural strength (MPa)**	**Loss (tanδ)**	**ε_r**	**d_{33} (pC/N)**	**g_{33} (Vm/N)**
0	95.45	2.85-12 (6.5)	561	73.5	0.0205	4215	450	11.61
0.5	97	0.3-2.2 (0.75)	608	75.55	0.0142	2842	218	8.69
1	98	0.23-1.1 (0.563)	681	92.35	0.0131	2821	126	5.06
1.5	98.7	0.36-1.35 (0.37)	807.2	93.4	0.0106	2865	16	6.51
2	99	0.3-2.5 (0.35)	630.9	105	0.0160	2640	11	5.03

Section 4: Effect of ZrO_2 addition on phase evolution, densification, electrical and mechanical properties of BZT-0.5BCT

Introduction

Though dense BZT-BCT with improved strength and hardness and reasonably good piezoelectric property can be obtained by incorporation of nano-Al_2O_3 in BZT-BCT matrix, but the dielectric property degrades.

Recently, significant improvement of mechanical properties, corresponding to a slightly sacrificed value of d_{33}, was achieved in PZT/ZrO_2 composites [34]. Wu et al.. reported the preparation of monoclinic and tetragonal ZrO_2reinforced PZT(Zr/Ti = 58/42) by in situ precipitation method. The PZT/ZrO_2nanocomposite attained significantly improved mechanical properties, while retaining its good piezoelectric properties [33].However, no data is available on the incorporation of tetragonal ZrO_2or ZrO_2(3Y) either in $BaTiO_3$ or in BZT-BCT for improvement of mechanical properties. It is worth investigating how dielectric, piezoelectric and mechanical properties varies with the volume% of ZrO_2(3Y).

In the present section, we report the dielectric, piezoelectric and mechanical properties of ZrO_2(3Y) added BZT-BCT and show that ZrO_2(3Y) addition improves the densification behavior, strength and hardness while retaining the high relative permittivity. However, in this case, piezoelectric property slightly degrades.

4.17 Powder characteristics

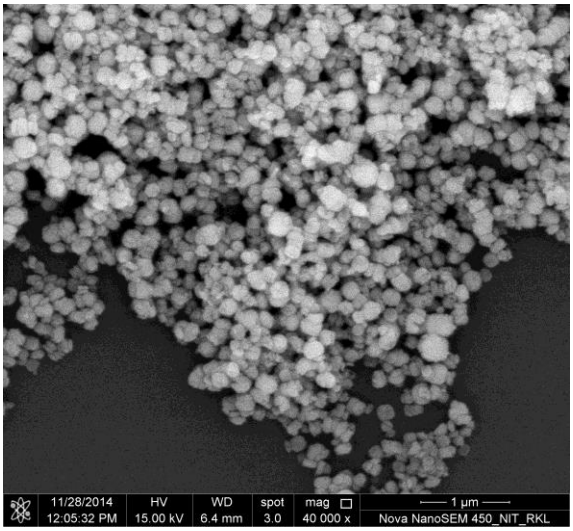

Figure 4.25: FESEM micrograph of nano ZrO_2powder.

Figure 4.25 shows the powder morphology of nano–ZrO_2 powder from which particle size comes out to be 100 nm or less. The particles have near equiaxed shapes. The primary particles appear to form secondary particles of the size, a one tenth of micrometer.

4.18 Phase Analysis of sintered sample

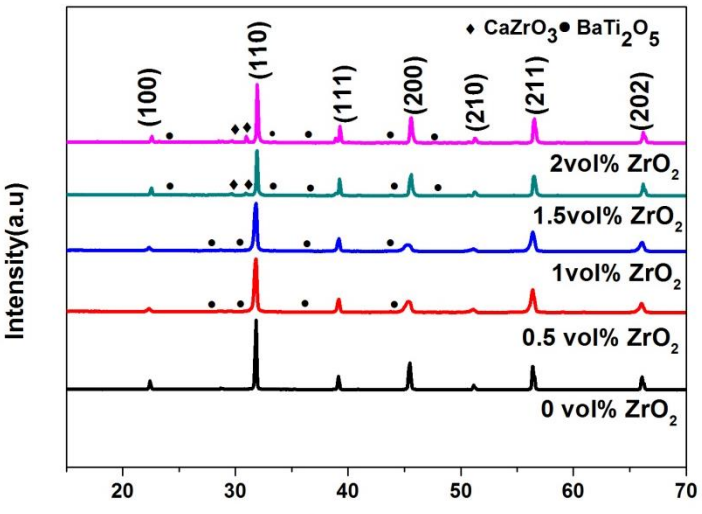

Figure 4.26 X-ray diffraction patterns of pure BZT-0.5BCT and different vol. % of nano-ZrO_2added sample sintered at 1350^{o}C/4hrs

Figure 4.26shows the X-ray diffraction patterns of nano-ZrO_2 (3Y) (0-2 vol %) added BZT-0.5BCT ceramics sintered at 1350^{o}C /4h.It can be observed that all the compositions exhibit perovskite structure. It is to be noted that $BaTi_2O_5$ secondary phase was generated for small addition of ZrO_2 (3Y) (0.5 vol%). In addition, the secondary phase of $CaZrO_3$ (JCPDS file no.09-0364) can be observed at higher vol% of ZrO_2 (x>1.5vol %). Splitting of (111) peak is more intense for higher addition of ZrO_2(x>1vol %), indicating that structure shifts towards rhombohedral symmetry. It may be producing a grain boundary region with Zr-rich BZT-0.5BCT and core with stoichiometric BZT-BCT.

For small addition of ZrO_2 in BZT-0.5BCT, Zr^{4+}can diffuse into B-site by replacing Ti^{4+} from the structure as because the Zr^{4+} ions are chemically more stable than Ti^{4+} ions. Probably, incorporation of Zr^{4+} in BZT-BCT destabilizes the structure and also expells Ba^{2+} ion which react with TiO_2 to form $BaTi_2O_5$. This is contrast to MgO addition (discussed in section 2), where $CaTiO_3$ phase was generated first. For higher addition of ZrO_2, Ca comes out from the structure and it reacts with excess ZrO_2 to form $CaZrO_3$.Rase and Roy determined the BaO-TiO_2 phase diagram with a stable $BaTi_2O_5$ phase [35]. Statton grew

needlelike crystals of $BaTi_2O_5$ from a TiO_2-rich solution of 68.4-mol% in the BaO-TiO_2 system [36].

Akinshige et al.. [37] and Waghmare et al.. [38] reported that the compound, $BaTi_2O_5$ can be a candidate material for lead-free high phase transition temperature ferroelectric materials.

4.19 Thermal Shrinkage behavior, Density Measurement and Microstructure

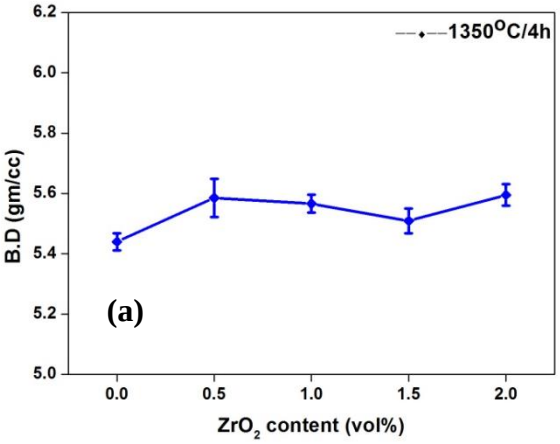

Figure 4.27 (a): Bulk density of nano-ZrO_2 added BZT-0.5BCT sintered at 1350°C

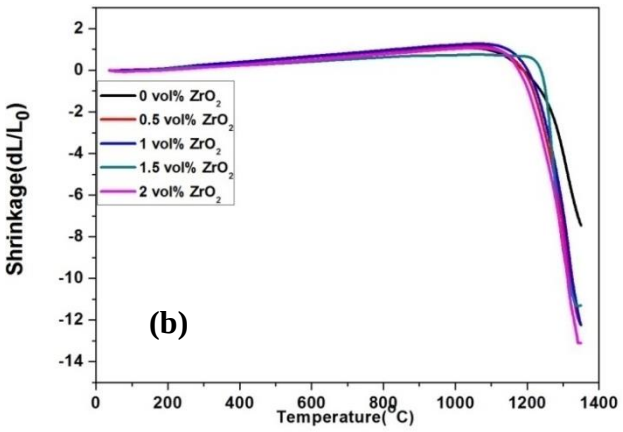

Figure 4.27 (b): Dilatometric analysis of pure BZT-0.5BCT and different ZrO_2 volume % (0 – 2) added BZT-0.5BCT

Figure 4.27 (a) depicts the effect of ZrO_2 (3Y) addition on the sintered density of the BZT-0.5BCT at 1350°C. From the figure, it is evident that the bulk density increased marginally with an increase in ZrO_2 addition, however no significant change was observed beyond 0.5 vol% addition. Thermal shrinkage increases from 7.5% in case of pure BZT-BCT to 12.2% with ZrO_2 addition (Figure4.27 (b)). Initially, the enhancement of the densification may be attributed to the formation of liquid phase. Expelled TiO_2 has a limited solubility in BZT-0.5BCT and results in the formation of TiO_2-rich separate phase and that melts below 1350°C and liquid phase sintering take place. A wide range of grain sizes (7-80 μm) results [Figure4.28]. Large grain size and sharp edge of the grains are also indication of presence of liquid phase at the time of sintering.

Microstructural characterization of BCZT + ZrO_2

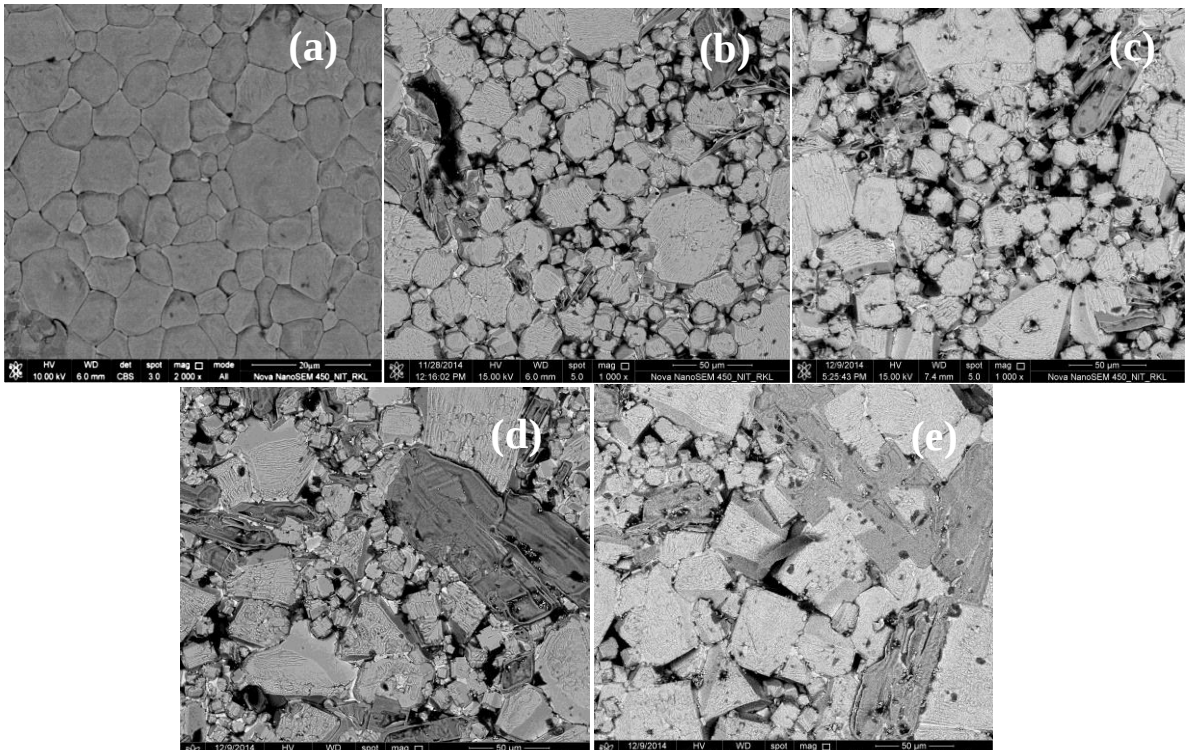

Figure 4.28: FESEM micrographs of nano ZrO_2added BZT-0.5BCT ceramic sintered at 1350^{o}C (a) x=0 (b) x=0.5 (c) x=1 (d) x=1.5 (e) 2 vol %

4.20 Dielectric properties

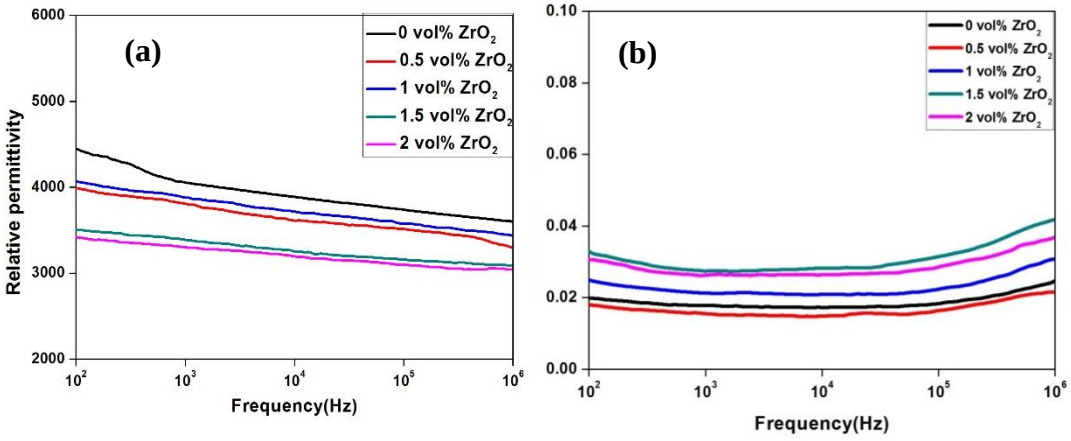

Figure 4.29: (a) Relative permittivity and (b) dissipation factor as the function of frequency for nano-ZrO_2 added BZT-0.5BCT ceramic sintered at 1350°C/4h.

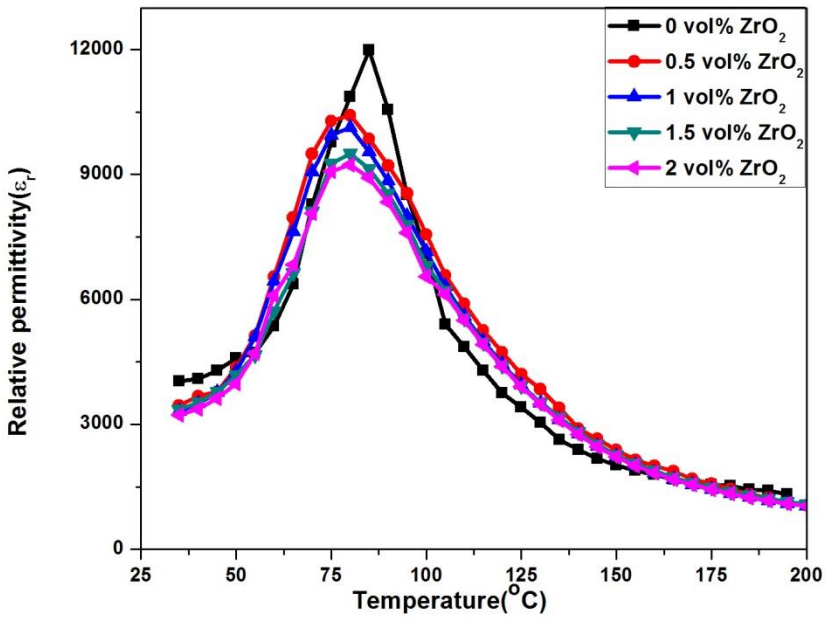

Figure 4.29 (c) Temperature dependence of relative permittivity of ZrO_2(3Y) added BZT-0.5BCT ceramics

Figure 4.29 (a) & (b) shows the relative permittivity and dissipation factor vs frequency for the different ZrO_2 (3Y) added BZT-0.5BCT samples (at room temperature). It can be observed that the room temperature relative permittivity of different ZrO_2 added samples (0, 0.5, 1, 1.5, and 2) are 4215, 3796, 3875, 3381, 3294 respectively at 1 kHz. The dissipation factor of all BCZT ceramics is less than 3% at 1 kHz and that increases marginally with ZrO_2 addition. The reduction of permittivity is less for small ZrO_2 (3Y) addition compared to MgO. Small ZrO_2 addition (up-to 1 vol%) generates Ti-rich $BaTi_2O_5$ secondary phase as confirmed from XRD and EDAX analysis. It is reported that $BaTi_2O_5$ may be a prospective material for lead-free high phase transition temperature ferroelectric materials. However, that may be a reason for less degradation of permittivity for small addition. Moreover, for higher amount of ZrO_2 addition (> 1 vol%) produces $CaZrO_3$ phase which is non-ferroelectric in nature and the ε_r value decreases sharply. Small shifting of the Curie peak towards low temperature [Figure4.29 (c)] may be due to composition fluctuation. Beyond a certain concentration of added ZrO_2, slightly Zr-rich phase should only affect the value of dielectric constant and dielectric loss without affecting the Curie temperature.

4.21 Piezoelectric properties

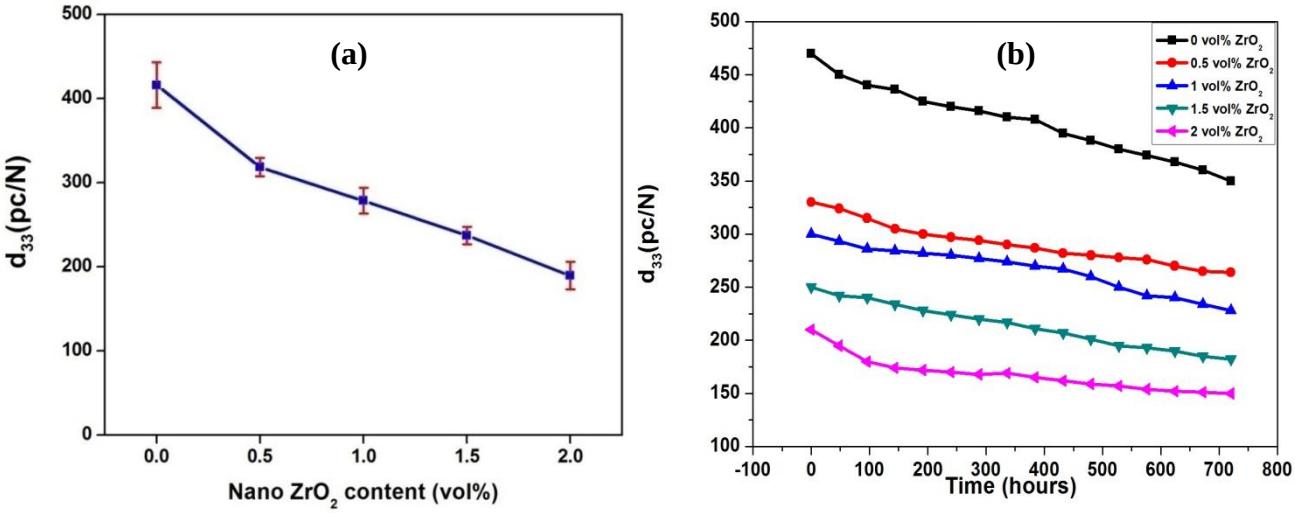

Figure 4.30: (a) Piezoelectric coefficient (d_{33}) (b) Piezoelectric coefficient (d_{33}) vs time (hours) values of ZrO_2(3Y) addition BZT-0.5BCT ceramics sintered at 1350°C for 4h.

Piezoelectric coefficient (d_{33}) value of ZrO_2 added BZT-0.5BCT ceramics are shown in figure 4.30(a).d_{33} of pure BZT-0.5BCT ceramic is 450pC/N quite close to the reported literature [21]**.** d_{33} of 318 pC/N was obtained for 0.5 vol% of ZrO_2 addition in BZT-0.5BCT which was 29% less than that of BZT-0.5BCT (450pC/N). For higher concentration of ZrO_2 content (beyond 0.5 vol %) piezoelectric constant degrades rapidly and that because of generation of ZrO_2-rich phase in the matrix. The d_{33} value decreases with increase in time (hours) as shown in figure 4.30 (b).The d_{33} value decreased gradually that obeyed logarithmic time dependence. Aging is attributed to the stabilization of domain structure over time. This stabilization can be due to direct pinning of domain walls by defects or the establishment of a preferred polarization direction by defect dipoles or volume effects. If the domains are immobile, they cannot contribute to the permittivity and permittivity will decrease.

4.22 Mechanical properties

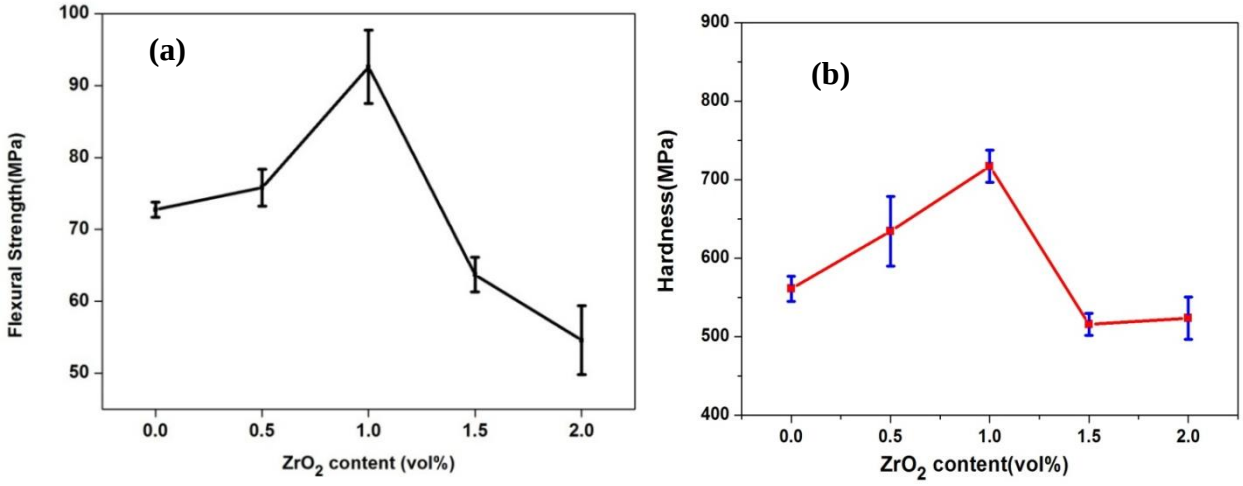

Figure 4.31: (a) Flexural Strength and (b) Hardness of ZrO_2(3Y) added BZT-0.5BCT ceramics.

Figure 4.31 (a) and (b) shows flexural strength and hardness of ZrO_2(3Y) added BZT-0.5BCT ceramics, respectively. It was found that the hardness and flexural strength, both increases with increase in ZrO_2concentration. In particular, the value of flexural strength of 1 vol. % ZrO_2 added BZT-0.5BCT was 91 MPa, which is approximately 21% greater than that of BZT-0.5BCT (73 MPa). Whereas, the hardness of BCZT composite was 715 MPa, which is almost ∼28% greater than the pure. Firstly the improved density [Figure 4.28 (a)] is helpful for enhancing the strength and hardness of the BZT-BCT composite ceramics. Secondly, a different grain boundary phase may form obstacles between the primary phases for crack propagation and increasing the crack propagation stress and that contributing to the strengthening [39]. For higher amount of addition (> 1 vol%) produces more amount of secondary phases and that was segregated and joined as seen from the fractured surfaces [Figure 4.32]. ZrO_2 addition also promotes significant grain growth [Figure 4.32 (b) surface]. As it is known that larger grain size ceramics have inferior mechanical properties [40].

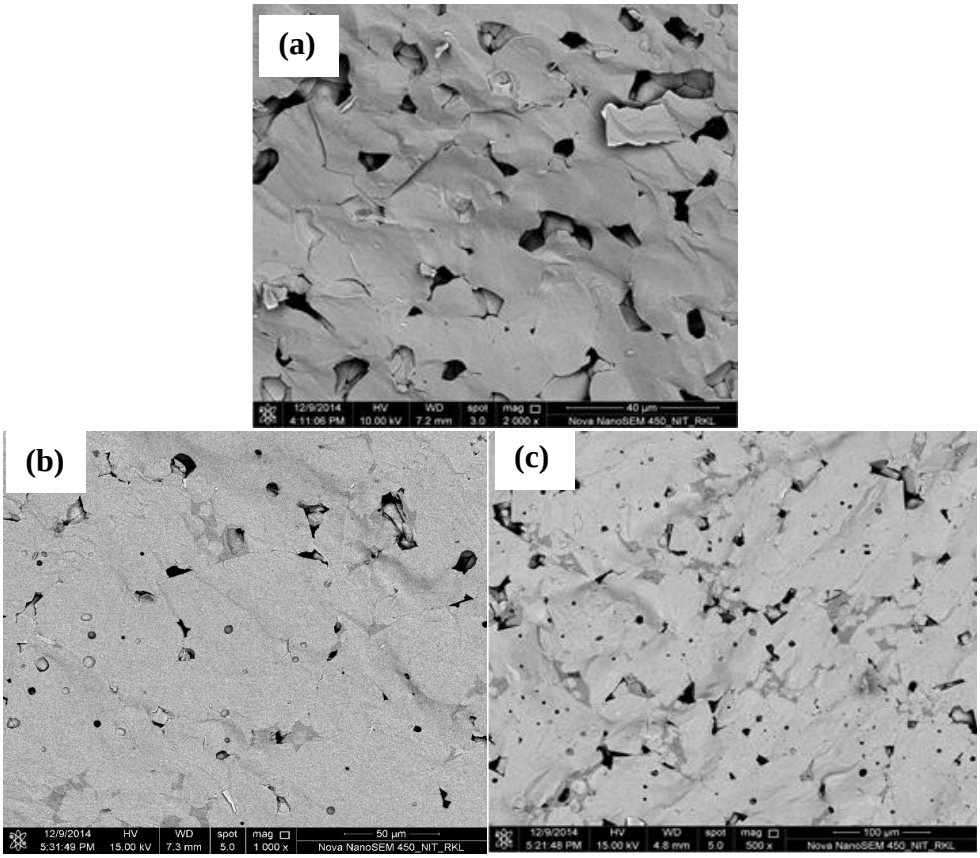

Figure 4.32: Fracture surface of sintered specimen with different volume fraction (a)V_f= 0 %,(b) V_f= 1% (c) 2 vol% ZrO_2 containing BCZT

Table 4.4: Table showing various mechanical and electrical properties of BZT-0.5BCT + ZrO_2 sintered specimens

ZrO_2 content	**Relative density (%)**	**Grain size (Min.-Max) (Average) (μm)**	**H_v (MPa)**	**Flexural strength (MPa)**	**Loss (tanδ)**	**ε_r**	**d_{33} (pC/N)**	**g_{33} (Vm/N)**	**kp**
0	95.45	2.85-12 (6.5)	561	73.5	0.0205	4215	450	11.61	41
0.5	97.63	9-60 (21)	634	77.6	0.0153	3796	318	10.15	49
1	97.2	7.5-80 (23)	717	90.6	0.0212	3875	278	9.37	41.12
1.5	96.32	8.3-70 (29)	515	65.4	0.0274	3381	237	9.94	41.42
2	97.8	7-85 (30)	523	58	0.0263	3294	189	10	40.8

References

[1] R. Yang, W. Fu, X. Deng, Z. Tan, Y. Zhang, L. Han, C. Lu, X. Guan, Adv. Mater. Res. **148** 1062 (2011)

[2] P Wang, Y. Li, Y. Lu, J. Eur. Ceram. Soc. **31** 2005 (2011)

[3] W. F. Liu and X. B. Ren, Phys. Rev. Lett. **10** 3257602 (2009)

[4] F. Benabdallah, A. Simon, H. Khemakhem, C. Elissalde, and M. Maglione, J. Appl. Phys.**109** 124116 (2011)

[5] X .G. Tang, Q.X. Liu, J. Wang, H.L.W. Chan, App. Phys. A **96** 945 (2009)

[6] N. Binhyeeniyi, P. Sukvisut, C. Thanachayanont, S. Muensit, Mat. Lett. **64** 305 (2010)

[7] N. Chakrabarti and H. S. Maiti, J. Mater. Chem. **6** 1169 (1996)

[8] M. Deluca, C. A. Vasilescu, A. C. Ianculescu, D. C. Berger. C. E. Ciomaga, L.P. Curecheriu, L. Stoleriu, A. Gajovic, L. Mitoseriu, C. Galassi, J. Eur. Ceram. Soc. **32** 3551 (2012)

[9] B.W. Lee, S.B. Cho, J. Eur. Ceram. Soc. **25** 2009 (2005)

[10] F.D. Morrison, D.C. Sinclair, A. R. West, J. Am. Ceram. Soc. **84** 531 (2001)

[11] A. Kaushal, S.M.Olhero, B. Singh, D. P. Fagg, I. Bdikin, J.M.F. Ferreira Ceram. Int., **40** 10593 (2014)

[12] S. Jiansirisomboon, A. Watcharapasorn, Curr. Appl. Phys. **8** 48 (2008)

[13] J. Wu, D. Xiao, W. Wu, Q. Chen, J. Zhu, Z. Yang, J. Wang, Scripta Mater. **65** 771 (2011)

[14] Y. Cui, X. Liu, M. Jiang, Y. Hu, Q. Su, H. Wang J. Mater. Sci. Mater. Electron.**23** 1342 (2012)

[15] J. G. Fisher , B. Lee, A. Brancquart, S. Choi, S.L. Kang, J. Euro. Ceram. Soc. **25** 2033 (2005)

[16] N. S. Hari and T.R.N.Kutty, J. Mater. Sci. **33** 3275 (1998)

[17] S. Su , R. Zuo, S. Lu, Z. Xu, X. Wang, L. Li, Curr. App. Phys.**11** S120 (2011)

[18] P Wang, Y. Li, Y. Lu, J. Eur. Ceram. Soc. **31** 2005 (2011)

[19] P.H. Xiang, X.L. Dong, C.D. Feng, N. Zhong, J.K. Guo, Ceram. Int. **30** 765 (2004)

[20] K. Tajima, H.J. Hwang, M. Sando, K. Niihara, J. Am. Ceram. Soc.**83** 651 (2000)

[21] J. Hao, W. Bai, W. Li, J. Zhai, J.Am.Ceram. Soc. **95** 1998 (2013)

[22] I. Coondoo, N. Panwar, H. Amor, M. Alguero, A.L. Kholkin, J. Appl. Phys. **113**, 214107 (2013)

[23] Ronald G. Polcawich and Susan Trolier-McKinstry J.Mater. Res.**15** 11 (2000)

[24] A. Kaushal, S. M. Olhero, B. Singh, R. Zamiri, V. Saravanam and J. M. F. Ferreira, RSC Adv. **4** 26993 (2014)

[25] W. Lee, Ceramic Microstructures, Kluwer Academic Publishers 89-96 (1994)

[26] T. Nagai, K. Iijima, H. J. Hwang and M. Sando, J. Am. Ceram. Soc. **83** {1} 107 (2000)

[27] Y. Sakabe, N. Wada, T. Hiramatsu and T. Tonogaki, Jpn. J.Appl. Phys. **41** 6922 (2002)

[28] J.S. Park and Y.H. Han, J. Eur. Ceram. Soc. **27** 1077 (2007)

[29] Moulson,K. Uchino, E. Sadanaga, and T. Hirose, J. Am. Ceram. Soc. **72** {8} 1555 (1989)

[30] J. R. Scholz "Aging Rates In PZT Ferroelectrics With Mixed Acceptor-Donor Dopants" MS thesis, Pennsylvania State University, (2009)

[31] K. L. Kendig and D. B. Miracle, Acta Mater. **50** 4165 (2002)

[32] K. Niihara, J. Ceram. Soc. Jpn. **99** 974 (1991)

[33] Y. Wu, T. Feng, J. Alloys Comp **491** 452 (2010)

[34] S.J. Jeong, J.B. Kim, Integr. Ferroelectr. **90** 12 (2007)

[35] D.E. Rase and R. Roy, J. Am. Ceram. Soc. **38** 102 (1955)

[36] W.O. Statton, J. Chem. Phys. **19** 33 (1951)

[37] Y. Akinshige, K. Fukano, and H. Shigematsu, J. Electroceram. **13** 561 (2004)

[38] U. Waghmare, M. H. F. Sluiter, T. Kimura, T. Goto, and Y. Kawazoe, Appl. Phys. Lett. **84** {24} 4917(2004)

[39] A. Sawaguchi, K. Toda, and K. Niihara, J. Am. Ceram. Soc. **74** P1142 (1991)

[40] M. Barsoum, Fundamentals of Ceramics, Mcgraw-Hill Publishers, ch 11 415 (1997)

CHAPTER 5

CONCLUSIONS

5.1 Conclusions

Addition of Al_2O_3 nano-particulates in the range of 0–2 vol% to BZT-0.5BCT matrix was found to promote densification upto 1vol% and enhances grain growth. The synthesized powder could be densified to 96% of relative density at a temperature of 1350^oC. Al_2O_3 addition improves the mechanical properties of composite ceramics. The dielectric constant, dielectric loss and piezoelectric coefficient were also influenced by Al_2O_3 addition. It was observed that the addition of Al_2O_3 up to 1 vol % could maintain the permittivity (ε_r) at 3600 with low tanδ value of about 0.02 and d_{33} of 350pC/N. BZT-0.5BCT/Al_2O_3 ceramics possess good mechanical properties viz. flexural strength of 92 MPa compared to pure BZT-BCT (74 MPa) ceramics. The increase in hardness and flexural strength up to 25% and 29%, respectively, could be achieved with addition of 1 vol% Al_2O_3. Better densification and stronger Al_2O_3-rich grain boundaries may be the reason for improved mechanical properties. In this present study, for 1 vol% of Al_2O_3 addition, $BaTiO_3$/ Al_2O_3 composite ceramics with good electrical and improved mechanical properties could be produced.

Addition of MgO was found to promote densification and reduces grain size significantly. Probably, MgO addition, up to a certain level, inhibits grain growth and helps in densification. The MgO addition also provided materials with superior mechanical properties but degrades the dielectric and piezoelectric properties drastically. The most interesting aspect of MgO added samples is their relative permittivity vs temperature response. It is clear that MgO additions effectively suppress the relative permittivity around phase transition temperature. In this case reduction in permittivity and flattened phase transition peak could be attributed to the significant reduction in grain size and generation of non-ferroelectric phase in the matrix. 1 vol% of MgO added sample may be suitable for capacitor application due to flat permittivity-temperature response with reasonably high permittivity (~2500) and improved mechanical strength.

In case of addition of ZrO_2 (3Y), the densities of the composite ceramics were improved by adding appropriate amount of ZrO_2 (3Y). Compared with the BZT-0.5BCT, incorporation of PSZ consistently improved the mechanical properties; however the piezoelectric properties degrades slightly. The strengthening of the material is attributed to the improved densities

and modification of the grain boundaries of the modified BZT-0.5BCT composite ceramics. The reduction of permittivity is least for ZrO_2 (3Y) addition compared to Al_2O_3 and MgO. The presence of grain boundary phase which has composition slightly different from the matrix may be ferroelectric. That may be the reason for less degradation of permittivity. The BZT-BCT/Al_2O_3 and BZT-BCT/ZrO_2, composites revealed good mechanical and electrical properties. These are suitable for application in highly reliable low power piezoelectric devices.

5.2 Scope of future work

Apart from the brief conclusion on the current research work there are several scopes for further work on comprehensive understanding of the certain issues regarding dielectric and piezoelectric and mechanical properties of BZT-0.5BCT. However, the study has not answered some of the following points, which can be taken up as the future study:

i) In order to carry out more detailed analyses of dielectric properties and its temperature dependence, impedance spectroscopy should be employed. It is observed that nano-oxide [Al_2O_3, MgO, ZrO_2(3Y)] addition in BZT-0.5BCT significantly modify microstructure and electrical properties. Impedance spectroscopy may correlate microstructure with electrical microstructure. It is necessary to understand the contribution of grain, grain boundary and ceramic interface effects, which greatly influence the electrical properties.

ii) To understand the conduction mechanism in BZT-0.5BCT/nano-oxide composite ceramics, complex electric modulus formalism can be studied which may provide some important information in determination of the bulk response in terms of localized, i.e., defect relaxation or non-localized conduction, i.e., ionic or electronic conductivity.

iii) Aging of the electrical properties is a very important and interesting phenomenon of ferroelectric or piezoelectric materials. Already some interesting observation are presented in the thesis and some plausible explanations are also provided. For further clarity of different aging mechanism in the composite BZT-0.5BCT ceramics, Rayleigh analysis of piezoelectric response and detail polarization hysteresis P(E) loop measurements should be performed.

iv) Hardness and flexural strength of the BZT-0.5BCT and composite ceramics provided in the thesis. It will be interesting to measure the fracture toughness (K_{Ic}) of BZT-BCT composite ceramics.

v) Further work is required to clarify the domain configuration and microstructure of grain-grain boundary region using HRTEM.

vi) Effect of different non-oxide particle (e.g. Si_3N_4, AlN) additions in BZT-BCT can be studied.

Publications resulting from the M.Tech(Res) work

List of publication related to thesis

1. **P. Adhikari,** Ranabrata Mazumder , Ganesh K. Sahoo**,** Electrical and Mechanical Properties of $0.5Ba(Zr_{0.2}Ti_{0.8})O_3–0.5(Ba_{0.7}Ca_{0.3})TiO_3$ (BZT–0.5BCT) Lead Free Ferroelectric Ceramics Reinforced with Nano-sized Al_2O_3, (**Accepted in Ferroelectrics**).
2. **P. Adhikari,** Ranabrata Mazumder , Ganesh K. Sahoo**,** Effect of Two Different Nano-oxide Addition on Densification, Microstructure, Electrical and Mechanical Properties of $Ba(Zr_{0.2}Ti_{0.8})O_3–0.5(Ba_{0.7}Ca_{0.3})TiO_3$ (BZT–0.5BCT) Ferroelectric Ceramics, (Under Review).
3. **P. Adhikari,** Ranabrata Mazumder, Dielectric and Mechanical Properties of nano-MgO added BZT–0.5BCT composite Ceramics. (Under Review)

List of presentation in conferences

1. P. Adhikari, R. Mazumder, G.K. Sahoo "Electrical and Mechanical Properties of $0.5Ba(Zr_{0.2}Ti_{0.8})O_3–0.5(Ba_{0.7}Ca_{0.3})TiO_3$ (BZT–0.5BCT) Lead Free Ferroelectric Ceramics Reinforced with Nanosized Al_2O_3" AMF-AMEC-2014 The Joint Conference of 9th Asian Meeting on Ferroelectrics & 9th Asian Meeting on Electroceramics, Oct. 26-30, 2014, Shanghai
2. **P. Adhikari,** Ranabrata Mazumder , Ganesh K. Sahoo**,** Electrical and Mechanical Properties of $0.5Ba(Zr_{0.2}Ti_{0.8})O_3–0.5(Ba_{0.7}Ca_{0.3})TiO_3$ (BZT–0.5BCT) Lead Free Ferroelectric Ceramics Reinforced with Nano-sized MgO (**selected for oral presentation in ICS,2015, Jamshedpur chapter**).

Curriculum Vitae

Mrs. PrativaAdhikari

W/o Subhanarayan Mishra
Qr. no- A/108, sector-22,
Rourkela Fertilizer Township,
Odisha, India 769002
Mob: +91-8018950080
Email:prativa.adhikari@gmail.com

Date of Birth: 17.02.1989

Education: M.Sc. (Physics)

Publications/Conference Publications:

- B.S. Sahu, **P. Adhikari**, J. Gorinta, A. Choudhary, R. Mazumder, S. Bhattacharyya, P. Choudhuri, Fabrication and Characterization of Li_2TiO_3 Pebbles by Extrusion and Spherodization Technique for Test Blanket Module in Fusion Reactor, **Journal of fusion Science and technology 65 (2014) 338-345.**
- **P. Adhikari,** Ranabrata Mazumder, Ganesh K. Sahoo**,** Electrical and Mechanical Properties of $0.5Ba(Zr_{0.2}Ti_{0.8})O_3–0.5(Ba_{0.7}Ca_{0.3})TiO_3$ (BZT–BCT) Lead Free Ferroelectric Ceramics Reinforced with Nano-sized Al_2O_3, (**Accepted in Ferroelectrics**).
- **P. Adhikari,** Ranabrata Mazumder, Ganesh K. Sahoo**,** Electrical and Mechanical Properties of $0.5Ba(Zr_{0.2}Ti_{0.8})O_3–0.5(Ba_{0.7}Ca_{0.3})TiO_3$ (BZT–BCT) Lead Free Ferroelectric Ceramics Reinforced with Nano-sized MgO, (**selected for oral presentation in ICS,2015, Jamshedpur chapter**).
- **P. Adhikari,** Ranabrata Mazumder, Ganesh K. Sahoo**,** Electrical and Mechanical Properties of $0.5Ba(Zr_{0.2}Ti_{0.8})O_3–0.5(Ba_{0.7}Ca_{0.3})TiO_3$ (BZT–BCT) Lead Free Ferroelectric Ceramics Reinforced with Nano-sized ZrO_2, (Manuscript under preparation).